Study of the Optical Spectral Variability of the Be/X-ray Binary Systems

University of Crete

Department of Physics

Nersesian Angelos

Thesis for the degree of
Master of Science on Physics

Supervisors: Dr. Pablo Reig, Prof. Iossif Papadakis

Contents

Abstract

X-ray binaries are an important group of sources to study because they are among the brightest objects in the sky and are characterized by dramatic variability in brightness on timescales from milliseconds to months and years. Neutron-star X-ray binaries divide into high-mass (HMXB) and low-mass (LMXB) systems according to the mass of the donor star. High-mass X-ray binaries ($> 8M_{\odot}$) divide further into supergiant X-ray binaries (SGXB) and Be/X-ray binaries (BeXB) depending on the evolutionary state of the optical companion. Be/X-ray binaries are primarily composed of a massive, early-type donor star (Oe or Be star) and a neutron star accretor. The rapidly rotating Be star is surrounded by a geometrically thin circumstellar disk in its equator. The variability of the structure of the disk can be studied by observing the Balmer emission lines in the optical spectra and in particular the H_{α} emission line (6563Å) which is the strongest and the best-studied of these lines. The interaction of the neutron star with the material in the disk results in transient X-ray behavior. Aim of this project is to perform a global study of the optical spectral properties of Be/X-ray binary systems. We analyzed the optical spectroscopic data for the optical counterparts of 14 BeXBs and study the long-term variability of the H_{α} emission line. In particular, we study the correlation between the X-ray activity and the strength of the H_{α} line, the long-term V/R ratio variations and the relationship between the disk size and the H_{α} line equivalent width. From the relationship between the peak separation and the equivalent width we confirm that the disks in BeXBs are Keplerian, as in the case of classical Be stars. However, the disks in BeXB are denser and smaller than those in isolated Be stars. Likewise, the characteristic timescales associated with the evolution of the disk are, on average, shorter in BeXB than in isolated Be stars.

Περίληψη

Η μελέτη των διπλών αστέρων εκπομπής ακτίνων Χ παρουσιάζει έντονο ενδιαφέρον καθώς είναι από τα πιο λαμπρά αντικείμενα στον ουρανό και χαρακτηρίζονται από δραματικές αλλαγές στην φωτεινότητά τους που μπορεί να διαρκέσουν από milliseconds έως μήνες ακόμη και χρόνια. Οι διπλοί αστέρες εκπομπής ακτίνων Χ, εκ των οποίων ο ένας είναι αστέρας νετρονίων, διακρίνονται ανάλογα με τη μάζα του συνοδού αστέρα σε συστήματα υψηλής - μάζας (HMXB) και χαμηλής - μάζας (LMXB). Τα υψηλής - μάζας διπλά συστήματα ($> 8M_{\odot}$) χωρίζονται περεταίρω σε διπλά συστήματα supergiant X-ray (SGXB) και Be/X-ray (BeXB) ανάλογα με την εξελικτική κατάσταση του οπτικού συνοδού. Τα διπλά συστήματα Be/X-ray αποτελούνται κυρίως από έναν γίγαντα αστέρα φασματικού τύπου Oe ή Be και από έναν αστέρα νετρονίων. Λόγω της γρήγορης περιστροφής του αστέρα Be δημιουργείται ένας γεωμετρικά λεπτός δίσκος στον ισημερινό του. Η ανίχνευση της μεταβολής της δομής του δίσκου γίνεται με τη μελέτη γραμμών εκπομπής και πιο συγκεκριμένα της γραμμής H_{α} του υδρογόνου (6563Å) της σειράς Balmer. Η αλληλεπίδραση του αστέρα νετρονίων με το υλικό του δίσκου οδηγεί σε παροδική εκπομπή ακτίνων Χ. Στόχος της παρούσας εργασίας είναι η μελέτη των ιδιοτήτων του οπτικού φάσματος των διπλών αστρικών συστημάτων τύπου Be/X-ray. Για την εργασία αυτή αναλύσαμε οπτικά φάσματα για τους οπτικούς συνοδούς 14 διπλών συστημάτων BeX και μελετήσαμε την μακροχρόνια μεταβολή της γραμμής εκπομπής H_{α}. Συγκεκριμένα, μελετήσαμε τη συσχέτιση μεταξύ της εκπομπής ακτίνων Χ και της ισχύος της γραμμής H_{α}, την μακροχρόνια μεταβολή του λόγου V/R και τη σχέση ανάμεσα στο μέγεθος του δίσκου και του ισοδύναμου πλάτους της γραμμής H_{α}. Από την σχέση μεταξύ του διαχωρισμού των κορυφών (peak separation) και του ισοδύναμου πλάτους προκύπτει ότι οι δίσκοι των διπλών συστημάτων BeX είναι Keplerian, όπως στην περίπτωση των κλασικών αστέρων Be. Ωστόσο, οι δίσκοι στα διπλά συστήματα BeX είναι πιο πυκνοί σε σχέση με τους δίσκους των κλασικών αστέρων Be. Παρομοίως, τα χαρακτηριστικά χρονικά διαστήματα της εξέλιξης του δίσκου είναι, κατά μέσο όρο, μικρότερα στα διπλά συστήματα BeX από τα αντίστοιχα στους κλασικούς αστέρες Be.

Acknowledgments

First and foremost, I would like to express my sincere gratitude to my supervisor Dr. Pablo Reig, who has supported me throughout my thesis with his patience and knowledge. I would also like to express my special thanks to Professor Iossif Papadakis for providing me his support.

In my daily work I have been blessed with a friendly and cheerful group of fellow students. I thank each and every one of them for their help and encouragement. Special thanks to Dialektopoulos K. for our detailed discussions on physics for the last two years, to Tritsis A. as well as Liodakis I. for helping me to get on the road to Python and to Psaradaki I. for sharing her knowledge and experience about astrophysical observations.

I thank PhD student Papageorgiou T. at University of Patrai for helping me with my first attempt to write IRAF scripts.

Finally, I am most thankful to my family for supporting me throughout all my studies at University.

Chapter 1

Introduction

1.1 X-ray Binary Systems

X-ray binary systems are a special class of binary stars. They are made up of a normal star, called donor star, and a compact star (a white dwarf, a neutron star or a black hole), called the accretor. These pairs of stars produce X-rays if the stars are in close enough proximity that material is pulled off the normal star by the gravity of the dense, collapsed star. If the compact star is a neutron star or a black hole, its gravitational field is enormous and so the material is accelerated to extremely high velocities. When the matter reaches the vicinity of the compact star, it decelerates and its free fall kinetic energy is converted into heat radiation, which is available to power the X-ray source.

1.2 X-ray Binaries Classification

Depending on the type of the compact object, the X-ray binary systems are divided into three major classes: cataclysmic variables, if the compact object is a white dwarf, neutron star X-ray binaries or black hole systems. X-ray binaries with neutron stars and black holes can also be divided into low mass X-ray binary or a high mass X-ray binary, depending on the physical properties of the optical star (donor star) [1.1].

1.3 Low Mass X-ray Binaries

1.3.1 Definition

A low mass X-ray binary (LMXB) is a binary system where one of the components is either a neutron star or a black hole. The other, donor, component usually fills its Roche lobe and therefore transfers mass to the compact star. The mass of the donor is typically $< 2M_{\odot}$ and can be on the main sequence, a degenerate white dwarf or an evolved star (red giant). A typical LMXB emits almost all of his radiation in X-rays, and typically less than one percent in visible light, so they are among the brightest objects in the X-ray sky, but relatively faint in visible light. The apparent optical

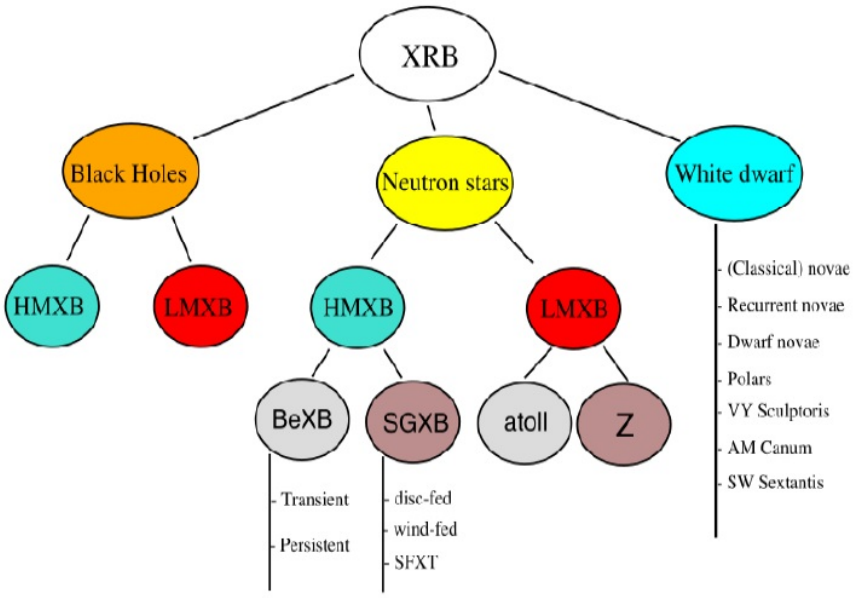

Figure 1.1: Classification of X-ray Binary Systems (Reig 2011)

magnitude is around 18 to 20. The brightest part of the system is the accretion disk around the compact object. The orbital periods of LMXBs range from minutes to hundred of days. Approximately one hundred LMXBs have been detected in the Milky Way, and of these, thirteen have been discovered in globular clusters.

1.4 High Mass X-ray Binaries

1.4.1 Definition

A high mass X-ray binary (HMXB) is a binary system that is strong in X-rays, and in which the normal stellar component is a massive star, usually of type O or B, a Be star, or blue supergiant. The compact, X-ray emitting, component is generally a neutron star, a black hole or possibly a white dwarf. A fraction of the stellar wind of the massive normal star is captured by the compact object, and produces X-rays as it falls onto the surface of the compact object. In a HMXB, the massive star dominates the emission of optical light, while the compact object is the dominant source of X-rays. The massive stars are very luminous and therefore easily detected with ground-base optical telescopes.

1.4.2 Classification

When the component of a HMXB is a neutron star the X-ray binaries are subdivided up into Be/X-ray binaries (BeXB) and supergiant X-ray binaries (SGXB). The separation of these two categories depends on the luminosity class of the binary system. When the optical star is a dwarf, subgiant or giant OBe star, i.e. of luminosity class III, IV or V, then we speak of BeXBs. On the other hand, if the optical star is of luminosity class I or II then we speak of SGXBs.

1.5 Supergiant X-ray Binaries

Supergiant X-ray binaries are HMXBs in which the compact objects orbit massive companions with orbital periods of a few days, 3-15 d, and in circular or slightly eccentric orbits. SGXBs show the typical hard X-ray spectra of accreting pulsars and most show strong absorption at low energies as obscured HMXBs. In SGXBs the optical star emits a substantial stellar wind, removing between $10^{-6} - 10^{-8} M_{\odot} yr^{-1}$ with a terminal velocity up to 2000 km s^{-1}. A neutron star in a relatively close orbit will capture some fraction of this wind, sufficient to power a bright X-ray source. Typical X-ray luminosity is of order $10^{36} erg\, s^{-1}$. If the mass transfer occurs via Roche lobe overflow, then the X-ray emission is highly enhanced and an accretion disk is formed around the neutron star. SGXBs are subdivided into low luminosity or win-fed systems, high luminosity or disk-fed systems and supergiant fast X-ray transients. At this time, there is known only one disk-fed SGXB in the Galaxy, Cen X-3, and three in total, SMC X-1 and LMC X-4, while there about a few tens of wind-fed SGXBs. Because of their brightness and persistent X-ray emission, SGXBs were the first to be discovered. They were initially thought to represent the dominating population of HMXBs, whereas BeXBs were considered atypical cases.

Since the launch of INTEGRAL in October 2002, the situation among the SGXBs was changed. INTEGRAL has unveiled a population of highly obscured HMXBs with supergiant companions and a new type of source displaying outbursts which are significantly shorter than typical BeXBs and which are characterized by bright flares with a duration of a few hours and peak luminosities of $10^{36} - 10^{37} ergs^{-1}$. These new systems have been termed as supergiant fast X-ray transients (SFXT) (Neguerulea et al. 2006; Neguerulea et al. 2008; Walter & Zurita Heras 2007). SFXTs differ from SGXBs because they are only detected sporadically, during very brief outbursts. The origin of these outbursts is not yet found, but there are some promising models that explain this phenomenon. One model to explain SFXTs invokes highly structured stellar winds. The outburst occurs as a result of the accretion of one of the clumps of dense matter from the wind. An alternative model assumes a very elliptical orbit for the binary. In this model the outbursts are triggered when the compact object travels through the periastron. Other models imply that SFXTs contain strongly magnetized neutron stars. The outbursts result from the overcoming of centrifugal and magnetic barriers.

1.6 Be/X-ray Binaries

BeXBs are X-ray sources composed of a Be star and a neutron star. The high energy radiation arise due to accretion of material associated with the Be star by the compact object. The name Be stars is used as a general term describing an early type non supergiant, fast rotating B type and luminosity class III-V stars, which at some time has shown emission in the Balmer series lines and hence the qualifier 'e' in their spectral type (Porter & Rivinius 2003). In comparison with normal stars of the same spectral type, both the emission lines and the strong infrared excess are attributed to the presence of circumstellar material in disk like geometry. The exact cause that give rise to the disk are not well understood. Different mechanisms have

been proposed but it seems none of them can explain the observed phenomenon on its own (Neguerulea 1998).

During periastron, the neutron star passes close to this disk, sometimes may even go through it causing major disruption. A large flow of matter is then accreted onto the neutron star. Then, the free fall kinetic energy of the matter is converted into thermal radiation which powers the X-rays. The Bexbs are by definition non supergiant systems with large orbital periods and hence they are within the Roche lobe. However, transient Roche lobe overflow may occur, during periastron passage in systems with large eccentric orbits or during giant X-ray outbursts when large fraction of the Be star's disk is believed to be accreted (Reig 2011).

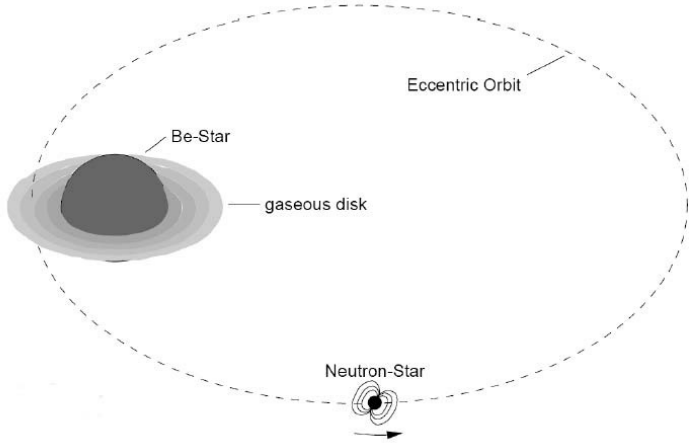

Figure 1.2: Typical representation of a BeXB system. The Be star has a circumstellar disc around its equatorial region and the neutron star is in an eccentric orbit around it. Material in the circumstellar disc may be accreted by the neutron star as it undergoes periastron passage.(Kretschmar1996).

BeXBs can have multiple states of X-ray activity:

- Persistent low luminosity ($L_x \leqslant 10^{36} ergs^{-1}$) X-ray emission.
- Short X-ray outbursts ($L_x \approx 10^{36} - 10^{37} ergs^{-1}$) separated by the orbital period (Type I outbursts), generally occurring close to the time of periastron passage of the neutron star.
- Giant (Type II) X-ray outbursts ($L_x \geqslant 10^{37} ergs^{-1}$), which do not show clear orbital modulation and last several weeks.

Some systems display only persistent emission, but most of them show outbursts and are termed Be/X-ray transients. Both kinds of systems seem to fall in a relatively narrow region of the P_{orb}/P_{spin} diagram [1.5].

1.6.1 Optical/IR Properties of BeXB

There are two main observational characteristics of Be stars, the emission spectral lines, as opposed to the normal absorption photospheric lines and an excess of IR

emission. The origin of these two properties come form the extended circumstellar envelopes of ionized gas surrounding the equator of the B star. They are the result of the free-free and free-bound emission from the disk. The common origin that this two properties share is strongly supported by the correlation among the intensities of continuous IR emission, as measured by fluxes at a certain wavelength, and the intensity of the H_α line, as measured either as equivalent width or fluxes. By studying the line variability one can obtain important constraints on the geometry and dynamics of the envelope.

1.6.2 H_α Line Profiles

H_α emission lines can be divided into two main classes based on the morphology of their profile. Class 1 includes the symmetric line profiles and Class 2 includes the asymmetric profiles with variability on time scale of years [1.3]. Each class does refer to the same groups of sources because individual Be stars can change slowly (of the order of years to decades in isolated Be stars and months to years for BeXbs), from the one class to the other. Symmetric profiles are generated in quasi-Keplerian disks. In contrast, asymmetric profiles are associated with distorted density distributions (Okazaki 1991).

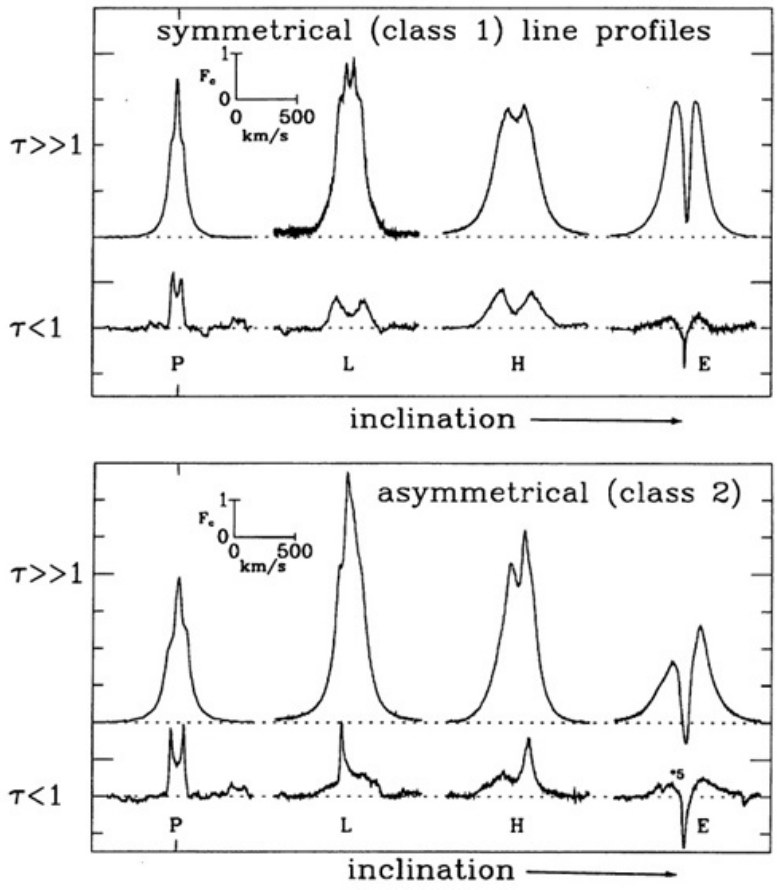

Figure 1.3: Typical emission line shapes of symmetrical and asymmetrical profiles for Be stars (Hanuschik et al. 1996).

Interferometric observations have clearly shown that there is a linear correlation between the net emission in H_α and the physical extent of the emitting region (Quirrenbach et al. 1997; Tycner et al. 2005). An important spectral parameter of the H_α line that measure the strength of the line is the equivalent width (EW). Therefore we would expect a correlation between the EW and the size of the disk (Grundstrom & Gies 2006).

1.6.3 V/R Variations of Binary Be Stars

Most of the BeXBs show asymmetric split H_α profiles. V/R variability refers to the variation of the relative strength of the blue to the red peak and it is crucial characteristic of the H_α line profiles of the BeXBs. The V/R ratio, defined as the ratio of violet-side to red-side peak intensities above continuum in units of continuum intensity, represents a measure of the asymmetry of the line. In practice it is common to use the logarithm of this ratio, $log(V/R)$.

The V/R variability can be explained by a non-axisymmetrical equatorial disk in which a one-armed perturbation, i.e. a zone in the disk with higher density, propagates (Reig 2011). Double-peak symmetric profiles are expected when the high-density part is in front or behind the star. On the other hand, asymmetric profiles are observed when the high-density perturbation is on one side of the disk. In figure [1.4] the curved arrow indicates the direction of the nearly Keplerian motion of the gas in the disk. This high density perturbation revolves around the star in the prograde sense on the time scale of V/R variations of the emission line profiles. For the four positions of the high-density part of the one-armed perturbation we indicate the expected H_α profile for an observer which sees the disk edge-on.

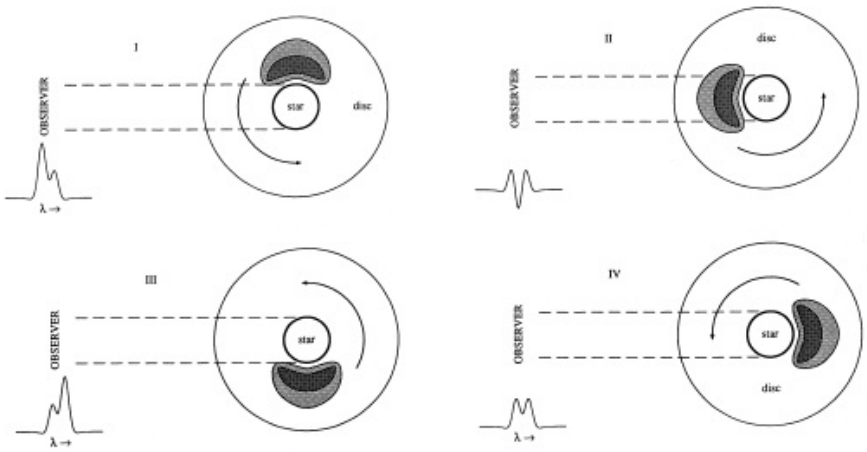

Figure 1.4: Schematic model of V/R variations (Telting et al. 1994).

- I) The gas in the high-density part of the disk moves towards the observer, therefore the emission lines have $V > R$.
- II) The high-density part is in front of the star, the emission lines have maximum shell absorption and $V = R$.

- III) The gas in the high-density part of the disk moves away from the observer, and the emission lines have $V < R$.
- IV) The high-density part is behind the star and also $V = R$.

1.7 Corbet's Diagram

Corbet's diagram [1.5] is a spin period versus orbital period diagram. A visual inspection of this diagram reveals that the different types of HMXBs occupy well-defined positions, which reflects the different types of mass transfer. SGXBs show no correlation or an anticorrelation. Disk-fed SGXBs (squares) show short orbital periods and short spin periods and display an anti correlation in the $P_{orb} - P_{spin}$ diagram. The small orbital separation and evolved companions make Roche lobe overflow the most likely mass transfer mechanism. Wind-fed SGXBs (triangles) show long spin periods and short orbital periods, occupying a more or less flat region in the Corbet diagram.

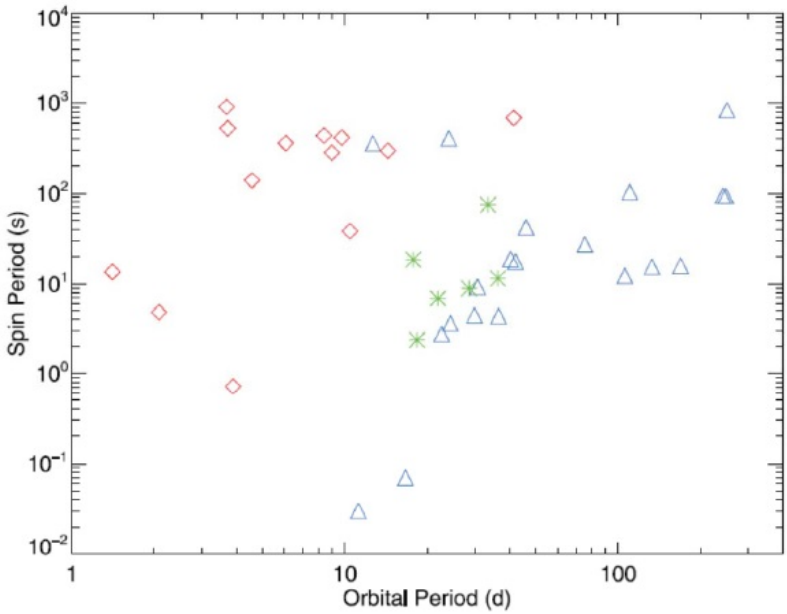

Figure 1.5: Corbet diagram (or $P_{orb} - P_{spin}$ diagram) for all the HMXBs that have known spin period excluding the PSR systems. The red diamonds represent the supergiant systems, the blue triangles are the Galactic Be/X-ray binaries and the green stars are the Small Magellanic Cloud Be/X-ray binaries (Townsend et al. 2011).

BeXBs (filled circles) show a positive correlation. The reason behind this correlation is explained in terms of equilibrium period. Equilibrium period is the period at which the the outer edge of the magnetosphere rotates with the Keplerian velocity. If the pulsar rotated far from the equilibrium period, then the accretion torque would increase its spin until the equilibrium is reached. If, on the contrary, the

neutron star rotates faster than the equilibrium period, then matter is spun away by the propeller mechanism.

The equilibrium period depends on the accretion rate because the accretion rate determines the size of the magnetosphere. The higher the accretion rate, the smaller the magnetosphere. In turn, the accretion rate depends on the orbital separation of the two components of the binary system. The larger the orbital period the lower the amount of mass captured by the compact object. The equilibrium period is given by

$$P_{\rm eq} \approx 1s \left(\frac{B}{10^{12}G}\right)^{6/7} \left(\frac{\dot{M}}{10^{-9}M_{\odot}yr^{-1}}\right)^{-3/7} \tag{1.1}$$

1.8 Circumstellar Disk

1.8.1 Disk Formation

Be stars have very large rotational velocities. A rotational velocity close to the critical velocity, i.e. the velocity at which centrifugal forces balance gravity, reduces the effective equatorial gravity to the extent that weak processes such as gas pressure or non radial pulsations may trigger the ejection of photospheric matter with sufficient energy and angular momentum to make it spin up into a Keplerian disk. The rotational velocity is a very important parameter and contributes to the formation of the circumstellar disk, but it is not the ultimate mechanism of mass ejection because the rotational velocity is smaller than the break-up velocity at which centrifugal forces balance gravity. The projected rotational velocities are determined by measuring the width of certain spectral lines. The rotational velocities and the width of the spectral lines are linearly related (Steele et al. 1999).

The gas origin in these disks seems to be ejected material from the stellar photosphere, although the mechanism that triggers this process is not known yet. There are some suggested models which attempt to explain the disk formation. One of them is the non-radial pulsations model (Cranmer 2009). Non-radial pulsations may give rise to propagating circumstellar waves, that can pass enough angular momentum to the upper stellar atmosphere to spin up a Keplerian disk.

1.8.2 Disk Loss Episodes

The determination of the spectral type and luminosity class of the Be star is not straightforward, because of the presence of the surrounding envelope, which distorts the photospheric spectrum. The hydrogen free-bound and free-free processes in the circumstellar envelope cause the Be stars to appear redder than the non-emission B stars. However, some of the Be stars display a disk loss episode. During this phenomenon we could identify the real luminosity of the Be star and then by subtracting the luminosity taken from the star with the disk, we get the luminosity of the disk. From the H_α line we can detect disk loss episode. The H_α line, during this episode, shows an absorption profile and at the time that the disk reappears the H_α line shows an emission profile [1.6].

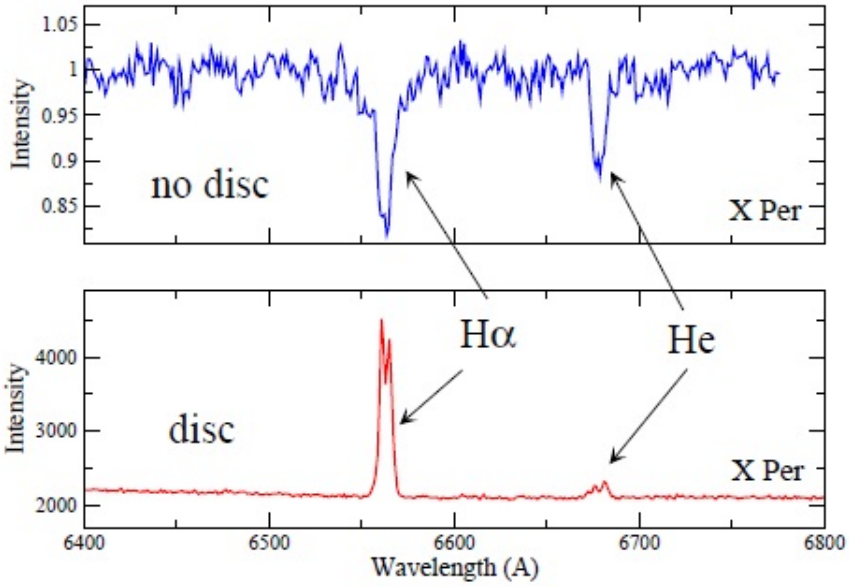

Figure 1.6: The H_α and H_e lines. Up: absorption. Down: emission. (Reig 2011)

1.9 X-ray Outbursts in Be X-ray Binaries

As we mention above, Be X-ray binaries are systems with one massive, early type donor star (Be) and one neutron star accretor. Gas from the decretion disk of the Be star can be accreted by the companion. The interaction of the neutron star with the material in the circumstellar disk leads to transient X-ray activity. This activity is characterized by two type of outbursts. Type I X-ray outbursts are periodic and coincide with periastron passage of the neutron star. These outbursts last for a few days and have typical luminosity of $L_x = 10^{36} - 10^{37} ergs^{-1}$. These outbursts can be produced when the neutron star captures a small fraction of low angular momentum gas at closest approach. Type II X-ray outbursts, although occur less frequently, they have a much larger luminosity of $L_x \geqslant 10^{37} ergs^{-1}$ and last from weeks to months. They don't show any preferred orbital phase and during these type of outbursts the formation of an accretion disk may occur.

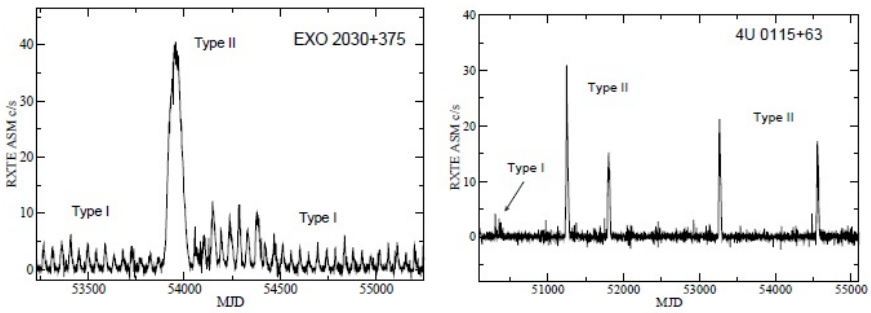

Figure 1.7: Typical light curves for Type I and Type II X-ray outbursts for two sources, EXO 2030+375 (left) and 4U 0115+63 (right). (Reig 2011)

1.10 Aims of the Project

The main goal of this project is to study the long-term optical spectral variability of BeXBs. The main source of variability in this kind of systems comes from the circumstellar disk around the Be star's equator. Since the H_α line is the prime indicator of the state of the disk, we have investigated the evolution of the line spectral parameters over time scales of years. Here we study the correlation between the X-ray activity and the strength of the H_α line, the V/R ratio variations and the relationship between the disk size and the H_α line equivalent width. In this project we used a sample of fourteen objects: 4U 0115+634, IGR J01363+6610, RX J0146.9+6121, IGR J01583+6713, V 0332+530, RX J0440.9+4431, A 0535+262, IGR J06074+2205, XTE J1946+274, KS 1947+300, GRO J2058+42, SAX J2103.5+4545, 4U 2206+54 and SAX J2239.3+6116.

Chapter 2

Observations and Methodology

The data used in this project come mainly from the 1.3 m telescope of the Skinakas observatory and 1.5 m telescope of the Fred Lawrence Whipple Observatory at Mt. Hopkins (Arizona). In addition, I had access to spectra taken in the framework of the University of Valencia/Southampton collaboration project (see e.g Reig et al. 1997). The spectra fom this collaboration were mainly obtained with the 1.0 m Jacobus Kapteyn Telescope (La Palma), are prior to 1998 and have been published in several articles. These data are supplemented with data from a series of telescopes: , 4.2 m William Hershel Telescope (La Palma; service time), and the Liverpool Telescope (La Palma).

2.1 Skinakas Observatory

The 1.3m telescope is the principal observing facility of Skinakas Observatory. It is a modified Ritchey-Chretien telescope that has a hyperbolic primary and a hyperbolic secondary mirror, in order to provide a large field of view with high image quality. There is also an auto guider with off axis guiding system.

Some technical details of the telescope are cited below :

- Aperture of main mirror: 129cm
- Aperture of secondary mirror: 45cm
- Central hole of main mirror: 35cm
- Distance main to secondary: 245.34cm
- Focal length: 985.7cm
- F-ratio: 7.64

Figure 2.1: Skinakas 1.3m telescope.

2.1.1 Focal Reducer and Slit Spectrograph

A Focal Reducer is mounted to the 1.3m telescope and it can be used in two different configurations:
1. In the imaging mode the focal length of the telescope is reduced by a factor of 1.87, enlarging by the same factor the imaged area of the sky on the CCD. A Filter Wheel with 6 filter positions is integrated to the Focal Reducer.

2. In the spectroscopy mode a reflection grating is introduced in the collimator path. Using different gratings, resolutions ranging from 0.57Å/pixel to 4Å/pixel are achievable with a 15μm pixel CCD camera. A Slit Wheel offering six positions with slit widths: 80μm, 160μm, 320μm and 640μm is part of this configuration.

A 2k x 0.8k CCD camera is attached to the slit spectrograph.

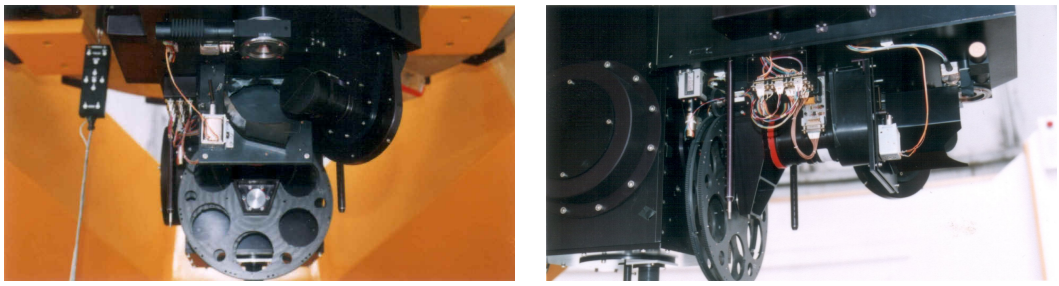

(a) Front View. (b) Side View.

Figure 2.2: Focal Reducer

The gratings of the focal reducer used for observations are given below:

Lines/mm	Zero order blaze wavelength (nm)	Dispersion (Å/nm)
1200	700	76.39
1302	430	70.44
1302	550	70.27

2.1.2 CCD

The CCD (Charge Couple Device) is attached to the slit spectrograph. Some of the characteristics of the camera are listed below:

- Pixel format: 2000 × 800
- Pixel size: 15 micron square
- Image area: 30 mm × 12 mm
- Field of view: 19.6 arcmin × 7.8 arcmin

2.2 Fred Lawrence Whipple Observatory

The Fred Lawrence Whipple Observatory (FLWO) is an astronomical observatory owned and operated by the Smithsonian Astrophysical Observatory (SAO) and is their largest field installation outside of their main site in Cambridge, Massachusetts. It is located near Amado, Arizona on the slopes of Mount Hopkins. FLWO telescopes includes the 1.5m Tillinghast spectroscopic telescope.

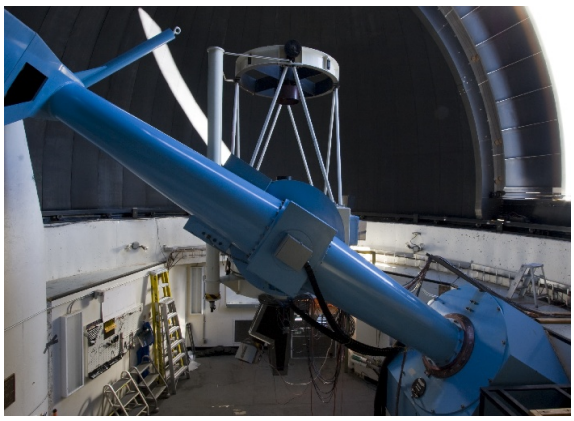

Figure 2.3: FLWO 1.5m Tillinghast spectroscopic telescope.

2.2.1 FAST Spectrograph

FAST is designed to accept gratings with rulings between 300 and 1200 lines per mm in first order. The following table gives the resolutions and spectral coverages for various gratings with a 53 mm long CCD. The spectrograph will vignette at the spectral extremes if a grating with an anamorphic factor exceeding 1.3 is used. This corresponds to a 1200 line grating centered at H_α, so of a 1200 line grating in the extreme red entails a modest loss in efficiency.

Ruling (gpm)	2 Pixel Res (Å)	Spectral Coverage (Å)	2 Pixel Slit Width (arcsec)
300	2.94	4000	1.21
600	1.48	2000	1.25
1200	0.75	1000	1.52

FAST has a conventional plane reflection grating geometry with an off-axis parabolic collimator and a Schmidt camera. The focal length of the collimator is 963mm and the effective focal length of the camera is 328mm, giving a reduction of 2.93, corresponding to a scale of 0.57 arcsec/15μ pixel along the slit. The unvignetted slit length is 3 arcminutes, or 13.72 mm at the slit. The angle between the collimated beams arriving at and leaving the grating is 35°.

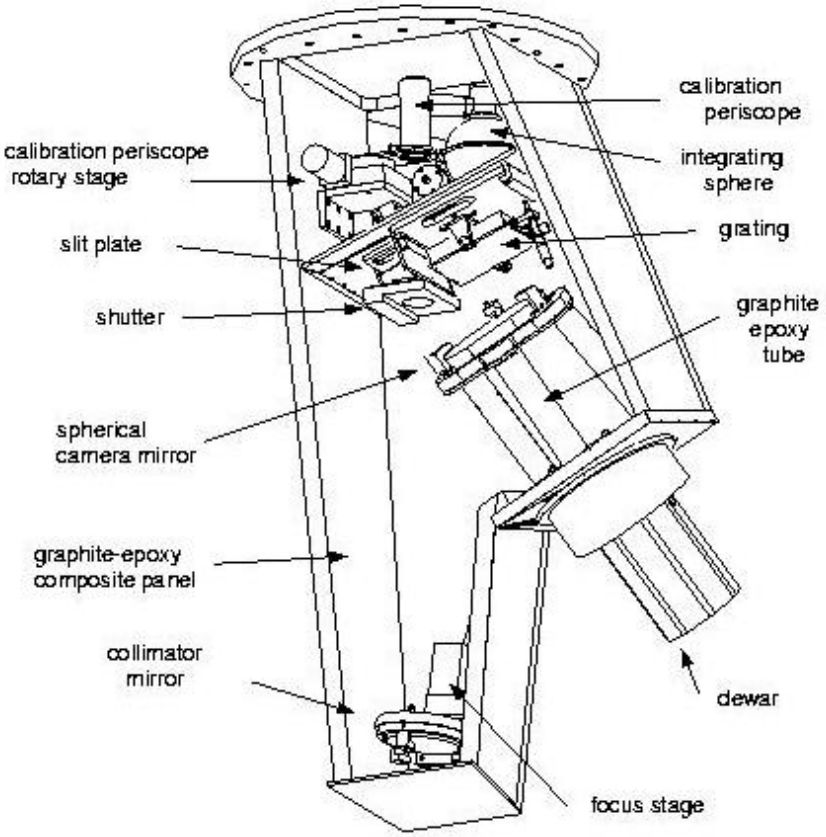

Figure 2.4: FAST spectrograph layout.

2.3 Methodology of the Data Processing

2.3.1 Data Reduction

For this project we used spectra that were already reduced. The data reduction was made by using proper packages of the IRAF[1] project. First, the raw images were BIAS subtracted. BIAS frames are images of zero second exposure time obtained with the telescope's shutter closed. So, the obtained images contain only noise due to the camera electronics. Then, the raw images were FLAT field corrected. This process is used to correct the pixel to pixel variations in the detector. Next we have to extract the spectrum. After we extract the stellar spectra we apply a last correction by subtracting the sky. This is done by measuring the sky spectrum and subtracting it from the images. Last step is the wavelength calibration of the source spectrum. For this process, the spectra of comparison lamps is taken before each exposure.

[1]Image Reduction and Analysis Facility, http://iraf.noao.edu

2.3.2 Data Analysis

The data processing was made by using PyRAF[2]. PyRAF is a command language for running IRAF tasks that is based on Python scripting language. PyRAF gives the ability to run IRAF tasks in an environment that has the power and the flexibility of Python. IRAF is a general Image Reduction and Analysis Facility providing a wide range of image processing tools for the user. IRAF is a product of the National Optical Astronomy Observatories (NOAO) and was developed for the astronomical community although researchers in other scientific fields have found IRAF to be useful for general image processing. For the spectra processing we used IRAF's splot command. Splot provides an interactive facility to display and analyze spectra.

To ensure the homogeneous processing of the spectra, they were normalized with respect the local continuum. Because we are interested in the spectral parameters of the H_α line, the continuum serves as a reference point. The definition of the continuum level is crucial because it represents the main source of uncertainty on the parameters. To normalize the continuum we fit a smooth curve in regions of the continuum devoided of spectral features. This process sets the continuum to 1.0, and allows us to measure the lines from spectrum to spectrum in a consistent way. For the normalization of the spectra we selected 5 different regions of the continuum near the H_α line profile, and two different functions to be fit to the spectra, i.e. 10 different fits for the continuum. The functions we used are chebyshev and legendre polynomials both of order 5.

To calculate the spectral line parameters we fit one or more line profiles to the data. This is done by using IRAF's deblending command. Deblending is a multi step process in splot. There are three different profiles that we can select to fit to our data:

- Gaussian
- Lorentzian
- Voigt

We test each of these profiles to a small portion of our data, and we conclude that the best option out of these three profiles was the Gaussian. From the Gaussian profile we measure the wavelength of the center or centers of the H_α line, the full width at half maximum and the equivalent width. If the line shows a split profile we fit two Gaussians. In some spectra the absorption between the two peaks is so pronounced that a third Gaussian (in absorption) is required to obtain a good fit.

[2]PyRAF is part of the stsci_python package of astronomical data analysis tools and is a product of the Science Software Branch at the Space Telescope Science Institute, http://www.stsci.edu/institute/software_hardware/pyraf/

2.4 Spectral Line Parameters

2.4.1 FWHM

Full Width at Half Maximum (FWHM) is the width measured at half level between the continuum and the peak of the line. The FWHM is expressed either in wavelength unit or in speed unit when the objective is to measure expansion or disk speeds. FWHM is used to investigate the broadening in the disk. The FWHM of the H_α emission lines are determined by the effective velocity of the envelope which are emitting a significant fraction of the H_α radiation (Zamanov et al. 2001).

2.4.2 Peak Separation

Peak separation is defined as the difference between the central wavelengths of the red minus the blue peak in velocity units ΔV.

$$\Delta V = \frac{\Delta\lambda}{\lambda} \times c \ \ (km/s) \tag{2.1}$$

where c is the speed of light, $\Delta\lambda$ is the difference between the central wavelengths of the red minus the blue peak and λ is the wavelength of the H_α line (6563Å).

2.4.3 Equivalent Width

Equivalent width (EW) is defined as the area of a surface counted between the level of the continuum, normalized to unity, and with reference zero, having a surface identical to the profile line. The equivalent width is measured in wavelength units (Å).

To measure the EW in IRAF we need to select two wavelengths that include the entire H_α line. These wavelengths may vary due to the different shapes and widths, not only among different sources but also in the same source. So we compute them by using the full width at half maximum (FWHM) of the Gaussian fit profile. If the Gaussian profile has two components we use the relations

$$\begin{aligned} \lambda_s &= \lambda - 2.5 * (FWHM\,V) \\ \lambda_f &= \lambda + 2.5 * (FWHM\,R) \end{aligned} \tag{2.2}$$

where λ_S and λ_f are the wavelengths near the start and the end of the line, FWHM V and FWHM R are the full width at half maximum of the V and R component of the Gaussian profile, and λ is the wavelength of the H_α line (6563Å).

If the Gaussian profile has one component then we simply use the FWHM of the line

$$\begin{aligned} \lambda_s &= \lambda - 2.5 * (FWHM) \\ \lambda_f &= \lambda + 2.5 * (FWHM) \end{aligned} \tag{2.3}$$

The factor 2.5 is somehow arbitrary but was chosen after numerous trials on different spectra and different sources.

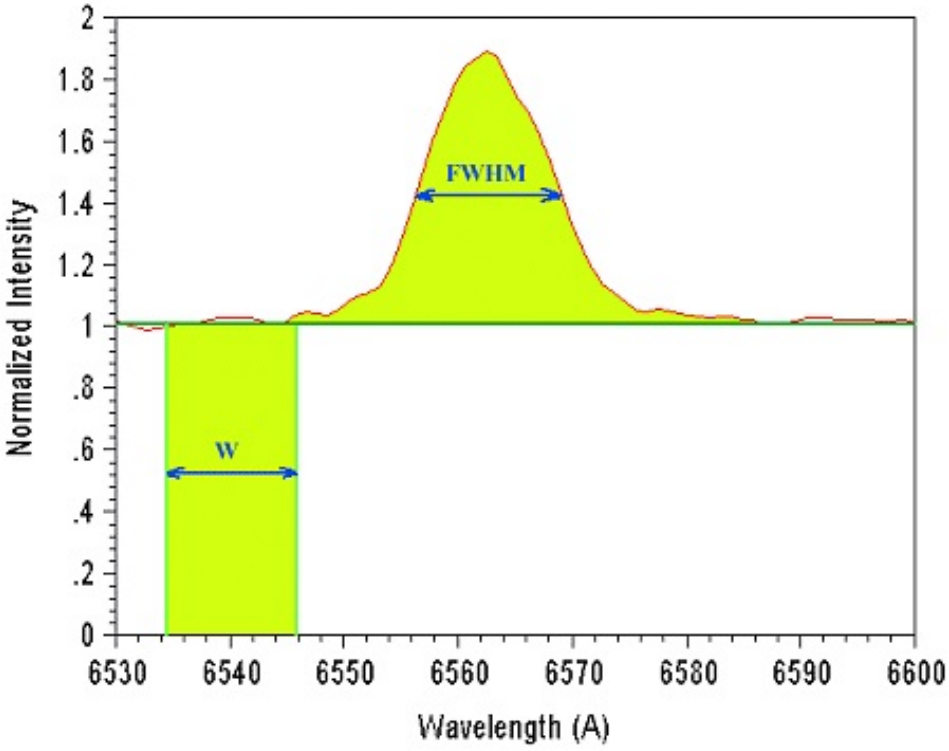

Figure 2.5: Equivalent width and full width at half maximum definitions (http://www.astrosurf.com/buil/us/spe2/hresol7.htm).

2.4.4 V/R Ratio

The ratio V/R, i.e. the ratio of the violet-to-red emission peaks, is used as one of the main characteristics describing the asymmetry of the double-peak emission lines of Be stars (Stefl et al 2007). The majority of the Be stars, both single and binary, show long-term variations of V/R ratio of H_α emission line, as well as for other lines like He_{II} and Fe_{II}. The V/R ratio represents also the measure of the asymmetry of the line profile. For convenience it is common to use the logarithm of this ratio.

2.4.5 Error Estimation

To calculate the quantities needed for this project, we took the average of ten measurements for different definition of the continuum.

$$\overline{x} = \frac{\sum x_i}{N} \tag{2.4}$$

To estimate the error for the values of the EW and the core intensity of the blue (V) and red peaks (R) we used the standard deviation.

$$S = \sqrt{\frac{\sum (\overline{x} - x_i)^2}{N - 1}} \tag{2.5}$$

Then by using the error propagation method we calculated the errors for the logarithm of the ratio V/R and the Peak Separation (ΔV).

$$\delta y = \sqrt{\sum \left(\frac{\partial y}{\partial x_i} * \delta x_i \right)^2} \tag{2.6}$$

The error for the logarithm of the ratio V/R is given by the resulting equation

$$\delta \left(log \frac{V}{R} \right) = \frac{1}{ln10} * \frac{R}{V} * \delta \left(\frac{V}{R} \right) \tag{2.7}$$

where

$$\delta \left(\frac{V}{R} \right) = \sqrt{\left(\frac{1}{R} * \delta V \right)^2 + \left(\frac{V}{R^2} * \delta R \right)^2} \tag{2.8}$$

The estimated error for the Peak Separation (ΔV) is given by the following equation

$$\delta \left(\Delta V \right) = \frac{c}{\lambda} * \sqrt{\left(\delta \lambda_V \right)^2 + \left(\delta \lambda_R \right)^2} \tag{2.9}$$

2.5 Disk Radius Determination

For rotationally dominated double peak profiles, the ratio $\Delta V/(2vsini)$ can be considered as a measure for the outer radius of the H_α emitting disk, R_H, Huang (1972):

$$\frac{\Delta V}{2vsini} = \left(\frac{R_H}{R_*} \right)^{-j} \tag{2.10}$$

where v and R_* are the stellar rotational velocity and radius, and j indicates the type of the disk rotation. $j = 0.5$ when the disk rotation is Keplerian and $j = 1$ for conservation of angular momentum. In the case of Keplerian rotation, the rotational velocity at the equator is given by

$$v_{rot} = \left(\frac{2GM_*}{R_*} \right)^{1/2} \tag{2.11}$$

If we plot the logarithm of normalized peak separation, $\Delta V/(2vsini)$, against log(-EW/Å), we notice that these two parameters are correlated. Hanuschik (1988) have derived the law

$$log \left(\frac{\Delta V}{2vsini} \right) = \frac{-j}{2} log \left(\frac{-EW(H_\alpha)}{\text{Å}} \right) + j \, log \left(\frac{N_e}{cm^{-3}} \right) \tag{2.12}$$

From the slope of this equation we can derive the value of j and thus we can conclude if the disk rotation is Keplerian or not.

Chapter 3

Results

In this chapter we present the results of the spectral analysis. We study the variability in the shape and strength of the H_α on timescale of years for fourteen different sources. We have measured the following spectral line parameters: centers λ_c, full width at half maximum (FWHM), peak intensities and equivalent width (EW). From these quantities we derived the peak separation ΔV and the ratio V/R. As mentioned in Chapter 1 the H_α line gives information about the conditions of the disk. Thus, by monitoring the H_α line we expect to understand the evolution of the disk. Table [3.1] gives the studied sources and some of their characteristics. In this chapter we also present some characteristic H_α line profiles for each source. The complete sample of the line profiles can be found in the Appendix.

Table 3.1: List of sources.

X-ray name	Optical name	Spectral type	v sin i (km s^{-1})	Radius ($R_\odot$)	Mass ($M_\odot$)	P_{orb} (d)	e	periastron ($R_\odot$)
4U 0115+634	V635 Cas	B0.2Ve	300 ± 50	8.3(1)	16(3)	24.3	0.34	60.4
IGR J01363+6610	–	B1Ve	–	6.3(2)	–	–	–	–
RX J0146.9+6121	LS I +61 235	B1Ve	200 ± 30	6.3(2)	–	330	–	–
IGR J01583+6713	–	B2IVe	–	–	–	–	–	–
V 0332+53	BQ Cam	O8.5Ve	< 150	8.8(1)	20(1)	34.3	0.3	86.4
RX J0440.9+4431	LS V +44 17	B0.2Ve	235 ± 15	8.3(1)	18(3)	130	–	–
1A 0535+262	V725 Tau	O9.7IIIe	225 ± 10	14.7(1)	20(3)	111	0.47	143.1
IGR J06074+2205	–	B0.5Ve	260 ± 20	8.0(1)	18(1)	–	–	–
XTE J1946+274	–	B0-1IV-Ve	–	8.0(1)	18(1)	169.2	0.33	231.9
KS 1947+300	–	B0Ve	–	8.3(1)	18(1)	40.4	0.03	129.2
GRO J2058+42	–	O9.5-B0IV-Ve	242 ± 51	8.5(1)	12(1)	110	–	–
SAX 2103.5+4545	–	B0V	240 ± 20	8.3(1)	18(1)	12.7	0.4	36.9
4U 2206+54	BD+53 2790	O9.5Ve	300 ± 40	8.5(1)	12(1)	9.5	0.3	31.4
SAX J2239.3+6116	–	B0-2III-Ve	–	6.8(2)	–	262.6	–	–

The radius of the companion star is determined from its spectral type and it is taken from (1)Vacca et al. (1996);(2)Moon et al. (1985);(3)Okazaki & Negueruela (2001).

3.1 4U 0115+634

4U 0115+634 is a recurrent hard X-ray transient system and is one of the BeXB that has been studied in great detail. The optical companion is a B0.2Ve star, V635 Cas, with an orbital period of 24.3 days. The distance of the system 4U 0115+63 is estimated to be 8 kpc (Negueruela & Okazaki 2001). The neutron star is in an eccentric orbit (0.34) around the Be star. The Be star is surrounded by a disk of relatively cool material, which gives rise to emission lines in the optical and infrared spectral regions. The hard X-ray emission is due to the accretion disk around the neutron star companion (Negueruela & Okazaki 2001). The source was detected in August 1969 by the Vella 5B satellite as three small outbursts separated by 180 days. Since then 17 outbursts have been reported. The most rescent X-ray outbursts were observed by Swift/BAT Hard X-ray transient monitor, one in April 2008 and the other in June 2011.

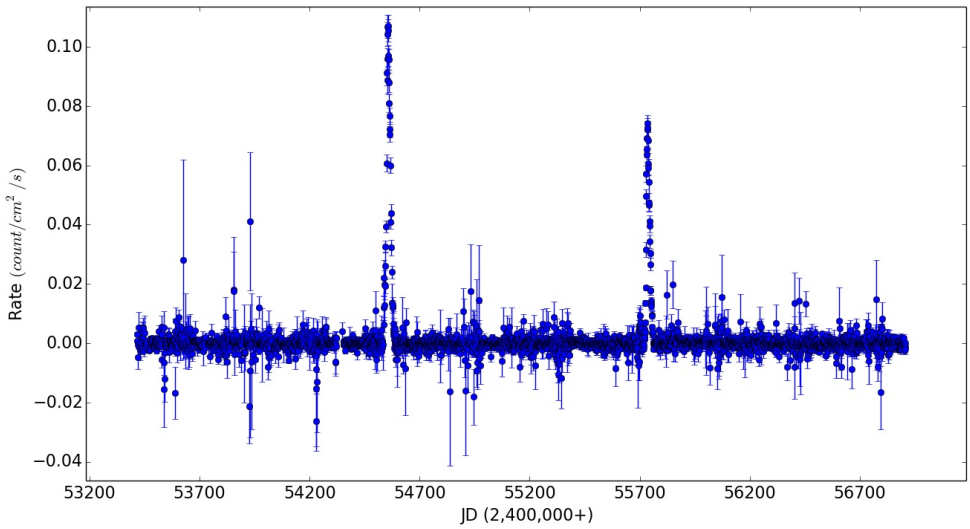

Figure 3.1: X-ray outburst light curve for the source 4U 0115+634 from the Swift/BAT X-ray transient monitor.

Variability of the H_α Parameters

The monitoring of 4U 0115+634 shows high variability of the H_α emission line, both in strength and shape. Figure [3.2] displays the variability of the equivalent width EW(H_α), the V/R ratio and the disk size in the time interval 1990-2014.

The second panel of figure [3.2] shows the variability of the ratio of the relative fluxes at the blue and red emission peak maxima. V/R variability is clearly seen, indicating that the structure of the equatorial disk is changing on timescales of years. The emission line profile of the $H\alpha$ shows both symmetric and asymmetric as well as single and double peak profiles. Asymmetric line profiles are associated with intermediate values of EW while symmetric line profiles are associated with higher

values of EW (Reig et al. 2007). In the time interval JD48252 - JD49340 we track two V/R cycles with quasi-periods $\sim$ 750d and $\sim$ 335d and $|log(V/R)| < 0.4$.

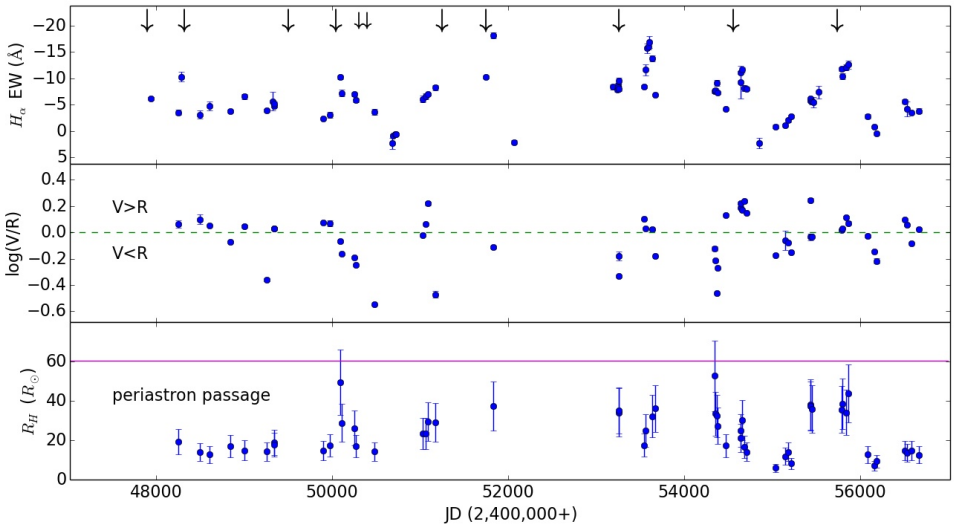

Figure 3.2: Long-term variability of the equivalent width EW(H_α), the V/R ratio and the calculated radius of the H_α emitting circumstellar disk for the source 4U 0115+634. The big arrows in the upper panel correspond to peak times of type II X-ray outbursts and the smaller ones to peak times of type I X-ray outbursts. The line in the lower panel indicates the periastron passage of the neutron star.

In our observations, EW of 4U 0115+634 varies in the interval -18.7 - 2.4Å, with average $\overline{EW} = -6.5$Å, and standard deviation of the mean $\sigma(EW) = 4.4$Å. Negative values of EW(H_α) indicates that the line displays an emission profile. In the earliest measurements the system underwent two type II X-ray outbursts, one in February 1990 (JD47900) and another in March 1991 (JD48320). After the first outburst EW decreased from -6.2 to -3.5Å in a timescale of ten months. Then it started to increase again and reached a peak (-10.3Å) in January 1991 (JD48280). In the following five years (JD48320 - JD50090) the disk was apparently in a disk-growth phase reaching a maximum of $50R_\odot$. In December 1995 (JD50040) a type II outburst observed. Following this outburst, EW as well as the disk radius started to decline. On the other hand, we observe that during the same period $|log(V/R)|$ increased.

In August 1997 (JD50683), EW was positive which means that the line displayed an absorption profile and reached its lowest value (2.4Å). In September 1997 EW increased from 0.8 to -18Å three years later (JD50695 - JD51833). The increase of EW suggests also the increase of the disk size, which we can clearly see in the lower panel of figure [3.2]. In that period of time we also notice that the disk reaches another maximum of $37.4R_\odot$. By the time EW reached that maximum, the system was already undergone two type II X-ray outbursts, the first in March 1999 (JD51250) and the second in August 2000 (JD51750). Soon after the second outburst the disk underwent a disk-loss episode. In July 2004 (JD53193) EW increased yet again, suggesting the formation of a new circumstellar disk. In September 2004

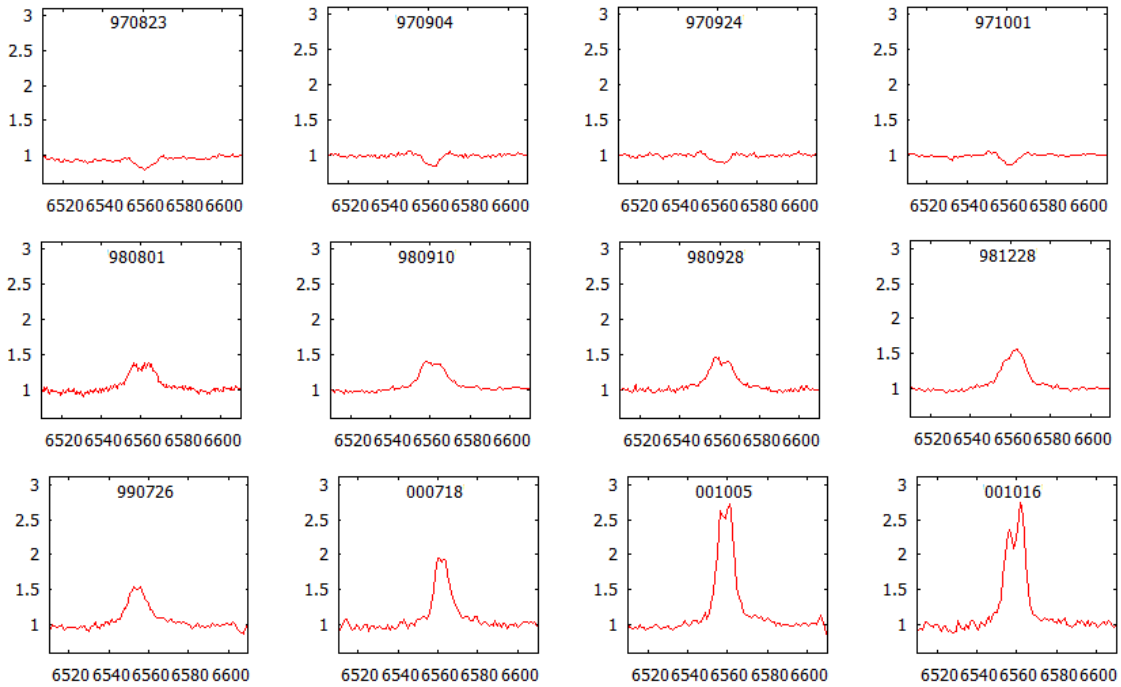

Figure 3.3: H_α line evolution from August 1997 to October 2000 (JD50683 - JD51840

(JD53260) the system underwent another X-ray outburst. In August 2005 (JD53600) the disk is in a disk-growth phase and the EW reaches a new peak at -16.9Å, and then drops off to -6.9Å in the timescale of two months. In September 2007 (JD54348) the disk reached sizes up to periastron passage. Then 4U 0115+634 underwent a type II X-ray outburst which peaked in April 2008 (JD54560). Following this outburst the disk started to decline and so did the EW reaching a new minimum at 2.3Å in January 2009 (JD54856). Ten months later the disk entered a new growth cycle, and during this phase the system underwent another X-ray outburst in June 2011 (JD55260). Since then the disk remains in a low state.

3.2 IGR J01363+6610

IGR J01363+6610 was discovered during INTEGRAL observations on April 19 2004 but was not detected 2 weeks later, indicating that the source is transient. IGR J01363+6610 was observed by XMM - Newton on July 31 2009 and confirmed as a Be X-ray binary with very low quiescent X-ray luminosity (Tomsick et al. 2011).

Variability of the H_α Parameters

IGR J01363+6610 is characterized by its strong H_α emission line profiles. V/R variability is absent because the emission lines are symmetric and single peaked. Through the time period that we monitor this source, the lines hardly change in strength. The strong emission lines suggest the existence of a very large (or dense) circumstellar disk around the Be star.

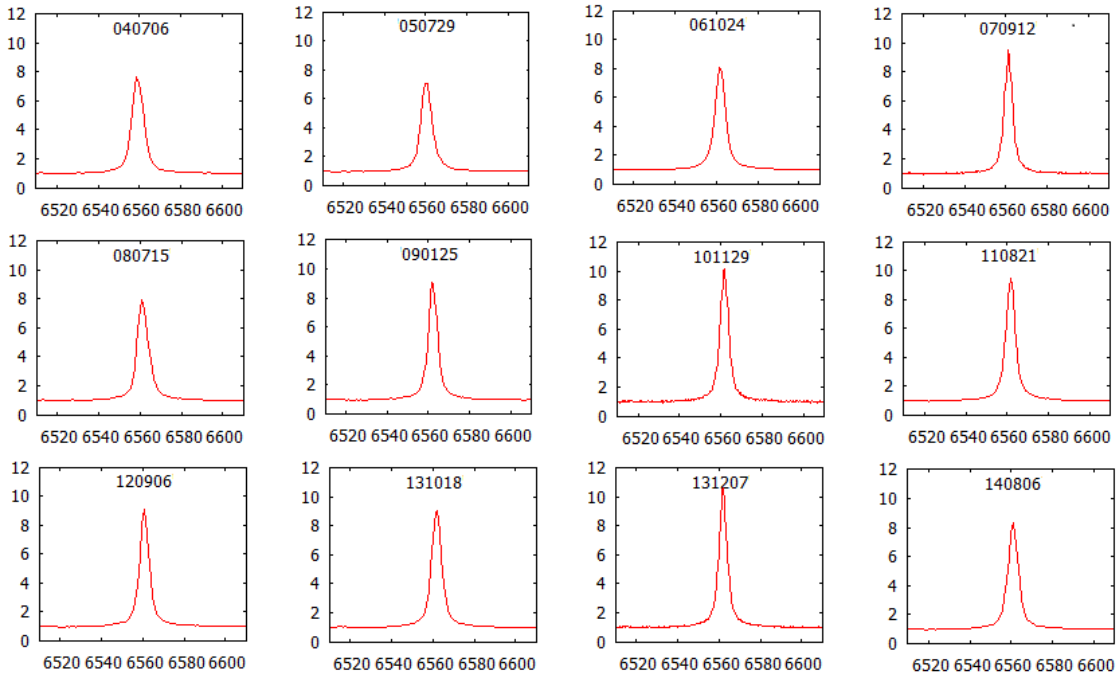

Figure 3.4: Characteristic H_α emission lines of the source IGR J01363+6610.

Figure [3.5] shows the evolution of EW with time. EW varies from -56 to -46Å, with average $\overline{EW} = -50.7$Å, and standard deviation of the mean $\sigma(EW) = 2.5$Å.

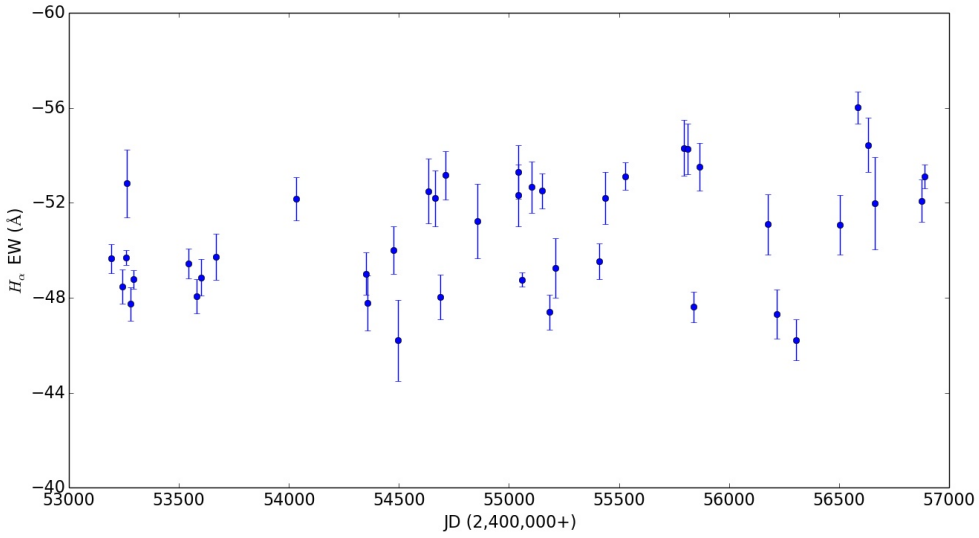

Figure 3.5: Long-term variability of the equivalent width EW(H_α) for the source IGR J01363+6610.

3.3 RX J0146.9+6121

The X-ray source RX J0146.9+6121 was discovered by Motch et al.(1991) from the ROSAT all-sky survey. Subsequently, they observed H_α emission in the optical counterpart LSI +61235, which confirms the source as BeX. RX J0146.9+6121 is a persistent low-luminosity BeX with low X-ray variability ($L_{max}/L_{min} \leqslant 10$) and it contains the slowest X-ray pulsar known with pulse period 1400s (Reig & Roche 1999). The orbital period of the binary system is about 330d (Sarty et al. 2008). The Be decretion disk of LSI +61235 has been intensively studied through the investigation of V/R variations in H_α emission line. The V/R variation of the H_α line correlates with long-term changes in H_α EW intensity.

Variability of the H_α Parameters

We monitor the BeXB RX J0146.9+6121 from August 1991 to December 2013 (JD48496 - JD56633). The H_α line has both single and double peak as well as symmetric and asymmetric profiles. From the second panel of figure [3.6] we can clearly notice that the V/R ratio is periodic. The variability in the V/R ratio indicates the existence of an one-armed density structure in the equatorial disk of the primary star.

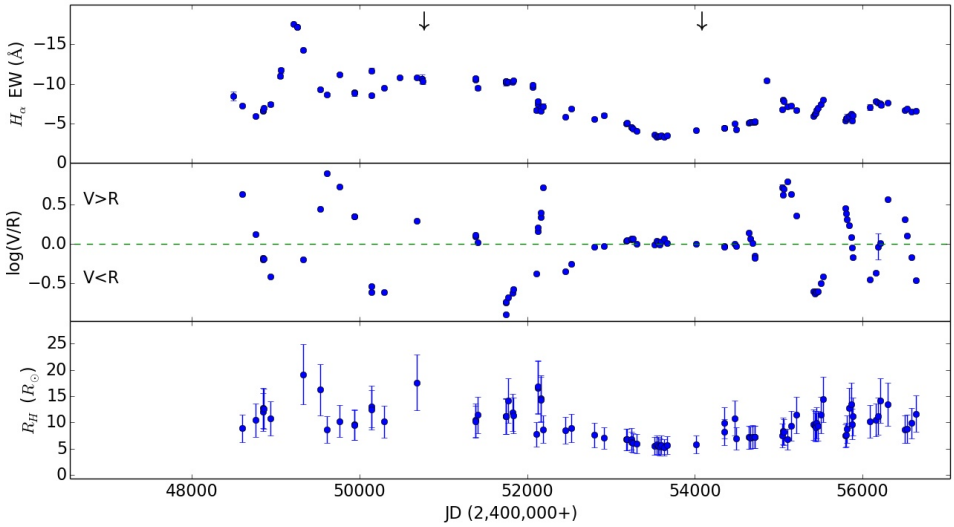

Figure 3.6: Long-term variability of the equivalent width EW(H_α), the V/R ratio and the disk radius R_H for the source RX J0146.9+6121. The arrows correspond to peak times of X-ray activity.

We monitor three cycles of the V/R variability from December 1991 to October 2001 (JD48603 - JD52190). By using the Lombe-Scargle (LS) periodogram (Lombe 1976; Scargle 1982) we searched for the V/R cycle quasi-period in this time interval and we found a period of 1300 days, with p-value 1.7E-06. In September 2002 the line intensity was reduced drastically and remained in this weak state for six years (JD52527 - JD54712). This phase coincides with the time when the disk was in a

low state. In January 2009 (JD54856) began a new V/R cycle with the line intensity returning to its previous state. We monitor two new V/R cycles in the time interval JD55042 - JD56303. From the LS periodogram we get a period of 636 days, with p-value < 0.001.

EW shows extreme variability through the studied time interval. It varies from -17.6 to -3.2Å and has a mean value of -7.5Å. In the earliest measurements EW is decreasing, reaching a minimum on May 18 1992 (JD48760) and 15 months later on August 11 1993 EW reaches a maximum at -17.6Å. The size of the disk follows the same evolution, reaching a maximum at $20R_{\odot}$. In September 1993 (JD49253) EW started to decline and for the next four years varied in the interval -12 - -8.5Å. In November 1997 (JD50769) we observe an increase of X-ray activity for which there is no optical coverage.

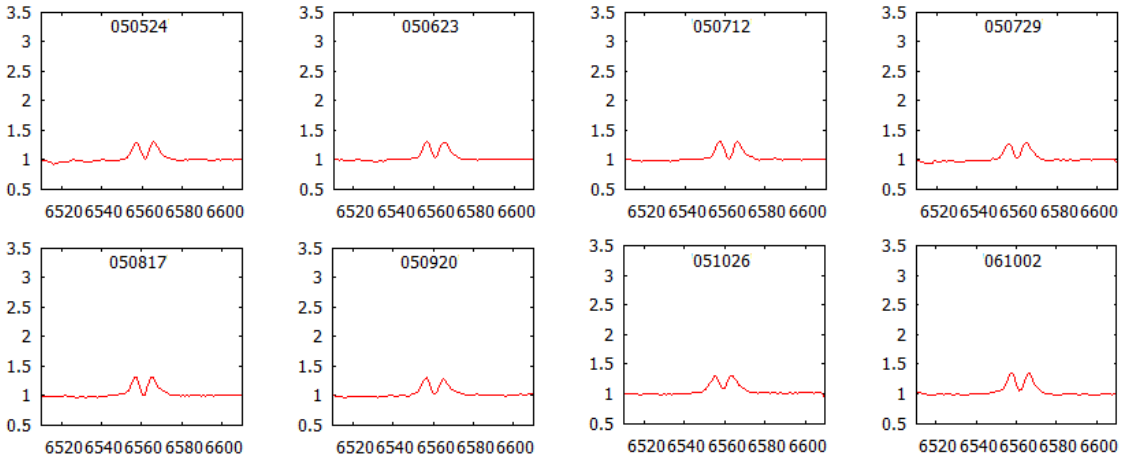

Figure 3.7: H_{α} line evolution from May 2005 to October 2006 (JD53514 - JD54010).

The system seems to be in a steady state from July to October 2000 (JD51740 - JD51830). After this phase EW drops off gradually, and reaches a minimum (-3.2Å) on June 23 2005 (JD53544). The disk radius is also in decay reaching a minimum at $6R_{\odot}$. In October 2005 (JD53669) EW starts to increase again, suggesting the formation of a new disk and at $\sim$ JD54100 the system entered a new phase of X-ray activity.

In January 2009 (JD54856) EW reaches a new peak at -10.4Å. In the following four years EW varies in the interval -8 - -5Å, and the disk radius changes in the interval 7 - $14R_{\odot}$.

3.4 IGR J01583+6713

The X-ray transient IGR J01583+6713 was discovered by INTEGRAL/IBIS hard X-ray surveys on December 6 2005. The source was detected with a mean flux of about 14 mCrab in the 20-40 keV band. After the outburst, the flux of IGR J01583+6713 decreased and could not be detected by IBIS after December 10 2005. Optical observations have provided evidence that it is a high mass X-ray binary (Wang 2010).

Variability of the H_α Parameters

As with IGR J01363+6610, the emission lines of IGR J01583+6713 are strong, symmetric and they have a single peak profile. Therefore, V/R variability is absent and we cannot estimate the size of the disk . Our data covers a time period of 3000 days with a sample frequency of 1 spectra every 3 months, from October 2006 to August 2014 (JD54032 - JD56875).

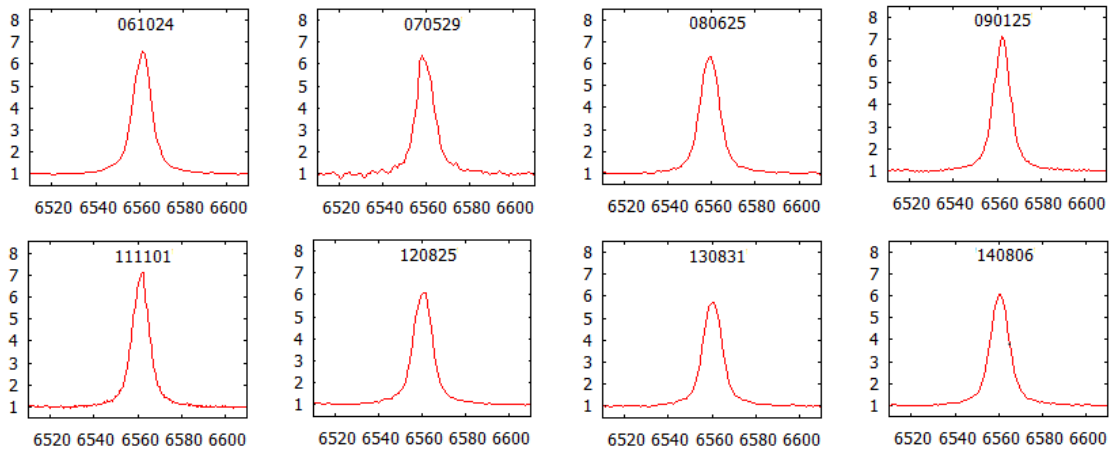

Figure 3.8: Typical H_α emission lines of the source IGR J01583+6713.

Figure [3.9] shows how EW changes with time. EW has a maximum at -72Å and a minimum at -58Å, remaining fairly constant with average $\overline{EW} = -61.5$Å and standard deviation of the mean $\sigma(EW) = 2.7$Å.

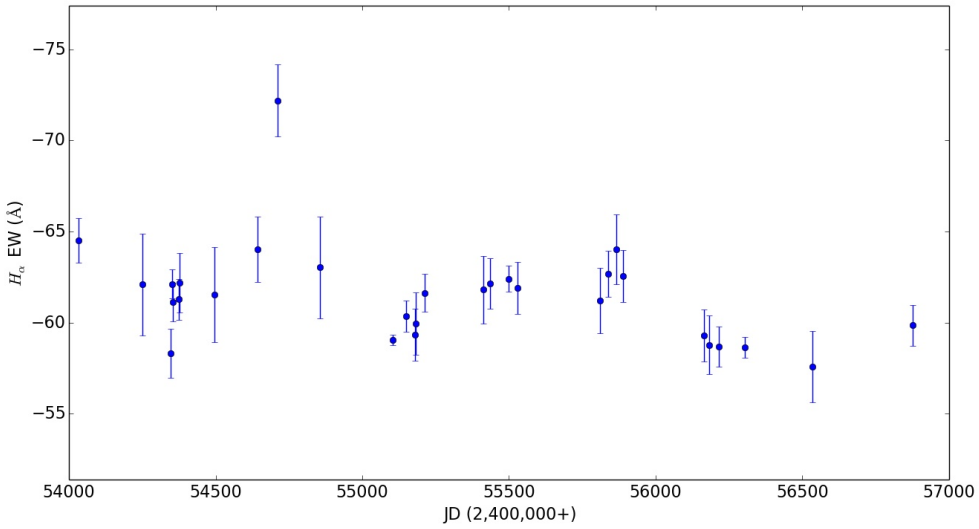

Figure 3.9: Long-term variability of the equivalent width EW(H_α) for the source IGR J01583+6713.

3.5 V 0332+53

V 0332+53 is a hard X-ray transient with a quiescent X-ray state. After 15 years of quiescence the BeX binary V 0332+53 underwent a giant outburst in December 2004 which lasted until January 2005. After that outburst, SWIFT/BAT mission observed two X-ray outbursts one in August 2008 and another in January 2010.

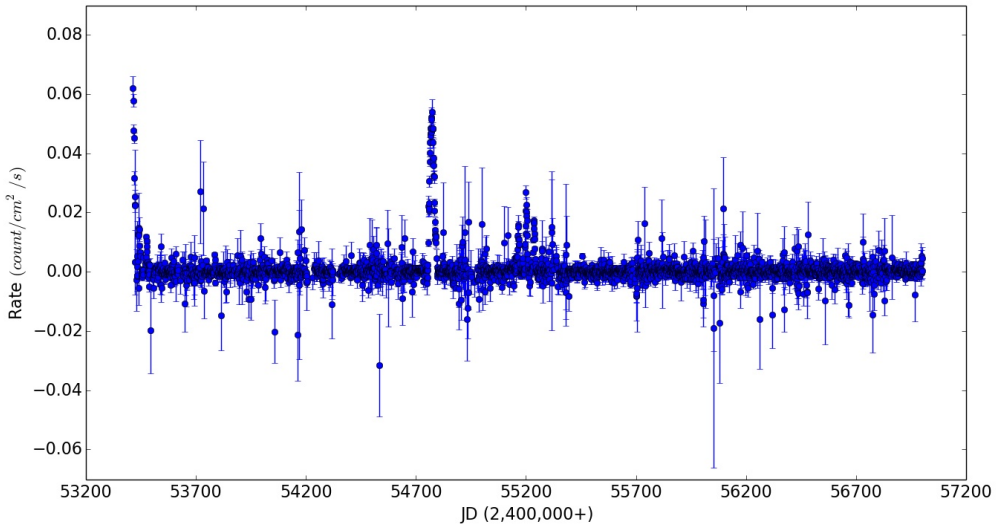

Figure 3.10: X-ray outburst light curve for the source V 0332+53 from the Swift/BAT X-ray transient monitor.

EXOSAT observations observations resulted in the discovery of X-ray pulsations with spin period 4.4s and the determination of the orbital parameters, $P_{orb} = 34.3d$ and e = 0.3 (Stella et al. 1985). The optical counterpart of V 0332+53 is BQ Cam and is an O8-9 Ve star at a distance of around 7 kpc, showing H_α emission and strong variable infrared emission (Bernacca et al. 1984;Negueruela et al. 1999).

Variability of the H_α Parameters

Our data cover V 0332+53 for almost 24 years, from January 1990 to August 2014 (JD47919 - JD56875), although there is an eight year gap between December 1991 and July 2000 (JD48604 - JD51744). Most of the time the emission line is symmetric and of low intensity. The average of EW is -5.6Å with standard deviation of the mean $\sigma(EW) = 1.2$Å. EW varies in the interval -8.3 to -2.5Å.

From figure [3.12] we notice that when the system underwent a giant type II X-ray outburst in January 2005 (JD53414), EW had reached a maximum on October 25 2004 (JD53303). Following this outburst the EW was decreased and after almost two years reached a new peak in October 2006 (JD54032). Another type II X-ray outburst occur when the EW was in a low state in August 2008. After that EW increased and reached a new peak in December 2009 (JD55183) and it was followed by another outburst in January 2010 (JD55200). Since then EW remains in a steady state, and in an X-ray quiescence.

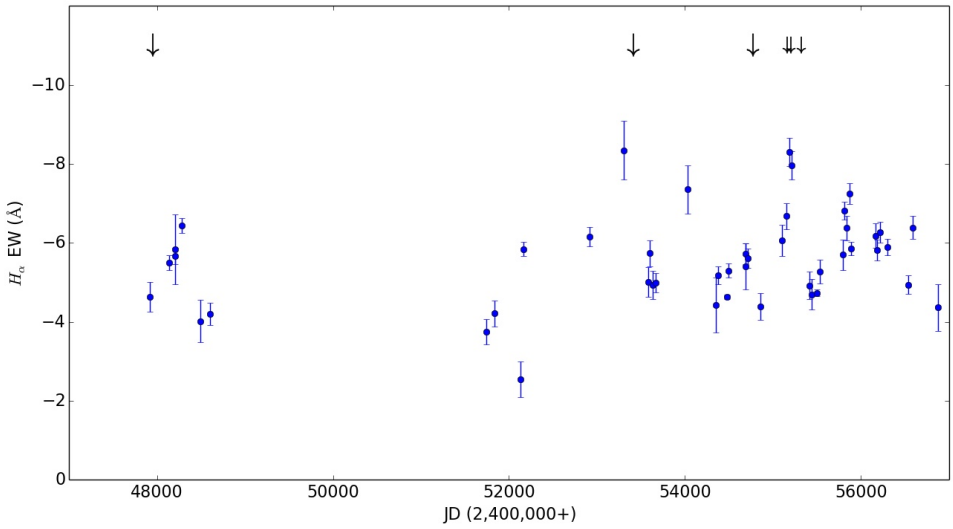

Figure 3.11: Long-term variability of the equivalent width EW(H_α) for the source V 0332+53. The big arrows correspond to peak times of type II X-ray outbursts and the smaller ones correspond to peak times of type I X-ray outbursts.

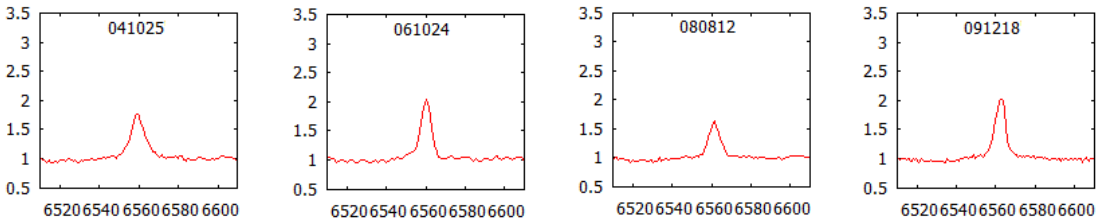

Figure 3.12: H_α emission lines before or after the occurrence of an X-ray outburst in the system V 0332+53.

3.6 RX J0440.9+4431

LS V +4417 is a bright star (V=10.8) of spectral type B_0 that is associated with the X-ray source RX J0440.9+4431. LS V +4417/RX J0440.9+4431 belongs to the subgroup of high mass X-ray binaries and was classified by Reig & Roche (1999) as one of the rare persistent neutron star Be/X-ray binaries. The distance of this source was estimated at 3.3 ± 0.5 kpc by Reig et al. (2005).

The first observed X-ray outburst observed from RX J0440.9+4431, was detected on March 26 2010. The Swift/BAT light curve showed that the source reached a peak luminosity of about 200 mCrab (15-150 keV). After a period of four months, a second outburst was detected on September 1 2010. These two intense X-ray emission episodes showed the typical properties of the type I outbursts, usually displayed when the neutron star in a BeXB approaches the system periastron and interacts with the companion's equatorial disk.

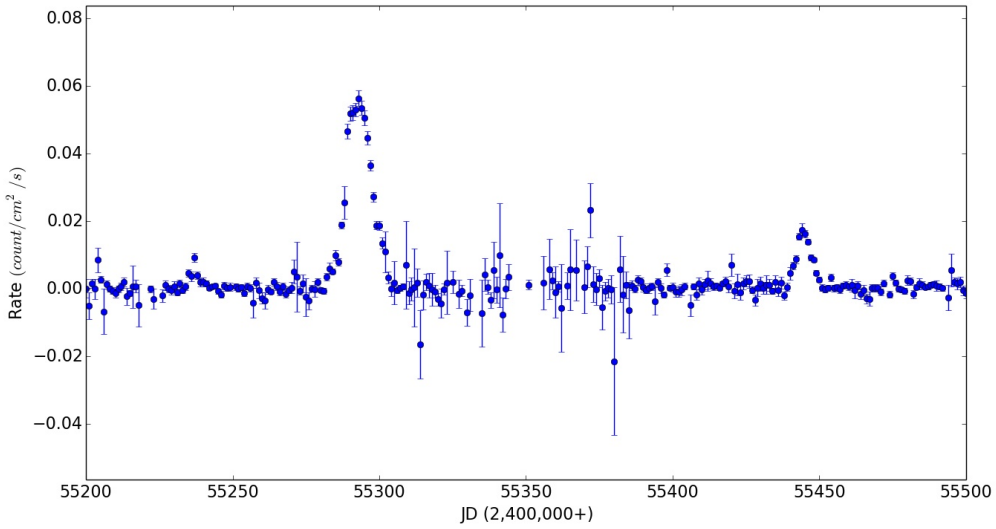

Figure 3.13: X-ray outburst light curve for the source RX J0440.9+4431 from the Swift/BAT X-ray transient monitor.

Variability of the H_α Parameters

We have monitored the BeXB RX J0440.9+4431 for eighteen years, from November 1995 to December 2013 (JD50050 - JD56633). Figure [3.14] shows the evolution of the H_α profile throughout the period covered by our observations. Double peak profiles, both symmetric and asymmetric are always present in this binary. By excluding the first two spectra the V/R ratio hardly changed over 10 years, which suggests that the density wave in the circumstellar disk gradually faded away (Reig et al. 2005). On January 25 2009 (JD54856) RX J0440.9+4431 entered a period of high V/R intensity which lasted over three years. This sudden behavior of the V/R ratio coincides with a major increase in size of the disk and X-ray activity. During the time interval JD55056 - JD55529 we track two V/R cycles with quasi-periods of $\sim$ 470d and $\sim$ 370d, and the log(V/R) of the lines varied from 0.2 to -0.5. In September 2012 (JD56184) the system returned to a low state variability with $|log(V/R)| < 0.05$.

In the earliest measurements EW(H_α) and the disk size seems to be steady, but in the time interval JD50750 - JD52130 we can clearly see the gradual decay both of the EW and the disk radius. EW has a minimum value of -0.03Å on August 7 2001 (JD52128). During this period EW remained always negative which suggests that the primary star didn't lost completely its disk ($5.5R_\odot$). Then EW increases slightly for three years and on October 5 2005 (JD53648) had a second minimum at -3Å. After that the EW increases continuously and has a maximum of -12.2Å on August 02 2010 (JD55410), which coincides with the period where the X-ray outbursts from the neutron star were observed by the Swift/BAT. After the second outburst in September 1 2010 (JD55440) EW starts gradually to decline reaching a minimum on August 30 2013 (JD56534). The disk size follows exact the same evolution of EW.

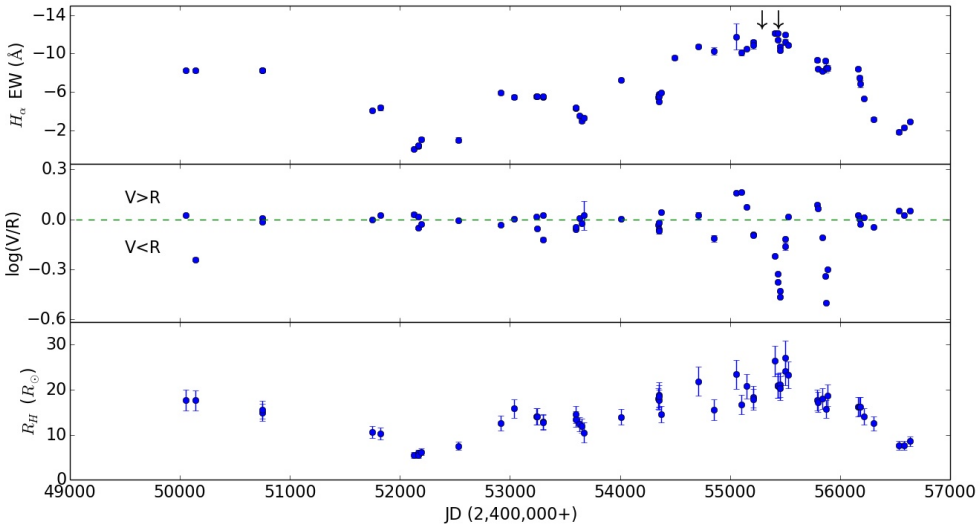

Figure 3.14: Long-term variability of the equivalent width EW(H_α), the V/R ratio and the calculated radius of the H_α emitting circumstellar disk for the source RX J0440.9+4431. The arrows in the upper panel correspond to peak times of X-ray outbursts.

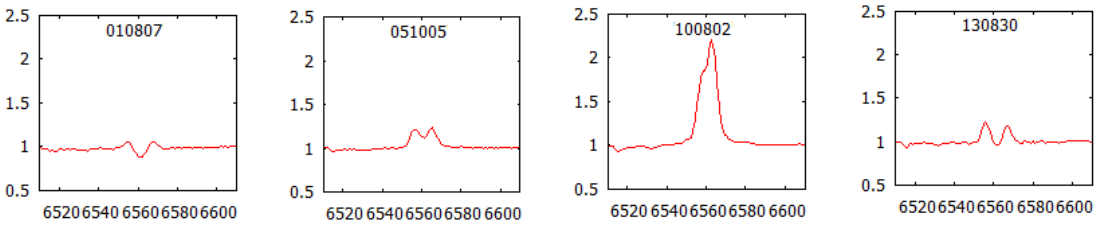

Figure 3.15: Characteristic H_α emission lines of the source RX J0440.9+4431. EW reaches a minimum on August 7 2001, October 5 2005, August 30 2013 and a maximum on August 02 2010.

3.7 1A 0535+262

1A 0535+262 is one of the best studied BeXB transient. The source was discovered by Ariel V satellite during a type II outburst. The system is associated with an O9.7III primary star (V727 Tau) and an X-ray pulsar in orbit around the primary (Steele et al. 1998). Orbital measurements of the binary system reveal an orbital period of 111d, a pulse period of 103.4d and an eccentricity of 0.47 (Finger et al. 1996). The system 1A 0535+262 is at a distance of 2kpc. 1A 0535+262 underwent its first outburst after a ten year quiescence X-ray state, which peaked at May/June 2005 and reached a flux of 4.5 Crab at 30 keV. This outburst was followed by two type I outbursts. The system had already begun undergoing X-ray activity, with a series of type I outbursts starting at JD54612 (May 2008). In December 2009 the system underwent a type II outburst with peak flux around 5.3 Crab in the energy range 15-50 keV which was followed by a series of type I outbursts. In February

2011 the system underwent another type II outburst with peak flux 3.1 Crab in the range 15-50 keV, and since then 1A 0535+262 has been in quiescence.

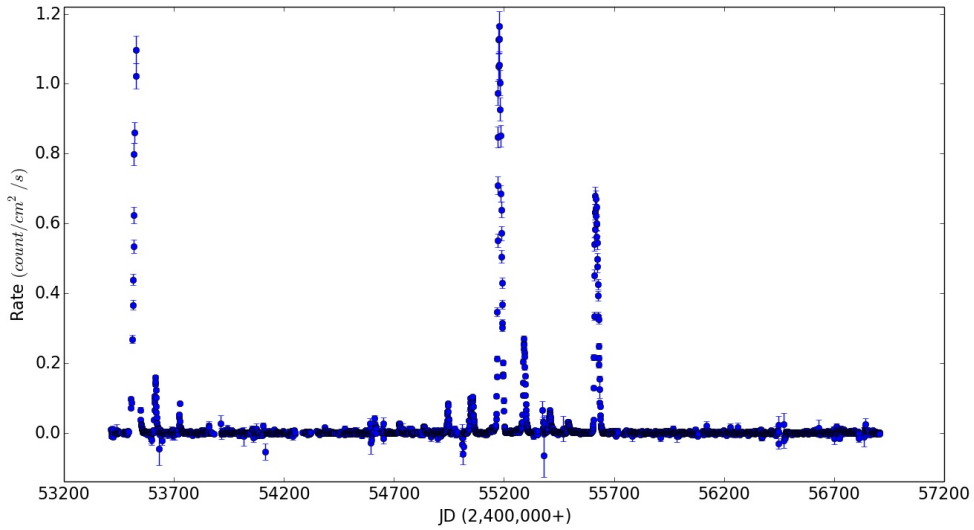

Figure 3.16: X-ray outburst light curve for the source 1A 0535+262 from the Swift/BAT X-ray transient monitor.

Variability of the H_α Parameters

We have monitored the behavior of the H_α emission line for the source 1A 0535+262 from December 1987 to January 2013. Figure [3.17] presents the long-term variability of the H_α parameters (EW, V/R ratio, disk radius). The line profile presents a diversity in shape and strength. It has both symmetric and asymmetric as well as single and double profiles.

In March 1989 (JD47600) 1A 0535+262 underwent a type II X-ray outburst which there was no optical coverage. Our earliest measurements coincide with the latest stages of a declining disk phase. This phase lasted until August 1992 (JD48850). On March 8 1993 (JD49054) seems that the source was in a disk-growth phase, but due to the single peak profile of the spectra we cannot compute the disk radius. In February 1994 (JD49400) another type II outburst was observed. During the period after the outburst, EW reached stability and so did the disk. This steady state lasted for almost 4 years (JD49436 - JD50747), and then the system entered a disk-loss phase. In this phase EW was positive which suggests that the line had an absorption profile and that the primary star lost completely its disk. EW reached a minimum value of 2.2Åon August 30 1998 (JD51055). In the next seven years a new disk started to form around the primary star, and after almost 10 years of X-ray quiescence 1A 0535+262 underwent a type II outburst at JD53528 followed by two type I outbursts. The result of these outbursts was the decline of the disk. In September 2007 (JD54350), we find again the system in a disk-growth phase which lasts over two years. During this time a series of type I X-ray outbursts had begun.

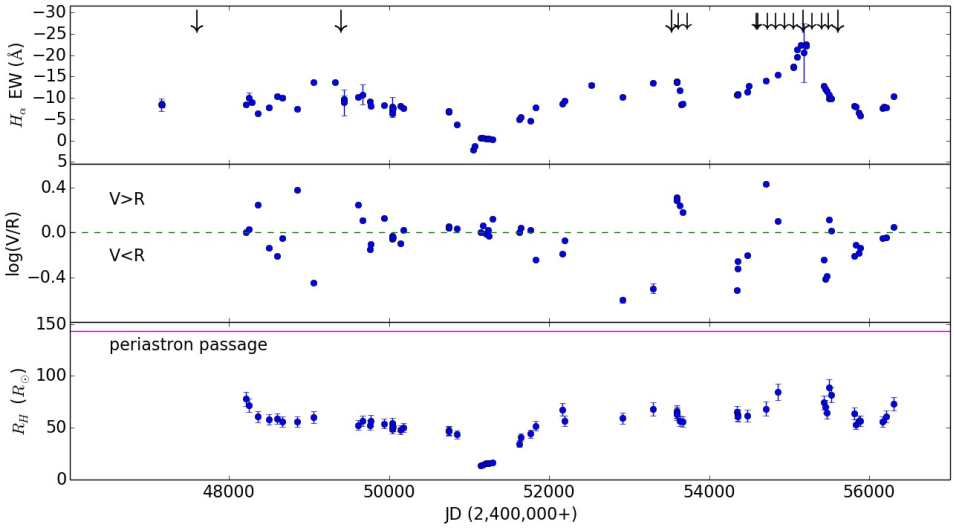

Figure 3.17: Long-term variability of the equivalent width EW(H_α), the V/R ratio and the calculated radius of the H_α emitting circumstellar disk for the source 1A 0535+262. The big arrows in the upper panel correspond to peak times of type II X-ray outbursts and the smaller arrows correspond to peak times of type II X-ray outbursts. The line in the lower panel indicates the periastron passage of the neutron star.

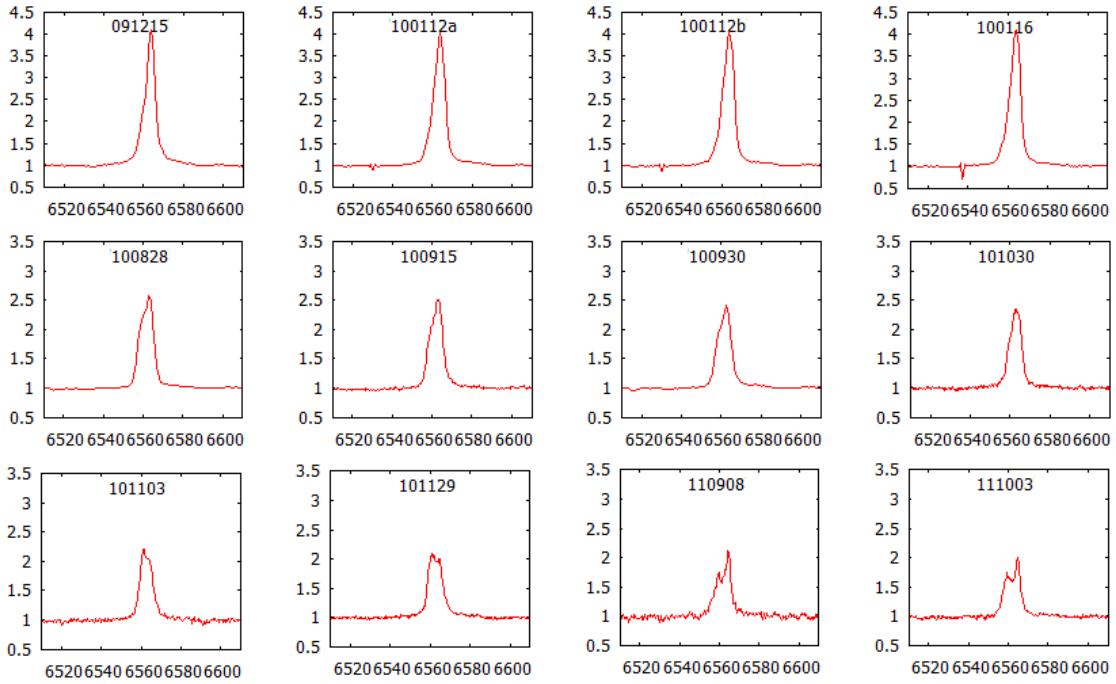

Figure 3.18: H_α line evolution from December 2009 to October 2011 (JD55180 - JD55837).

On 13 December 2009 (JD55178) a giant type II X-ray outburst occur and on January 12 2010 (JD55208) EW reached a maximum of -22.6Å. Three type I outbursts followed in the next ten months and the disk size was declined. On February 22 2011 the system underwent another type II X-ray outburst and in January 2013 (JD56300) the disk entered a new phase of growth.

1A 0535+262 also shows H_α emission lines with significant variability in their shape. The logarithm of the V/R ratio varies in the interval -0.4 - 0.4 from November 1990 to April 1996 (JD48200 - JD50180) and over a year later the ratio of the intensities of violet over red peak seems to be weakened. The lines had $|log(V/R)| < 0.1$ from October 1997 to August 2000 (JD50740 - JD51770), which coincides with the decline of the disk and suggests that the density perturbation faded away. Two months later the amplitude of log(V/R) started to increase indicating the existence of a new density wave in the new formed disk. In the time interval JD54348 - JD55454 when the system showed high X-ray activity and EW reached a maximum, the lines had $|log(V/R)| < 0.5$, and we found a quasi-period of $\sim$ 1100d, from $V < R$ (2007 - 2008) to $V > R$ (2008 - 2009) back to $V > R$ (2010).

3.8 IGR J06074+2205

IGR J06074+2205 was discovered by INTEGRAL/JEM-X on 15 February 2003. The source was detected with a flux around 7 mCrab at 3-10 keV and 15 mCrab at 10-20 keV. Optical spectroscopic observations with MDM 2.4 telescope found a Be star orbiting the source, exhibiting H_α emission. Reig et al. (2010) confirmed that IGR J06074+2205 is a BeX binary. The spectral type of the primary star is B0.5V, and an estimation of the rotation velocity of the underlying B star is 260 km s^{-1}. The distance of IGR J06074+2205 is around 4.5 kpc.

Variability of the H_α Parameters

The monitoring of IGR J06074+2205 reveals high variability of the H_α line profile. The line has mainly an asymmetric double peak profile. The following figure (3.19) shows how the EW(H_α), the V/R ratio and the disk radius change on timescale of seven years.

EW varies in the interval -12 - 3Å and has a mean value $\overline{EW} = -4.5$Å. Clearly EW takes positive values indicating an absorption profile for the H_α line. Our measurements coincide with a disk-loss phase and EW as well as the disk radius reached a first minimum on January 25 2009 (JD54856). After a period of eight months the disk started to increase gradually, but on March 28 2010 (JD55283) EW presents another minimum and we can assume that the primary star of IGR J06074+2205 lost its circumstellar disk completely. Five months later we find that a new disk started to form, but due to the observational gap in our data in the interval JD55530 - JD55800 we cannot see when the disk-size reached a peak. In September 2011 (JD55810) EW is in decline reaching a minimum around JD56250 and again the disk seems to vanish completely. A new disk started to form three months later and continued to increase in size until it reached a steady state.

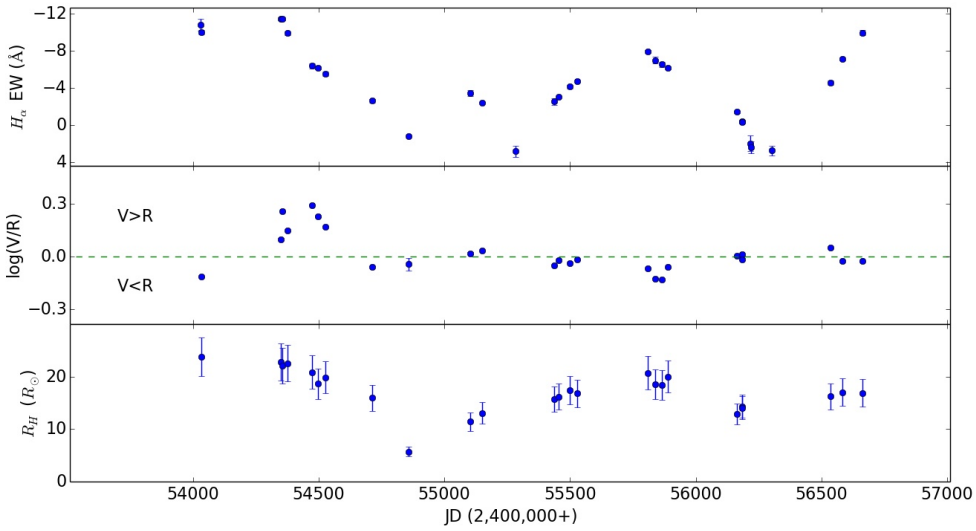

Figure 3.19: Long-term variability of the equivalent width EW(H_α), the V/R ratio and the calculated radius of the H_α emitting circumstellar disk for the source IGR J06074+2205.

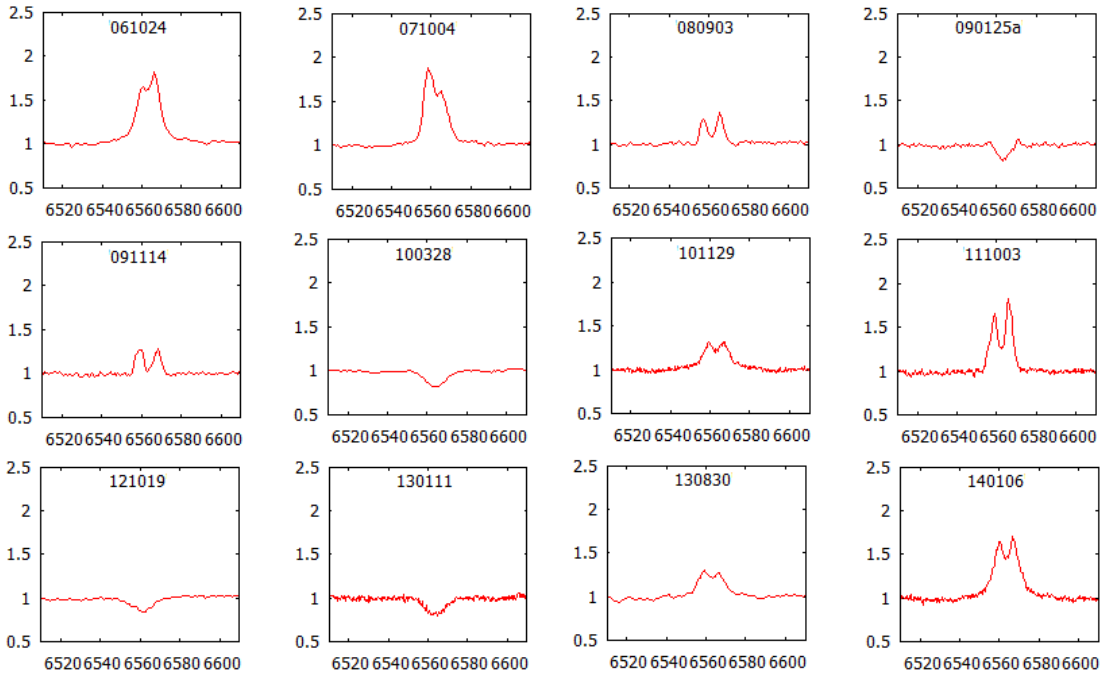

Figure 3.20: Characteristic H_α emission and absorption profiles of IGR J06074+2205.

Except EW and disk size, IGR J06074+2205 shows high V/R ratio variability, suggesting that the structure of the circumstellar disk changes significantly. In the earliest measurements log(V/R) seems to varied in the interval -0.1 - 0.3, but from September 2008 (JD54710) and for the next five years $|log(V/R)| < 0.1$. This time

period coincides with the long-term decline of EW and the decay of the equatorial disk.

3.9 XTE J1946+274

XTE J1946+274 is a hard X-ray transient Be/X-ray binary system. The system showed two main transient X-ray activity phases between 1998 and 2011. The first phase lasted almost three years (from September 1998 to August 2001) and it was the first and the longest X-ray activity of the system. During the initial outburst of these series (13 consecutive outbursts) it was revealed that the system had an X-ray pulsar with spin period of 15.83s orbiting its Be companion with a period of 169.2d in an 0.33 eccentric orbit. After, 9 years of quiescence in X-rays, the system underwent a new outburst phase starting on June 2010. From Swift/BAT we can see that the outburst that initiates the second phase of X-ray activity is about 142 mCrab at 15-50 keV. Similarly with the first phase the initial giant outburst is followed by four fainter outbursts ((Arabaci et al. 2014).

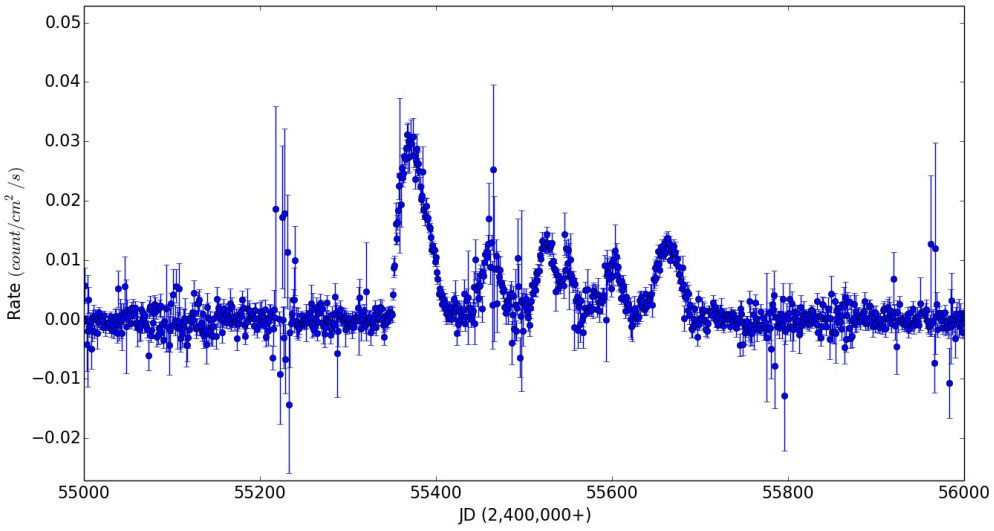

Figure 3.21: X-ray outburst light curve for the source XTE J1946+274 from the Swift/BAT X-ray transient monitor.

The optical counterpart of XTE J1946+274 was discovered by Verrecchia et al. (2002). It is a relatively faint B0-1 IV-Ve type star having strong H_α emission line in its spectra indicating the existance of an accretion disk.

Variability of the H_α Parameters

XTE J1946+274 emits a very strong, single peaked H_α line from June 2001 to August 2014, indicating the existence of a very large (or dense) circumstellar disk around the Be star. EW varies from -51.2 to -32Å and has an average value of -39.4Å with standard deviation of the mean 4.6Å. In the time interval JD52060

- JD54710 EW varied from -51 to -34Å. Although the system showed high X-ray activity starting on June 2010, EW seems to be unaffected by the outbursts. After the end of this phase EW slightly decreased from -43Å (JD56215) to -32Åtwo years later (JD56874).

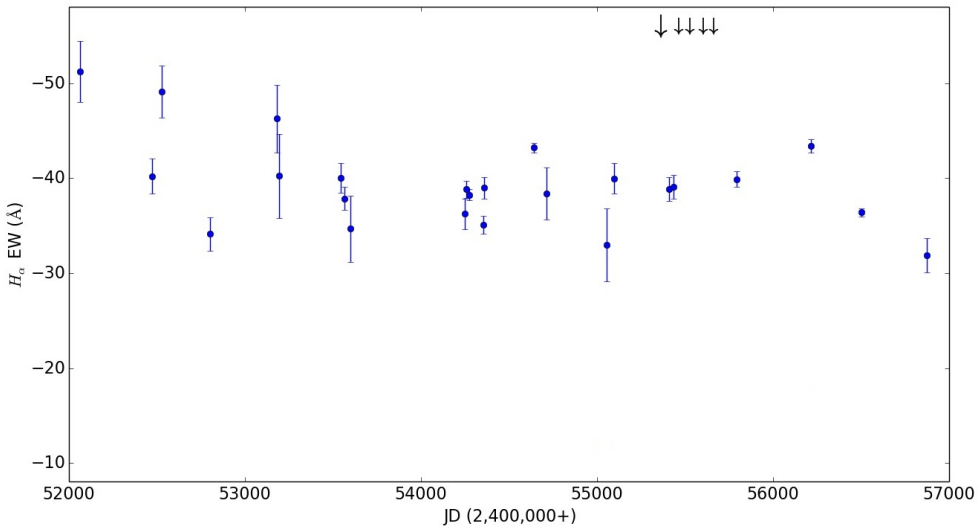

Figure 3.22: Long-term variability of the equivalent width EW(H_α) for the source XTE J1946+274. The big arrow corresponds to peak time of a type II X-ray outburst and the small arrows correspond to peak times of type I X-ray outbursts.

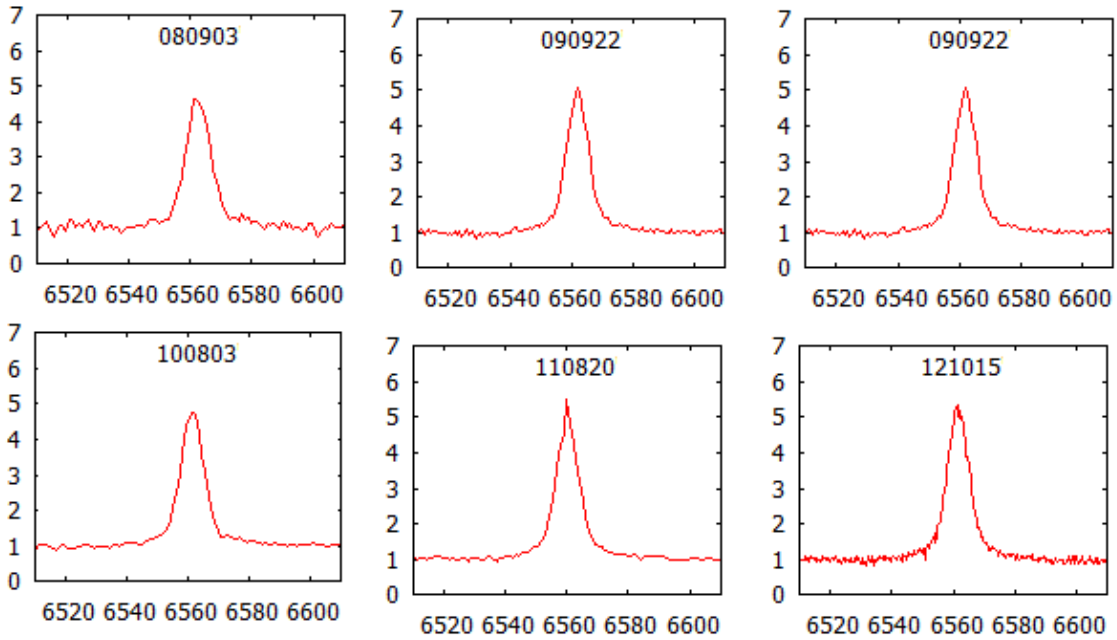

Figure 3.23: Characteristic H_α emission lines of XTE J1946+274.

3.10 KS 1947+300

The BeX binary KS 1947+300 was first detected in the X-ray band on June 8 1989 by the TTM coded mask X-ray spectrograph on the Kvant module of the Mir space station with a peak flux of 70 mCrab. The source remained in quiescence until the beginning of 2001, when the source reached a maximum flux of 120 mCrab.

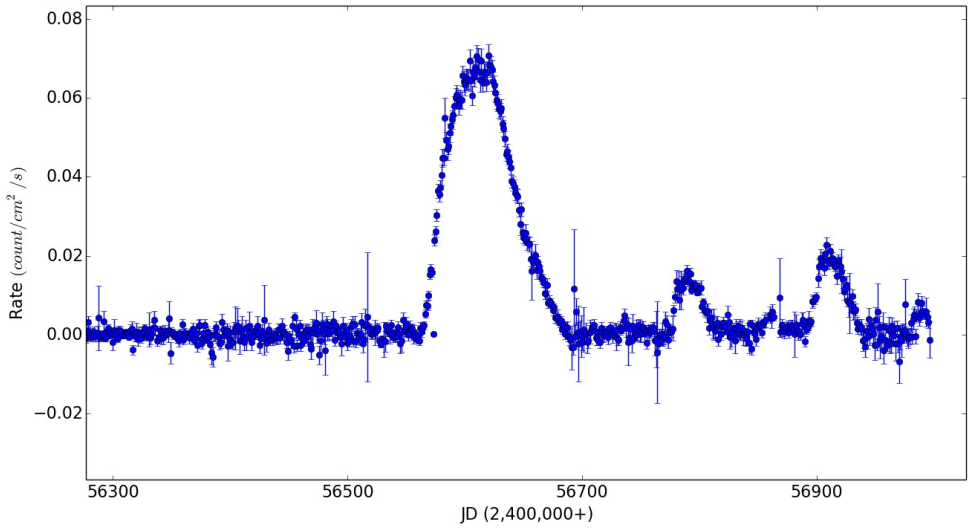

Figure 3.24: X-ray outburst light curve for the source KS 1947+300 from the Swift/BAT X-ray transient monitor.

After that outburst, the source remained in quiescent X-ray state for 12 years until November 2013, when the source underwent a giant outburst around 322 mCrab at 15-50 keV, the highest in its history. This outburst lasted about 120d. In 2014, the source underwent three more outbursts with peak flux lower than 70 mCrab (figure 3.24).

Pulse timing analysis showed the orbital parameters of the system. The binary system has orbital period of 40.4d and eccentricity 0.03. It's identification was suggested by Negueruela et al. (2003). KS 1947+300 is associated with a star of B0Ve spectral type and it is located at 10 kpc (Reig 2008).

Variability of the H_α Parameters

Similarly to XTE J1946+274, KS 1947+300 has a symmetric, single peaked H_α emission line but of lower strength. Because the line profiles of KS 1947+300 are single peaked we don't observe V/R variability. Our observations for this source start from early 2001 until August 2014. The interval which EW varies is from -18.3 to -12.8Å and it has a mean value of -15.7Å. The standard deviation of the mean is 1.2Å. Through the time we study this source we notice that the intensity of the emission line slowly declines with time. After the outburst at the beginning of 2001 the system remained in an X-ray quiescence state for 12 years. In November 2013 a series of X-rays started which lasted until September 2014.

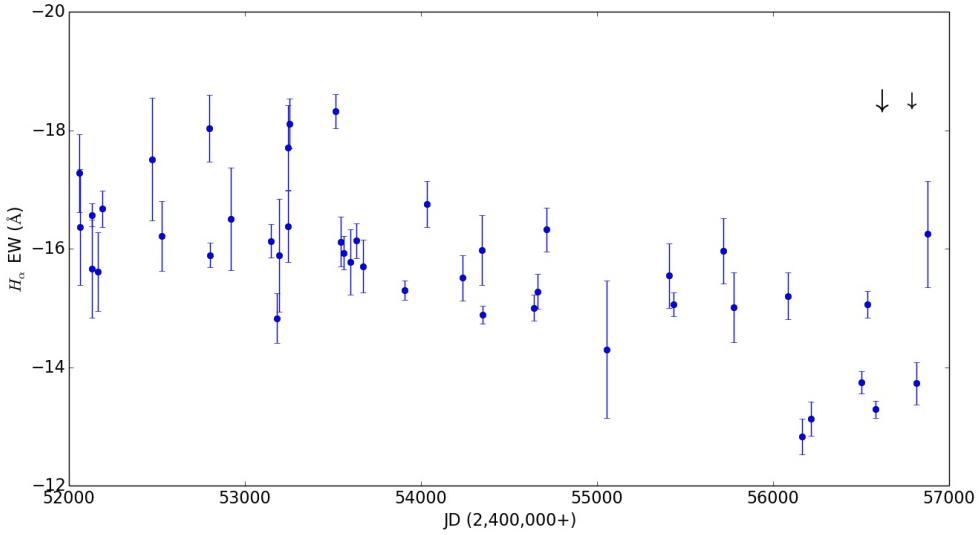

Figure 3.25: Long-term variability of the equivalent width EW(H_α) for the source KS 1947+300. The big arrow corresponds to peak time of a type II X-ray outburst and the smaller one corresponds to peak time of a type I X-ray outburst.

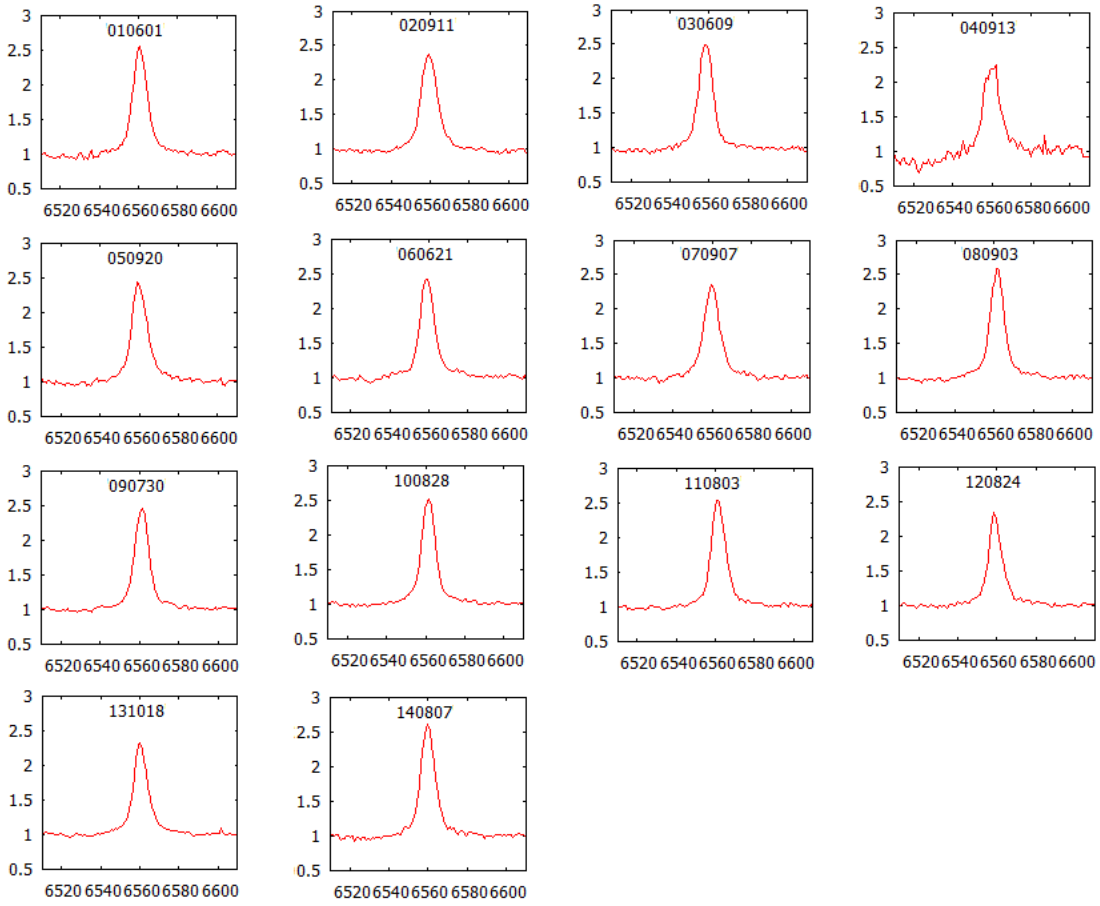

Figure 3.26: Characteristic H_α emission lines of KS 1947+300.

3.11 GRO J2058+42

GRO J2058+42 is a transient X-ray pulsar discovered in 1995 with BATSE, during a giant outburst that lasted 46d (Wilson et al. 1998). That outburst was followed by a series of type I outbursts. The peak flux reached about 300 mCrab at 20-50 keV. The optical counterpart of GRO J2058+42 has been identified with an O9.5-B0 IV-Ve star. The system is located at a distance of 9 kpc. GRO J2058+42 entered a quiescence X-ray state after a phase of high X-ray activity (from 1995 to 2002), that continues up to the present. The system exhibits H_α emission line with peak separation of $417 \pm 5 kms^{-1}$, which indicates that the Be star did not lose the circumstellar disk completely, despite the fact that the system showed a quiescent X-ray state (Reig et al. 2005).

Variability of the H_α Parameters

GRO J2058+42 is yet another source that its H_α line shows long-term variability. In the upper panel of figure [3.27] we can see how the EW(H_α) varies with time. EW seems to have sinusoidal behavior. In our earliest measurements EW increased slightly and then drops off. In July 2005 (JD53560) EW has a minimum -0.3Å which indicates that the disk is almost disappeared. Less than a month later the EW started to slowly increase and after almost four years, on September 22 2009 (JD55096) EW had a maximum of -10Å. In the following five years EW follows the same trend, a slow and gradual decrease, reaching a minimum around September 2012 and a gradual increase. This long-term variability suggests the dissipation and subsequent formation of the equatorial disk around the primary star.

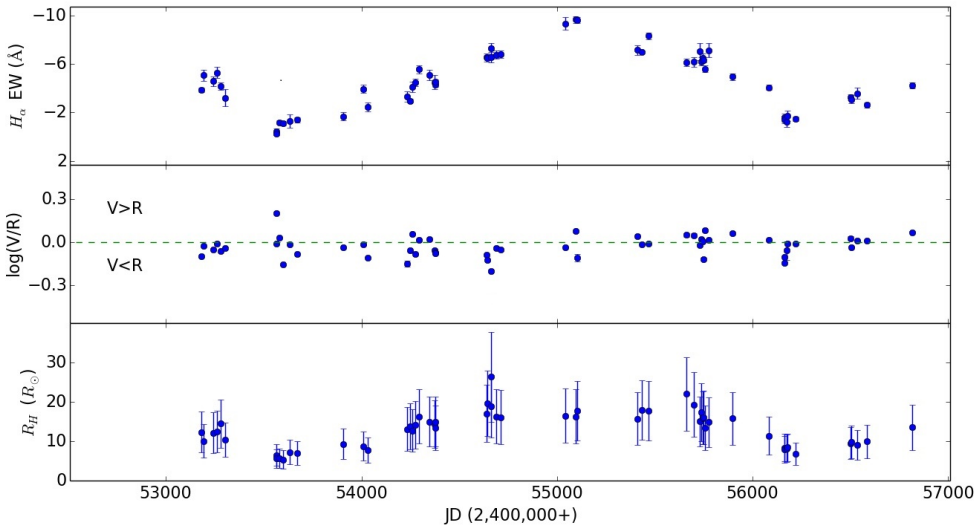

Figure 3.27: Long-term variability of the equivalent width EW(H_α), the V/R ratio and the calculated radius of the H_α emitting circumstellar disk for the source GRO J2058+42.

The second panel of figure [3.27] presents how the intensities of the V and R peaks

varied with time. The H_α line has only double peaked, symmetric or asymmetric profiles. The variability of the logarithm of the V/R ratio seems to be constant between the interval -0.2 - 0.2 ($|log(V/R)| < 0.2$).

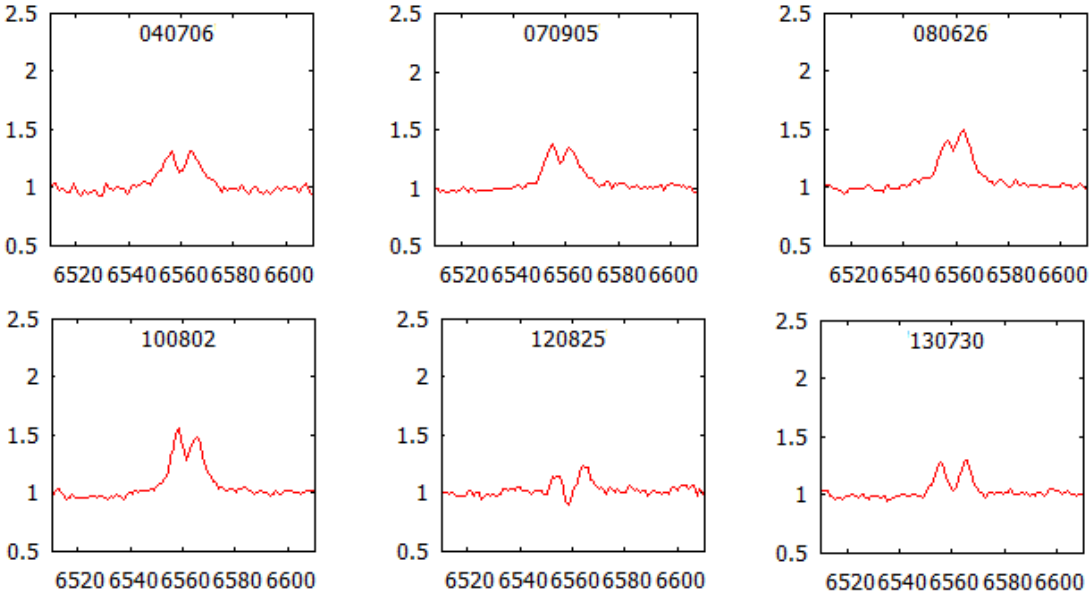

Figure 3.28: Typical H_α emission line profiles of the source GRO J2058+42.

3.12 SAX J2103.5+4545

SAX J2103.5+4545 is a HMXB. The compact object in this system is a neutron star due to the observed X-ray emission pulsations. The optical companion is a moderately reddened B0V_e star (Reig et al. 2014). The distance estimated by Baykal et al. (2007), from X-ray observations to 4.5 kpc. The orbital period is 12.7 days and has a moderately eccentric orbit with eccentricity 0.4 Baykal et al. (2007).

SAX J2103.5+4545 shows extended bright and faint X-ray states that last for several months. During this quiescence state, the X-ray intensity does not change with orbital phase, and the spin frequency of the neutron star remains constant (Baykal et al. 2007). In this state the companion of the neutron star shows H_α in absorption (Reig et al. 2010) which indicates the recession of the circumstellar disk.

SAX J2103.5+4545 underwent two X-ray outbursts, one in 2007 and another in 2010, with peak flux 170 mCrab and 130 mCrab at 20-50 keV respectively [3.29].

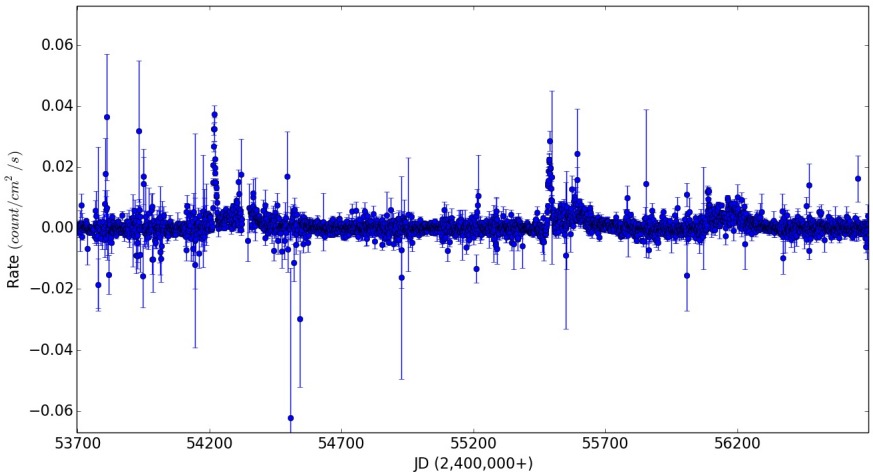

Figure 3.29: X-ray light curve for the source SAX J2103.5+4545 from the Swift/BAT X-ray transient monitor.

Variability of the H_α Parameters

The H_α line profile of SAX J2103.5+4545 show low variability and for most of the time is an absorption profile. We have monitored this source for over ten years from August 2003 to January 2014 (JD52852 - JD56660). In the earliest measurements EW(H_α) was decreasing and around August 2004 (JD53240) reached a minimum of 3Å.

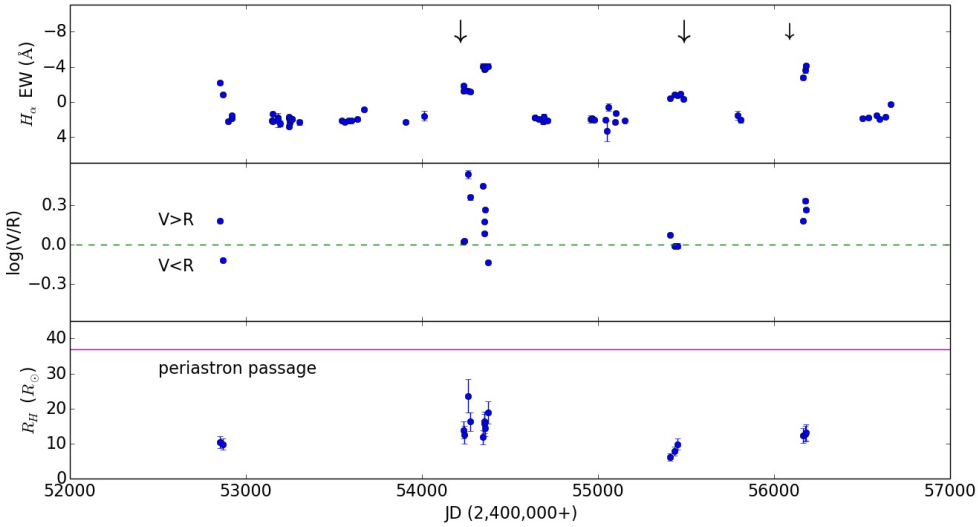

Figure 3.30: Long-term variability of the equivalent width EW(H_α) for the source SAX 2103.5+4545. The big arrows in the upper panel correspond to peak times of type II X-ray outbursts and the small arrow correspond to a type I X-ray outburst. The line in the lower panel indicated the periastron passage of the neutron star.

For almost three years, September 2003 - October 2006 (JD52890 - JD53900), the H_α line had an absorption profile. So, it is safe to assume that during this period the equatorial disk of the primary star had disappeared completely. In April 2007 (JD54218) the system underwent an X-ray outburst. In May 2007 (JD54230) EW started to increase gradually, and around September 2007 (JD54350) reached a maximum of -4Å. In the same period SAX J2103.5+4545 shows short-term variability of the V/R ratio. Also the appearance of H_α emission line profiles suggests that a circumstellar disk was formed around the primary star. We estimate the size of the disk to be around $30R_\odot$. Two years later EW declined and reached a new minimum at 3Å. In August 2010 (JD55410) EW started to increase again, but around JD55489 the source underwent another X-ray outburst resulting the gradual decline of the EW. It seems that EW followed the same trend the next three years but we cannot describe with detail the cycle due to the long observational gaps in our data.

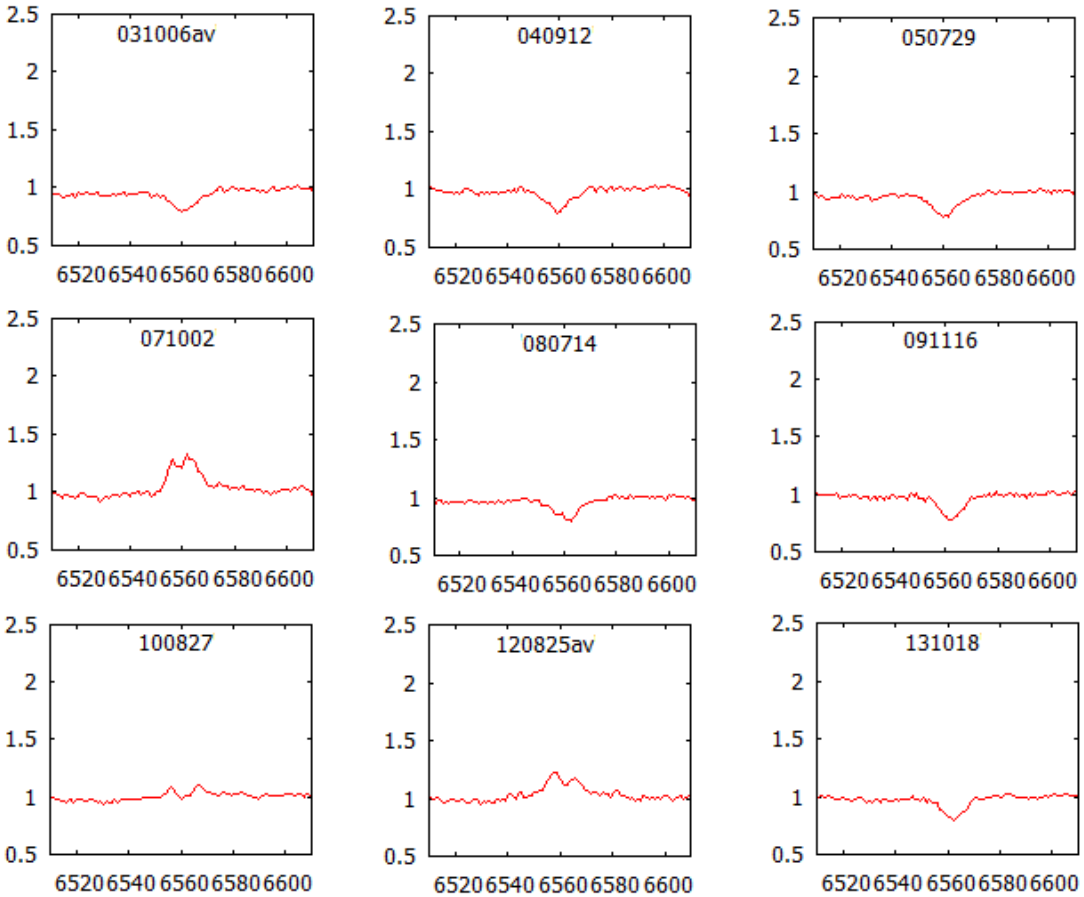

Figure 3.31: Characteristic H_α absorption and emission line profile of SAX 2103.5+4545.

3.13 4U 2206+54

4U 2206+54 is a persistent high-mass X-ray binary star at a distance of 2.6 kpc (Blay et al. 2006). It was detected as an X-ray source by the Uhuru satellite (Giacconi et al. 1972). The primary star (BD+53 2790) is classified as an O9.5 Ve star (Ribo et al. 2006). The compact object is a neutron star (Torrejon et al. 2004) with spin period 5549s (Finger et al. 2010).

Variability of the H_α Parameters

We have monitored 4U 2206+54 from July 1999 to August 2014 (JD51385 - JD56875). Through the years the H_α line profile of 4U 2206+54 remains in emission indicating the existence of an equatorial disk around the primary star. In addition, the line has always a double-peaked profile, both symmetrical and asymmetrical. Figure [3.32] shows the changes of EW(H_α), V/R ratio and disk radius. EW varies in the interval -4 - -0.9Å and has an average value -2.7Å with standard deviation of the mean $\sigma(EW) = 0.95$Å. The disk varies in the interval 11 - 17$R_\odot$ with a mean value 13.5$R_\odot$ and standard deviation of the mean 1.4$R\odot$. This means that the size of the disk hardly changes through time.

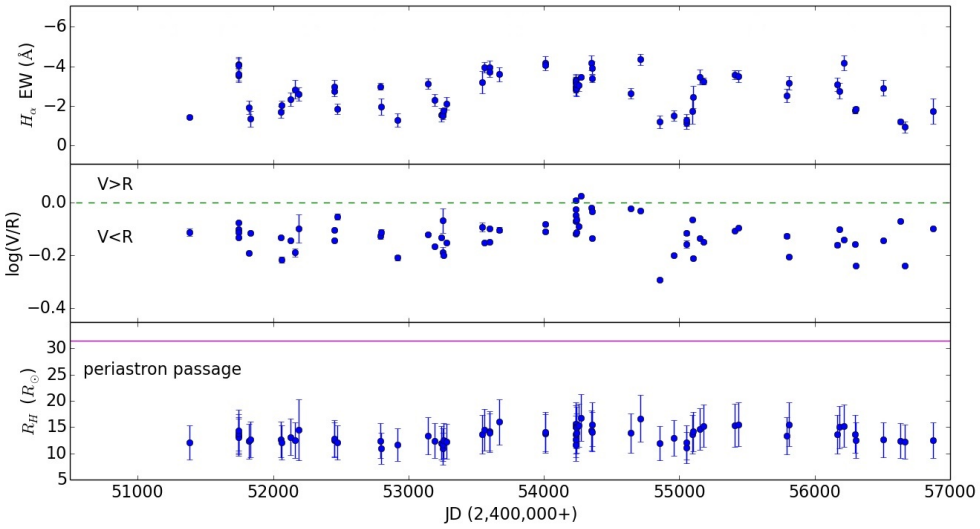

Figure 3.32: Long-term variability of the equivalent width EW(H_α), the V/R ratio and the calculated radius of the H_α emitting circumstellar disk for the source 4U 2206+54. The arrows in the upper panel correspond to peak times of X-ray outbursts. The line in the lower panel indicates the periastron passage of the neutron star.

On the other hand the intensity of the red peak of the $H\alpha$ line seems to have significant variability. By excluding the two cases where $V > R$, the logarithm of the V/R ratio is negative ($V < R$) and varies from -0.3 - 0, with an average value of -0.13.

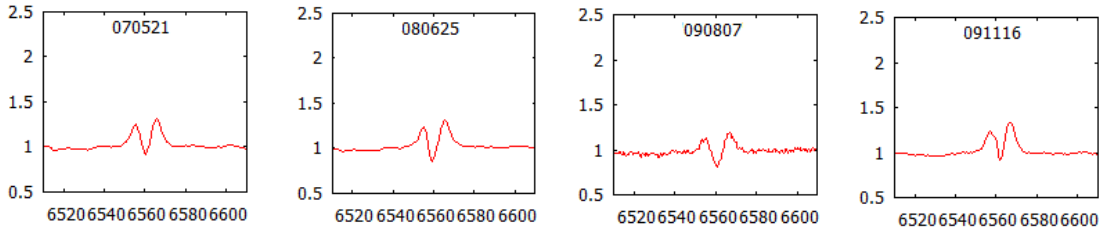

Figure 3.33: Typical H_α emission lines for the source 4U 2206+54.

The shape of the H_α has a deep absorption core going down below the continuum level resembling the expected spectrum from a Be star seen very close to edge-on (Hanuschik 1995, 1996; Negueruela & Reig 2001)

3.14 SAX J2239.3+6116

SAX J2239.3+6116 was discovered as a fairly bright X-ray transient by the Wide Field Cameras (WFCs) on BeppoSAX in 1997. An archival search from the All-Sky Monitor on RXTE showed five X-ray outbursts from the same source during 1996-1999. The five outbursts occurred with regular intervals of $262 \pm 5d$. Optical observations revealed an optical counterpart, a Be star with spectral type B0-2 III-Ve. An estimated distance of the system is 4.4 kpc. In't Zand et al. (2000) classified SAX J2239.3+6116 as Be/X-ray binary system with orbital period of 262d.

Variability of the H_α Parameters

We monitor the source SAX J2239.3+6116 for 13 years from May 2001 to August 2014 (JD52060 - JD56876). The H_α emission line has both a symmetric and asymmetric double peak profiles. V/R variability is clearly seen in the lower panel of figure [3.34] indicating a precessing perturbation in the disk. The lines have $|log(V/R)| < 0.3$. EW varies with time from -10.3 to -1.8Å. As we clearly see from the upper panel of [3.34] EW reach a peak at October 2003 (JD52920) and since then continued to decline gradually until August 2014 (JD56876) which reached its lowest point. Because the rotational velocity of SAX J2239.3+6116 is not yet determined we cannot estimate the disk size from Huang's law [2.10].

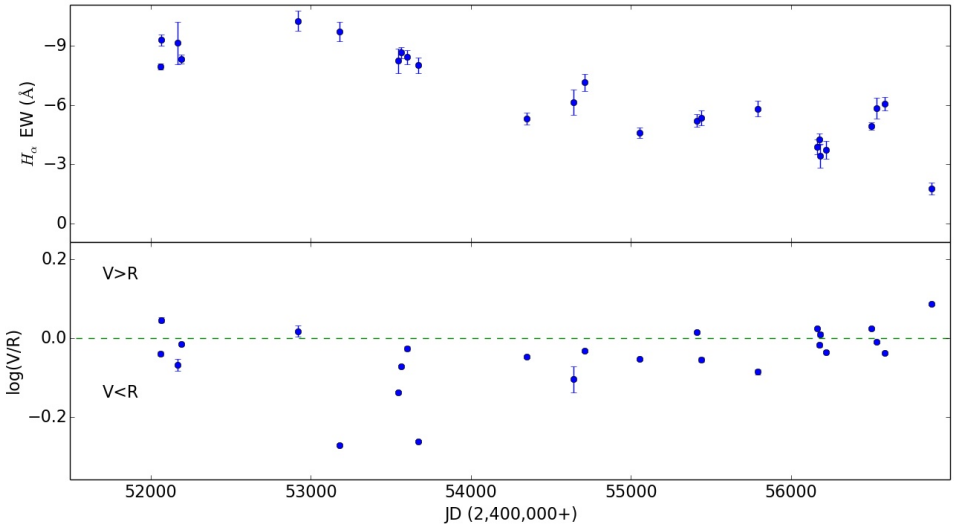

Figure 3.34: Long-term variability of the equivalent width EW(H_α) for the source SAX J2239.3+6116.

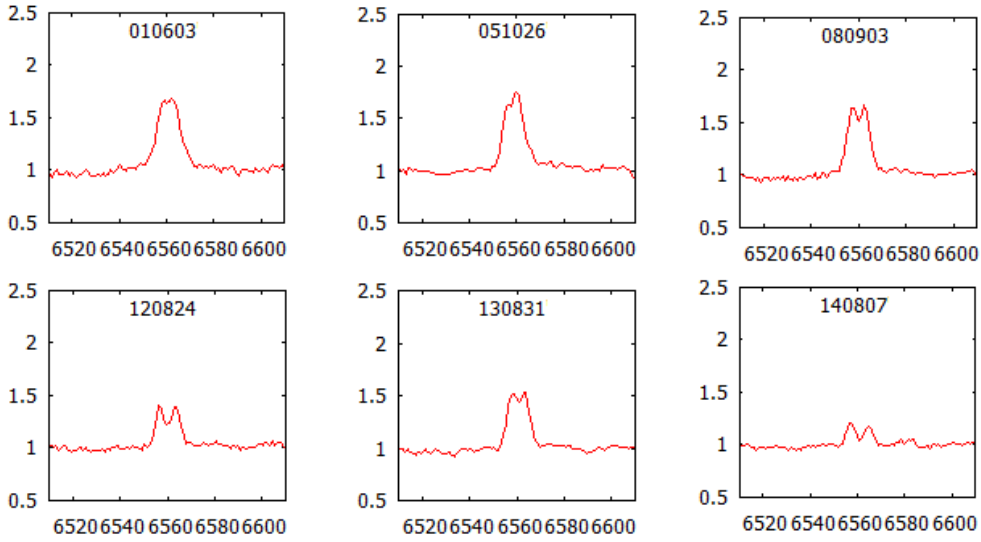

Figure 3.35: H_α emission lines for the source SAX J2239.3+6116.

Chapter 4

Discussion

Be stars show emission in the Hα line due to the recombination of radiation emitted by the star in the equatorial disk. As explained in Chapter 1, this line is the main indicator of the state of the disk. In this project we have studied the variability of the H_α spectral parameters in a group of 14 BeXBs with the aim to

- determine the disk rotational law
- investigate the relationship between the extension of the disk with the H_α line equivalent width
- investigate the relationship between the optical and X-ray activity.
- study the V/R variability

4.1 Disk Rotational Velocity Law

The radial dependence of the rotational velocity in the disk is given by

$$v_{rot} = v \left(\frac{R_H}{R_*} \right)^{-j} \tag{4.1}$$

where v and R_* are the stellar rotational velocity and radius. j is a parameter that defines the dependence of the velocity of the gas particles in the disk with distance: j=0.5 for Keplerian rotation and j=1 for conservation of angular momentum. According to Huang's law (1972), the peak separation can be given as $\Delta V = 2 v_{rot} sini$. Hence

$$\frac{\Delta V}{2 v sini} = \left(\frac{R_H}{R_*} \right)^{-j}$$

On the other hand, EW(H_α) for an optically thick gas is a function of the square of mean electron density and visible envelope area

$$EW \propto N_e^2 \left(\frac{R_H}{R_*} \right)^2$$

So, the normalized peak separation can be expressed as

$$\frac{\Delta V}{2vsini} \propto \left(\frac{EW}{N_e^2}\right)^{-j/2}$$

or by taking the logarithm of this expression

$$log\left(\frac{\Delta V}{2vsini}\right) = \frac{-j}{2} log\left(\frac{-EW(H_\alpha)}{\text{Å}}\right) + j\, log\left(\frac{N_e}{cm^{-3}}\right) + constant \Rightarrow$$

$$log\left(\frac{\Delta V}{2vsini}\right) = \alpha\, log\left(\frac{-EW(H_\alpha)}{\text{Å}}\right) + b \tag{4.2}$$

where $\alpha = -j/2$ and $b = log(N_e/cm^{-3}) + constant$.

Here we investigate the type of rotational law for BeXBs. We wish to tell if the disks in BeXBs differ from those in classical (isolated) Be stars.

In figure [4.1] we plotted the logarithm of $\Delta V/(2vsini)$ against the logarithm of -EW/Å for six of our sources that present long-term V/R variability. This diagram is quite useful to investigate the rotational velocity law parameter j.

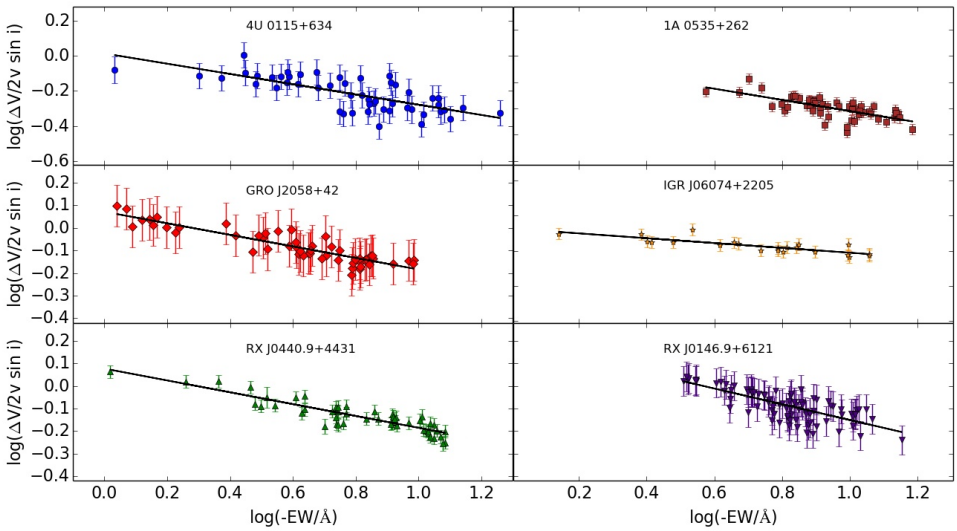

Figure 4.1: $log[\Delta V/(2vsini)]$ versus $log(-EW/\text{Å})$. The straight line is the linear least square fit from equation [2.12].

In table [4.1] we present the results from the least square fit for each source. From the slope α we calculate the rotational velocity parameter $j = -2\alpha$. For all six BeXBs we get a value for j which is close to the expected value for a Keplerian disk (j=0.5). Therefore, we can conclude that the rotational velocity of the disk around their Be stars is quasi-Keplerian.

Table 4.1: Results from the least square fit for six BeXBs.

X-ray name	Slope α	Error	Intercept b	Error	j	Error
4U 0115+634	-0.29	0.04	0.01	0.04	0.58	0.08
RX J0146.9+6121	-0.35	0.05	0.20	0.04	0.70	0.10
RX J0440.9+4431	-0.26	0.02	0.08	0.01	0.52	0.04
1A 0535+262	-0.21	0.01	-0.10	0.02	0.42	0.02
IGR J06074+2205	-0.14	0.03	-0.07	0.02	0.28	0.06
GRO J2058+42	-0.26	0.05	0.07	0.03	0.52	0.10

For isolated Be stars, it is known that H_α peak separation and EW are correlated (Hanuschik et al. 1988). Hanuschik (1989) derived the law

$$log\left(\frac{\Delta V}{2vsini}\right) = -0.32\, log\left(\frac{-EW(H_\alpha)}{\text{Å}}\right) - 0.2 \tag{4.3}$$

for 93 isolated Be stars. In figure [4.2], we gathered all data points for the previous six BeXBs and we plotted $log\Delta V/(2vsini)$ versus $logEW$. The dashed line represent the average behavior of Be stars as defined by Hanuschik (1989). From this figure it can be noticed that all the data points for the BeXBs are above the average line. This suggests that the circumstellar disks in the BeXBs are denser than disks in isolated Be stars. In fact, we find that on average the disks of BeXBs are ~ 2 times denser than isolated Be stars:

$$\Delta log\left(\frac{N_e^{BeXB}}{N_e^{Be}}\right) \simeq 0.3 \Rightarrow \frac{N_e^{BeXB}}{N_e^{Be}} \simeq 2 \tag{4.4}$$

Zamanov et al. (2001) found the same result, i.e. that the disks in BeXBs are about ~ 2 times more dense than disks in typical Be stars. Negueruella et al. (1998) also suggests that the disks in BeXBs are denser due to the observation of shorter periods of V/R variability.

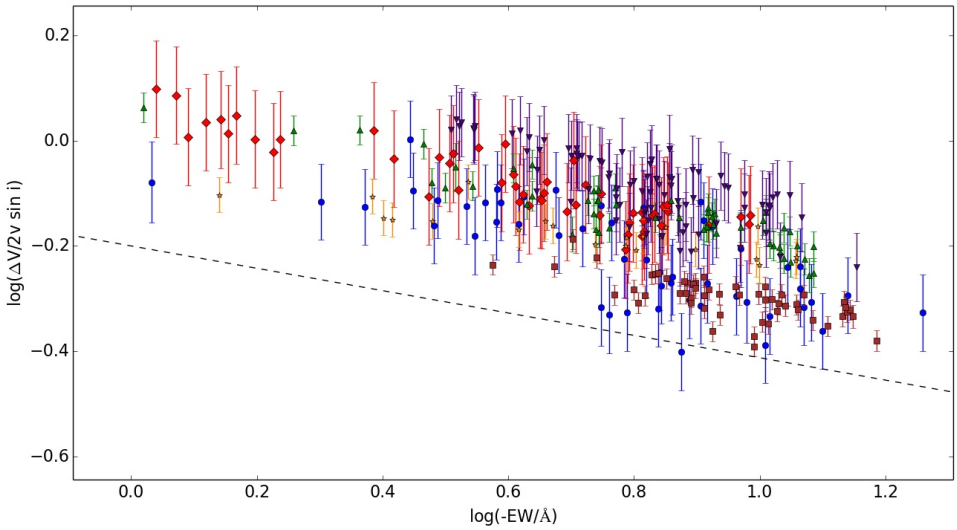

Figure 4.2: Plot of $log[\Delta V/(2vsini)]$ versus $log(-EW/\text{Å})$ of BeXBs. The dashed line represents the average behavior of the Be stars (Hanuschik 1989). Legend: circles (blue) - 4U 0115+634, triangles down (indigo) - RX J0146.9+6121, triangles up (green) - RX J0440.9+4431, squares (brown) - 1A 0535+262, stars (orange) - IGR J06074+2205, diamonds (red) - GRO J2058+42.

4.2 Correlation Between EW and Disk Size

In Chapter 3 we studied the evolution of the EW(H_α) and disk radius with time for each source. In the systems that show large amplitude of variability in the Hα line parameters we observe a general agreement between the strength of the line and the radius of the disk: BeXBs that have strong H_α emission lines, i.e. large equivalent width, also have very large circumstellar disks. On the other hand, for weak emission lines the disk seems to have small size. Here we study the relationship between disk size and strength of the Hα line in more detail.

According to Huang (1972) and Hanuschik (1988), rotationally dominated double peak profiles, $\Delta V/(2vsini)$ can be regarded as a measure for the outer disk radius R_H[2.10]. We showed in the previous section that the disk in BeXB follow a Keplerian velocity law. Thus we can estimate the radius of the disk from the peak separation assuming Keplerian rotation, that is j=1/2.

Substituting the rotation velocity parameter j in Huang's law [2.10] with 1/2

$$\left(\frac{R_H}{R_*}\right)^{-1/2} = \frac{\Delta V}{2vsini} \Rightarrow \left(\frac{R_H}{R_*}\right)^{-1} = \left(\frac{\Delta V}{2vsini}\right)^{2} \Rightarrow$$

$$R_H = R_* \left(\frac{\Delta V}{2vsini}\right)^{-2} \tag{4.5}$$

Figure [4.3] shows the disk radius as a function of EW(H_α). As suspected, the larger the equivalent width, the larger the size of the disk.

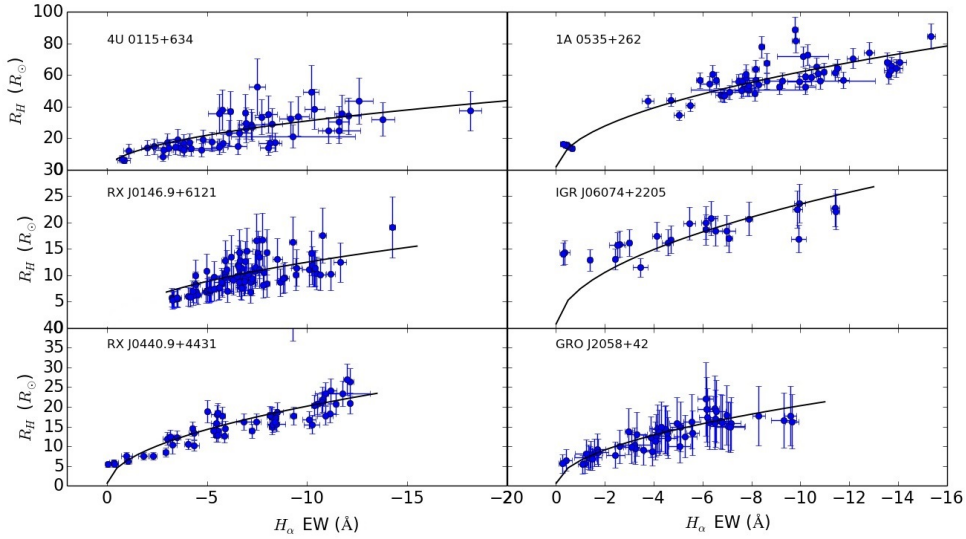

Figure 4.3: Disk radius R_H versus EW(H_α). The solid line in corresponds to a fit $R = \alpha_0 \sqrt{-EW}$.

From a Keplerian disk and according to equation [4.2], the dependence between R_H and EW should be $R_H \propto \sqrt{EW}$. The solid line in figure [4.3] corresponds to a fit

$$R = \alpha_0 \sqrt{-EW}$$

4.3 Optical/X-ray Correlations

In a BeXB the neutron star interacts with the circumstellar disk of its Be companion, resulting X-ray transient behavior. This behavior is characterized by two type of outbursts: 1) Type I, which are regular and periodic outbursts; 2) Type II, which represent major increase of the X-ray flux. In particular, type II outbursts are major events fueled by the material in the circumstellar disk, causing the variability in the structure of the disk. The changes in the structure of the disk are observable in the H_α line parameters. In fact, after a type II X-ray outburst we expect a decrease of EW because a large portion of the disk has been accreted by the neutron star. Normally we expect to observe outbursts when the disk grows in size and reaches or passes the distance to periastron. Here we investigate the relationship between X-ray activity and the strength of the line, which in theory gives a measure of the size of the disk. In our data we came across with some interesting results. In some cases we found that that type II X-ray outbursts occurred with very large disk sizes, as expected, and in another cases the outbursts occurred when the disk had a small size.

4.3.1 X-ray Activity With Very Large Disk Sizes

In these cases we observe major outbursts occur when the disk extends to very large sizes. When the X-ray activity end, we observe decline in the strength of the H_α emission line. This is the normal behavior that we expect to observe in BeXBs because the disk material is accreted from the Be star to the neutron star causing the dissipation of the disk. Such cases can be seen in systems 4U 0115+634, RX J0440.9+4431, 1A 0535+262 and SAX 2103.5+4545. 4U 0115+634 underwent type II X-ray outbursts at JD50200, JD51800, JD54560 and JD55900 with the disk radius reaching up to periastron passage ($\sim 63R_\odot$) and there is suspicion that might even cross it, figure [4.4].

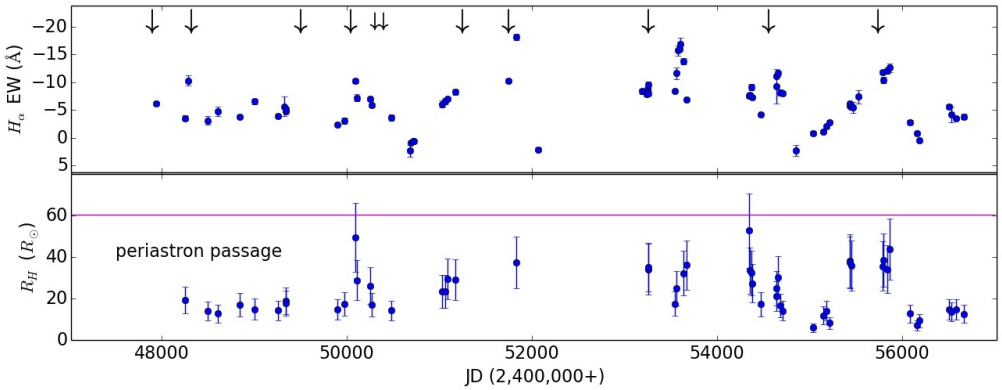

Figure 4.4: Long-term variability of the equivalent width EW(H_α) and the disk radius R_H for the source 4U 0115+634. The big arrows in the upper panel correspond to peak times of type II X-ray outbursts and the smaller ones to peak times of type I X-ray outbursts. The line in the lower panel indicates the periastron passage.

RX J0440.9+4431 had two X-ray outbursts at JD55410 and JD55440 with the disk radius reaching up to $30R_\odot$. After the outbursts EW as well as the disk radius declined as we expected.

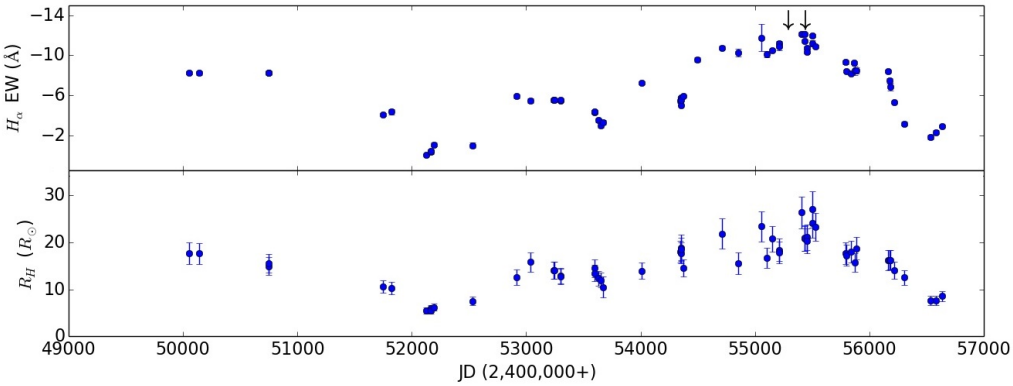

Figure 4.5: Long-term variability of the equivalent width EW(H_α) and the disk radius R_H for the source RX J0440.9+4431. The arrows in the upper panel correspond to peak times of X-ray outbursts.

1A 0535+262 underwent a type II X-ray outburst at JD55620 with the size of the disk reaching up to periastron passage ($\sim 143R_{\odot}$). This is suggested by the very large EW(H_{α}) measurements during the outburst. Both EW and the disk size decreased after the outburst, figure [4.6].

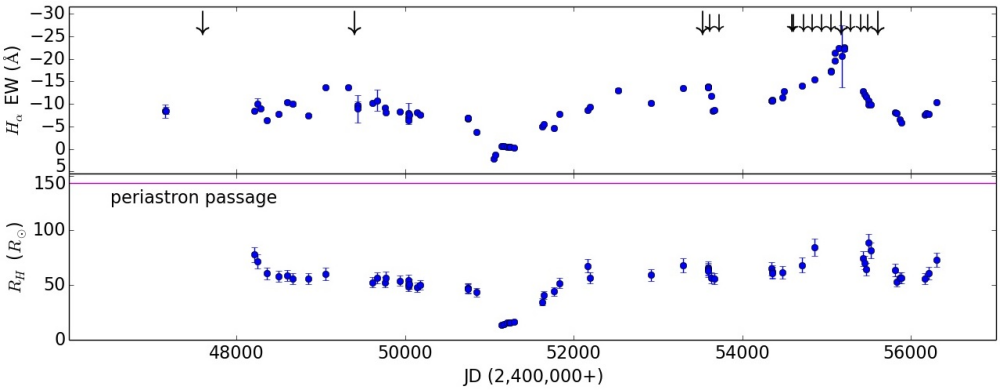

Figure 4.6: Long-term variability of the equivalent width EW(H_{α}) and the disk radius R_H for the source 1A 0535+262. The big arrows in the upper panel correspond to peak times of type II X-ray outbursts and the smaller ones to peak times of type I X-ray outbursts. The line in the lower panel indicates the periastron passage.

SAX 2103.5+4545 mainly shows H_{α} absorption profiles indicating the absence of a disk around the Be star. However, in the time interval JD54234 - JD54375 SAX 2103.5+4545 shows H_{α} emission lines suggesting the existence of a circumstellar disk. The disk ranged between 12-24$R_{\odot}$ and with the periastron in a distance of $\sim 37R_{\odot}$. The system showed enhanced X-ray emission at JD54220 which lasted for $\sim$ 25 days and coincides with the highest calculated value of R_H in our data. After the emission in X-rays, EW increased and reached a maximum value of -4Å, $\sim$ 115d later at JD54347, figure [4.7].

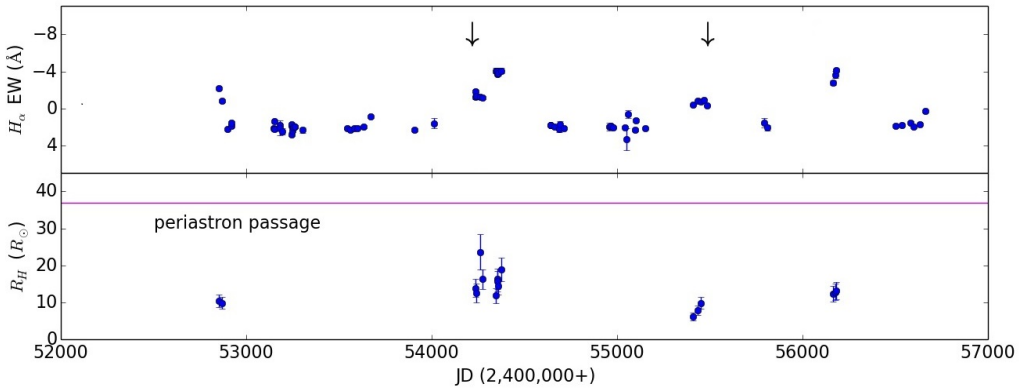

Figure 4.7: Long-term variability of the equivalent width EW(H_{α}) and the disk radius R_H for the source SAX 2103.5+4545. The arrows in the upper panel correspond to peak times of X-ray activity. The line in the lower panel indicates the periastron passage.

4.3.2 Unexpected Cases

Beside the typical behavior of BeXBs that we expected to observe, we came across with some peculiar and interesting cases. In these cases there is a suspicion of a large disk around the Be star and during or after the appearance of X-ray outbursts the structure of the disk seems to be unaffected by this activity. These peculiar cases are seen in sources XTE J1946+274 [fig.4.8] and KS 1947+300 [fig. 4.9]. An interpretation of this behavior is given by Reig & Fabregat (2015), which the neutron star accreted a small fraction of the material of the circumstellar disk ($< 10\%$).

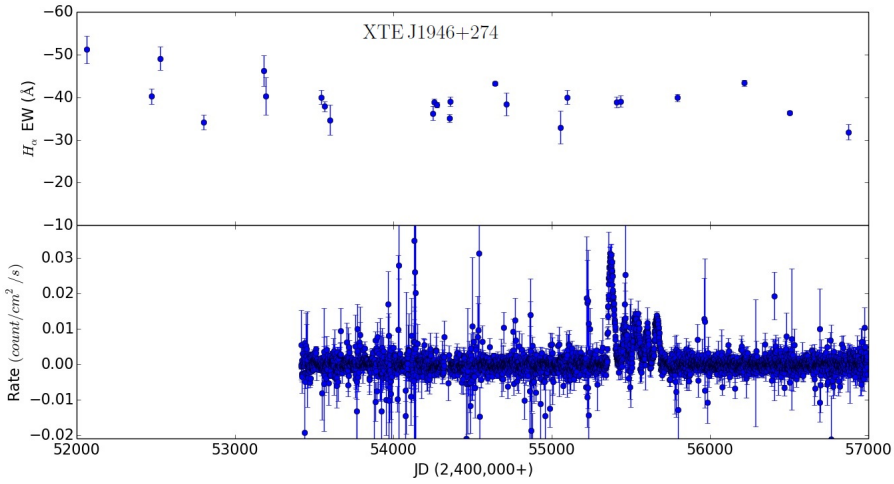

Figure 4.8: Long-term variability of the equivalent width EW(H_α) and X-ray activity for the source XTE J1946+274.

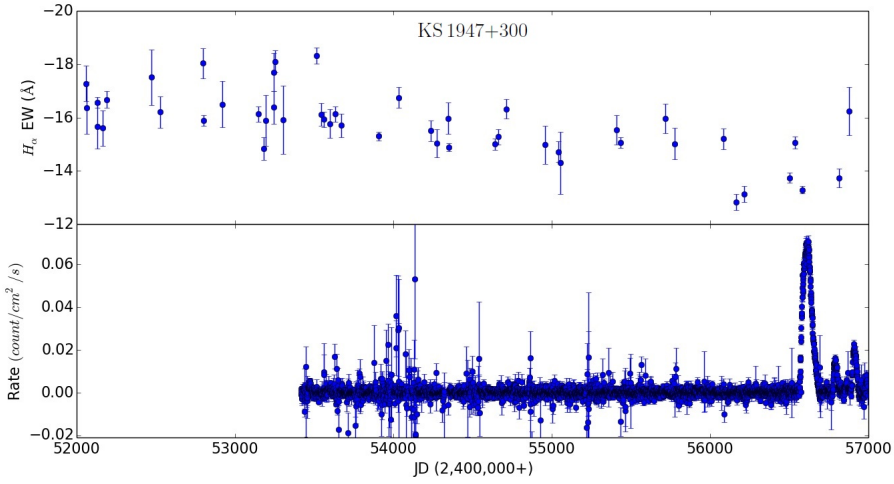

Figure 4.9: Long-term variability of the equivalent width EW(H_α) and X-ray activity for the source KS 1947+300.

4.4 V/R Variability

H_α line profiles in BeXBs show a large range of different shapes. The emission lines may be single or double peaked and these shapes come in symmetric or asymmetric varieties. As mentioned in Chapter 1, class 1 H_α profiles are symmetric, often double peaked, with $V \approx R$. On the other hand, class 2 H_α profiles are asymmetric, often with one dominant single peak, with $V \neq R$. Class 2 profiles, apart from their characteristic asymmetric shape, have a second property ; their time variability pattern. Class 2 profiles tend to change their shape greatly over years. V/R variability is believed to be caused by the gradual change of the amount of the emitting gas approaching the observer and that resending from the observer due to the precession of a density perturbation in the disk. By studying this long-term variability we may get information about the physical conditions of the equatorial disk around the Be star, mainly its kinematic state.

One particular source that show long-term cyclic behavior is RX J0146.9+6121. In figure [4.10], three cycles of V/R variability can be seen from December 1991 to October 2001 (JD48603- JD52190). Then the disk dissipated and the amplitude of V/R variability decreased significantly for six years (JD52527 - JD54712). In January 2009 (JD54856) began a second period of high V/R variability. In the second time interval (JD55042 - JD56303) we monitor two new V/R cycles.

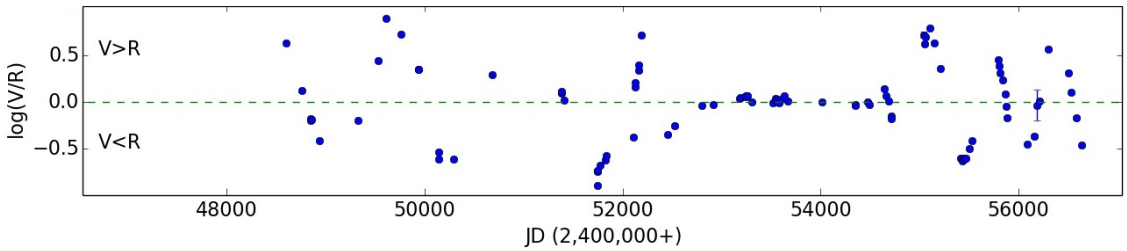

Figure 4.10: V/R variability of the source RX J0146.9+6121.

To find if the V/R cycle has any significant period we used NASA's periodogram service and in particular the LS periodogram (Lombe 1976; Scargle 1982).

We found a quasi-period of 1300 days, with p-value 1.7E-06, when the disk was bigger in size. In particular, the radius of the disk varied from 10 to $20R_\odot$ and possibly in the earliest measurements $R_H > 20R_\odot$. Then $V \approx R$ for 6 years indicating that the density perturbation in the disk faded away. At $\sim$ JD55000 the EW began to increase. When EW reached -10Å a new density perturbation formed with V/R quasi-period of 636 days, and p-value$<$ 0.001. Its radius varied roughly from 10 to $15R_\odot$. The low size of the disk as well as the short period of the V/R cycle, indicate that the density perturbation is closer to the Be star than it was before. In figure [4.12] we plot log(V/R) with the respective phase.

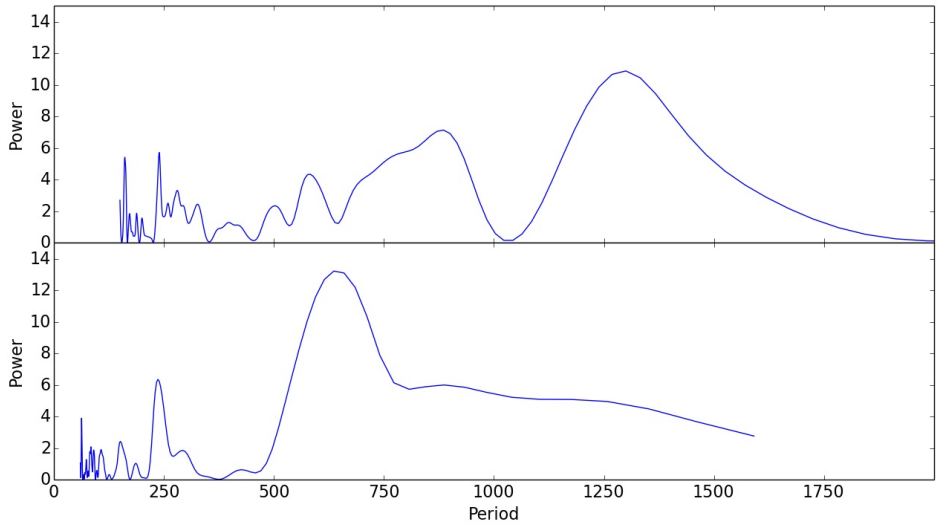

Figure 4.11: LS periodograms for the source RX J0146.9+6121. Upper panel: Period for the time interval JD48603 - JD52190. Lower panel: Period for the time interval JD55042 - JD56303.

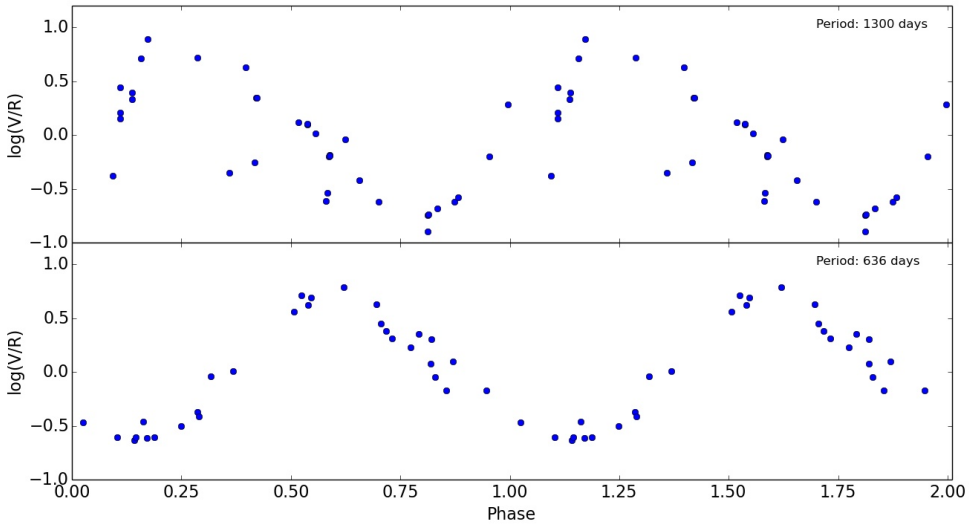

Figure 4.12: Plot of log(V/R) versus time phase. Upper panel: V/R cycle with 1300 days period. Lower panel: V/R cycle with 636 days period.

Other than RX J0146.9+6121, typical V/R variability can be seen in the systems 4U 0115+634, RX J0440.9+4431, 1A 0535+262 and IGR J06074+2205. In the earliest measurements of 4U 0115+634 and specifically in the time interval JD48252 - JD49340 we found two V/R cycles, the first with quasi-period of $\sim$ 750d and the second with $\sim$ 335d, figure [4.13].

Common behavior of the long-term V/R variability can be seen in the sources RX J0146.9+6121 (figure 4.10), RX J0440.9+4431, 1A 0535+262 and IGR J06074+2205.

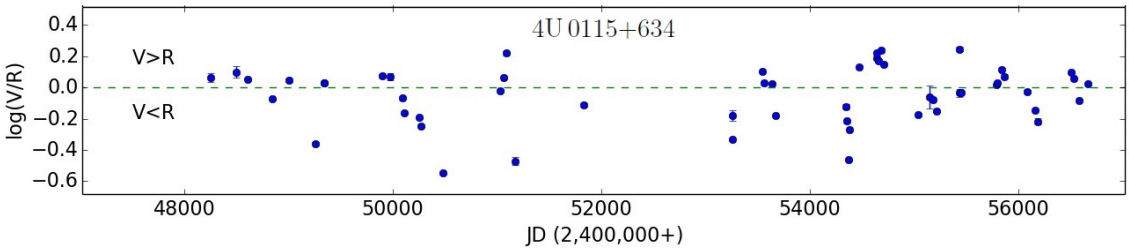

Figure 4.13: V/R variability of the source 4U 0115+634

During the period when the disk is almost dissipated, the emission lines of these systems have $|log(V/R)| < 0.1$. This behavior is expected because tenuous disks with very small sizes cannot support very large density waves.

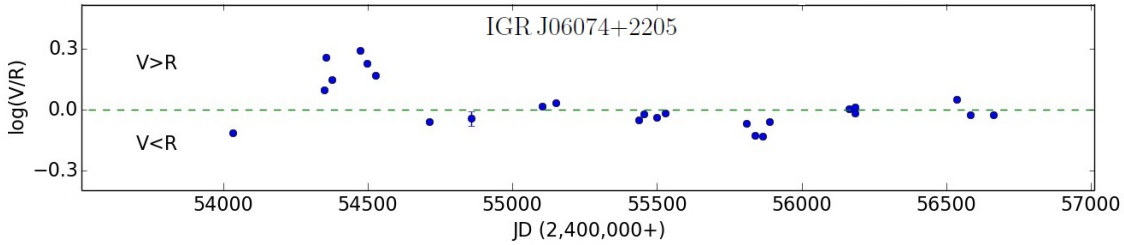

Figure 4.14: V/R variability of the source IGR J06074+2205

For RX J0440.9+4431, a new disk was formed between the time interval JD55056 - JD55529 and the system entered a period of X-ray activity. During this period we found: 1) a major amplitude increase of the log(V/R); 2) V/R cyclic behavior and specifically two cycles with quasi-periods of $\sim$ 470d and $\sim$ 370d.

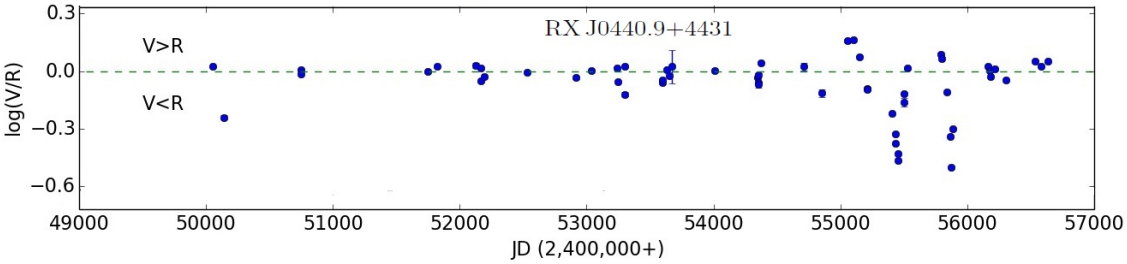

Figure 4.15: V/R variability of the source RX J0440.9+4431

Similarly, when 1A 0535+262 had a very large disk and showed high X-ray activity in the time interval JD54348 - JD55454, the asymmetry of the H_α emission line increased and we found at least one V/R cycle with quasi-period of $\sim$ 1100d.

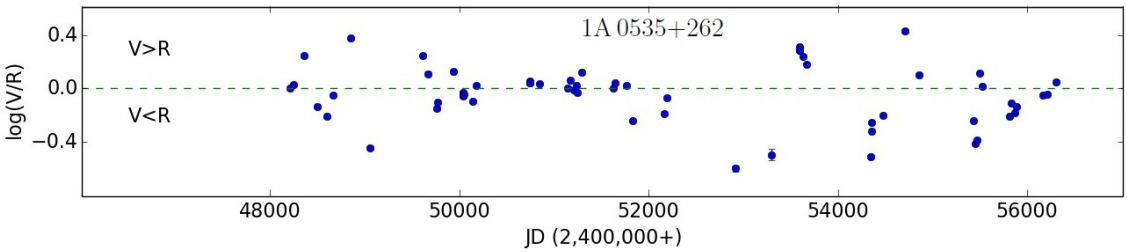

Figure 4.16: V/R variability of the source 1A 0535+262

Okazaki (1997) found that the periods of V/R variations in isolated Be stars range from years to decade, with a statistical mean of 7 years, which is much longer than the rotational period of the central star. In contrast, what we found here is that in BeXBs the V/R quasi-periods are significantly shorter (< 3.5yr) which can be interpreted as the result of smaller disks in BeXB because the neutron star affect significantly the structure and the size of the circumstellar disk.

Chapter 5

Conclusions

The aim of this project was to perform a global study of the optical spectral properties of Be/X-ray binary systems. We analyzed the optical spectroscopic data for the optical counterparts of 14 BeXBs and study the long-term variability of the H_α emission line. The reason to study so many different sources was to find: 1) if BeXBs share common properties as a group; 2) similarities or differences between Be stars, in a X-ray binary system, and isolated Be stars. At first we found evidence of the interaction of the neutron star and the disk in BeXBs. After major X-ray activity the strength and the shape of the H_α line exhibit significant changes. During the period when the Be star had a very large equatorial disk had undergone a type II X-ray outburst . Following the outbursts EW(H_α) declined which indicate the dissipation of the disk. Most of our sources followed the same trend, however this is not the case with sources XTE J1946+274 and KS 1947+300. Although both systems show very strong H_α emission lines, after a period of major X-ray activity the disk remains unaffected. In addition, based on the data analysis we found that the disks around the Be stars of the systems 4U 0115+634, RX J0146.9+6121, RX J0440.9+4431, 1A 0535+262, IGR J06074+2205 and GRO J2058+42 are quasi-Keplerian. So it is safe to assume that the disks formed in BeXBs have essentially Keplerian velocity. It is also confirmed by Hanuschik (1989) that the disks in a sample of 93 isolated Be stars are Keplerian and therefore the disk formation on both cases must be the same, although the neutron star in BeXBs prevents the disk from developing freely. We also found that the disks in BeXBs are smaller in size and denser than isolated Be Stars. From the data analysis rises also the confirmation of the correlation between EW(H_α) and the size of the disk R_H. This correlation can be seen in all sources in our collective data that showed long-term variability. Therefore the evolution of the H_α line and EW by extension must be the prime indicator of the physical state of the disk. Finally, from the study of the V/R variability we conclude that the effects of the density perturbation do not appear until the disk is properly developed. This fact can be seen in the cases of BeXBs 4U 0115+634, RX J0146.9+6121, RX J0440.9+4431, 1A 0535+262, IGR J06074+2205 and SAX J2103.5+4545, where the V/R cyclic behavior coincides with the observation of a fully developed circumstellar disk. Also the V/R quasi-periods of BeXBs are much shorter (< 3.5 years) than the quasi-periods of isolated Be stars which range from years to decades with statistical mean of 7 years (Okazaki 1997).

Appendix A

Evolution of the H_α Line

In this chapter we present the plots that show the evolution of the H_α emission line, for the 14 BeXBs 4U 0115+634, IGR J01363+6610, RX J0146.9+6121, IGR J01583+6713, V 0332+530, RX J0440.9+4431, A 0535+262, IGR J06074+2205, XTE J1946+274, KS 1947+300, GRO J2058+42, SAX J2103.5+4545, 4U 2206+54 and SAX J2239.3+6116.

4U 0115+634

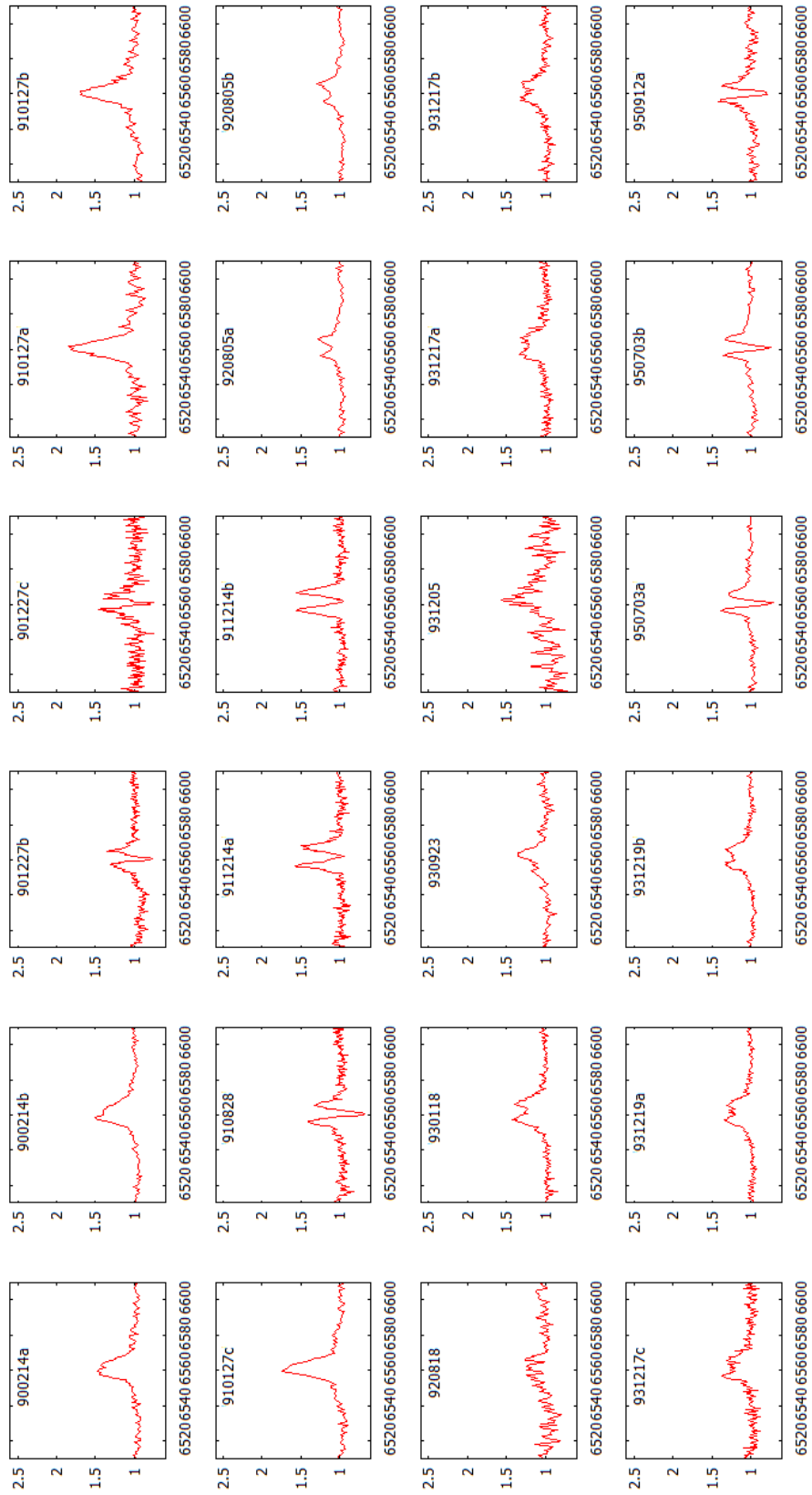
900214a
900214b
901227b
901227c
910127a
910127b
910127c
910828
911214a
911214b
920805a
920805b
920818
930118
930923
931205
931217a
931217b
931217c
931219a
931219b
950703a
950703b
950912a
2.5
2
1.5
1
6520 6540 6560 6580 6600

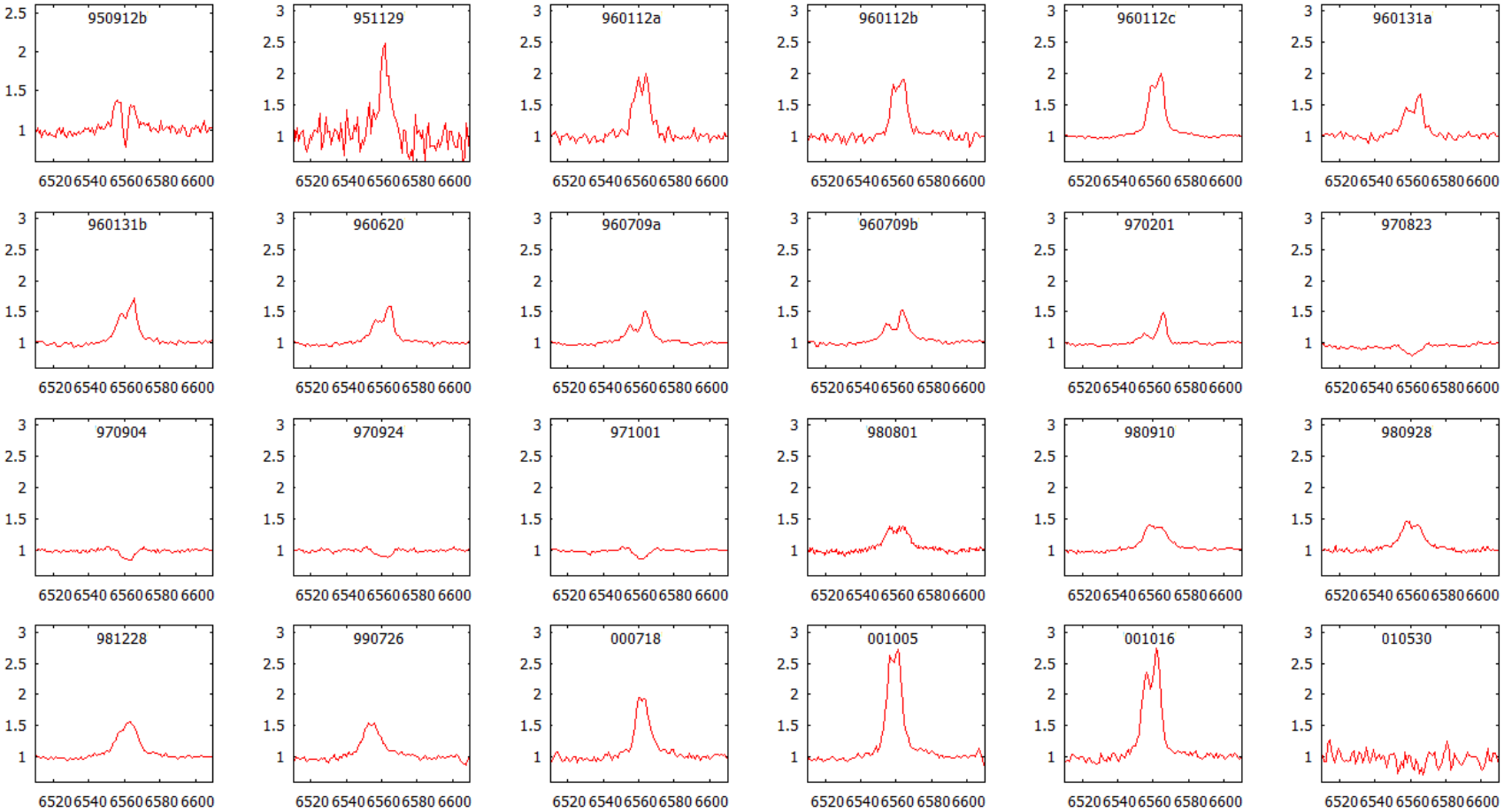
950912b
951129
960112a
960112b
960112c
960131a
960131b
960620
960709a
960709b
970201
970823
970904
970924
971001
980801
980910
980928
981228
990726
000718
001005
001016
010530
2.5
2
1.5
1
3
6520 6540 6560 6580 6600

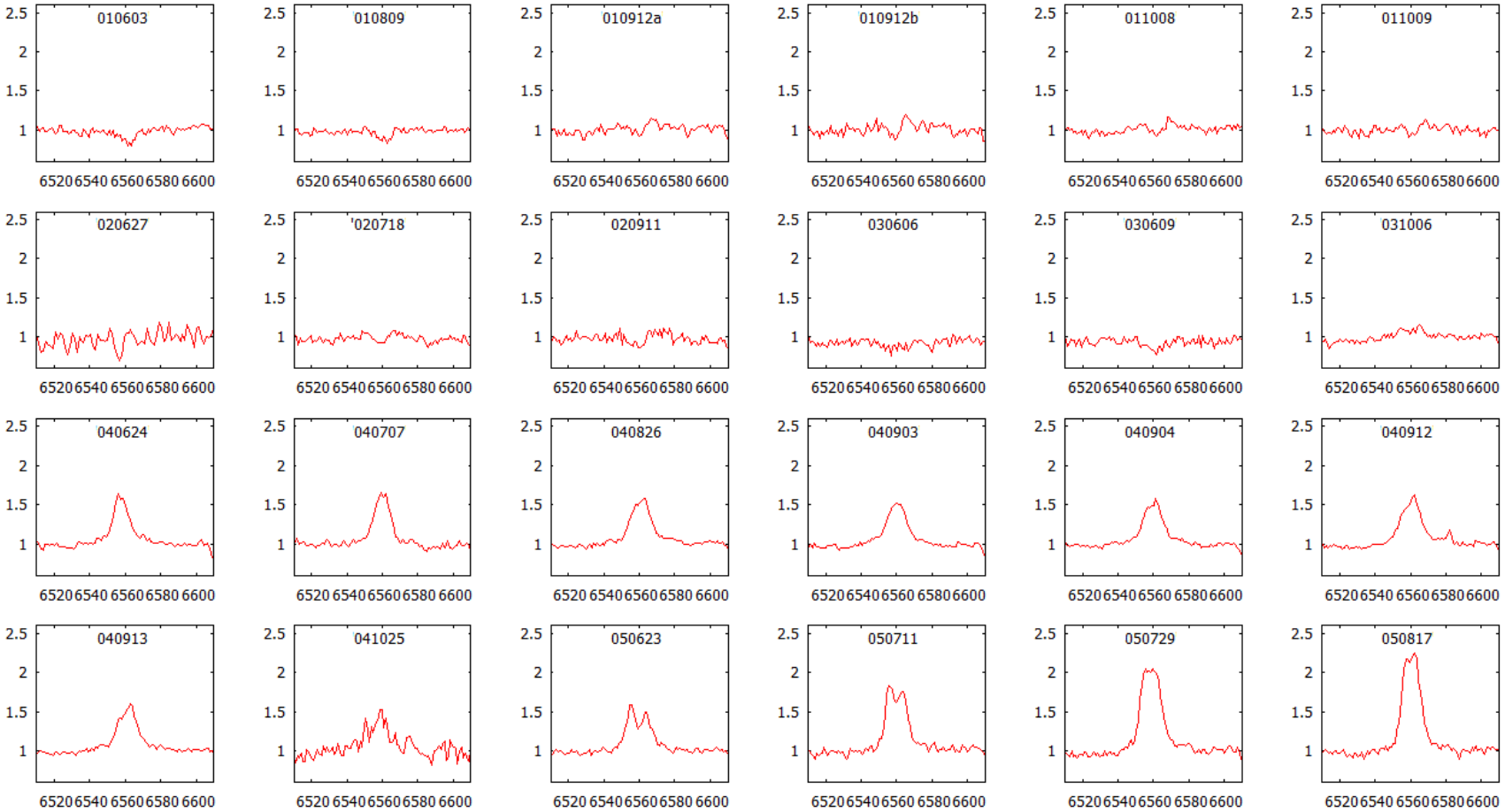
010603
010809
010912a
010912b
011008
011009
020627
'020718
020911
030606
030609
031006
040624
040707
040826
040903
040904
040912
040913
041025
050623
050711
050729
050817
2.5
2
1.5
1
6520 6540 6560 6580 6600

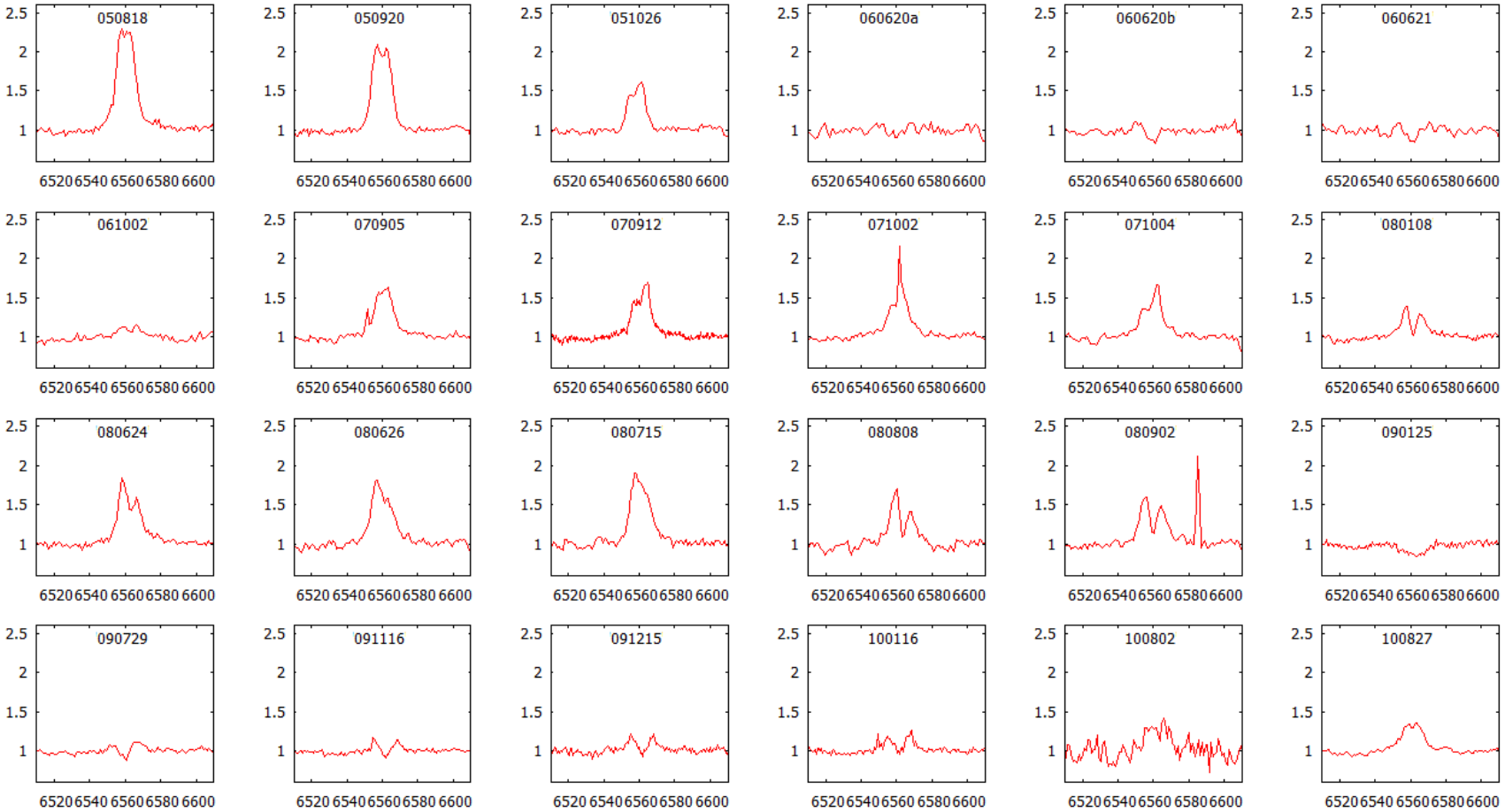
050818
050920
051026
060620a
060620b
060621
061002
070905
070912
071002
071004
080108
080624
080626
080715
080808
080902
090125
090729
091116
091215
100116
100802
100827
2.5
2
1.5
1
6520 6540 6560 6580 6600

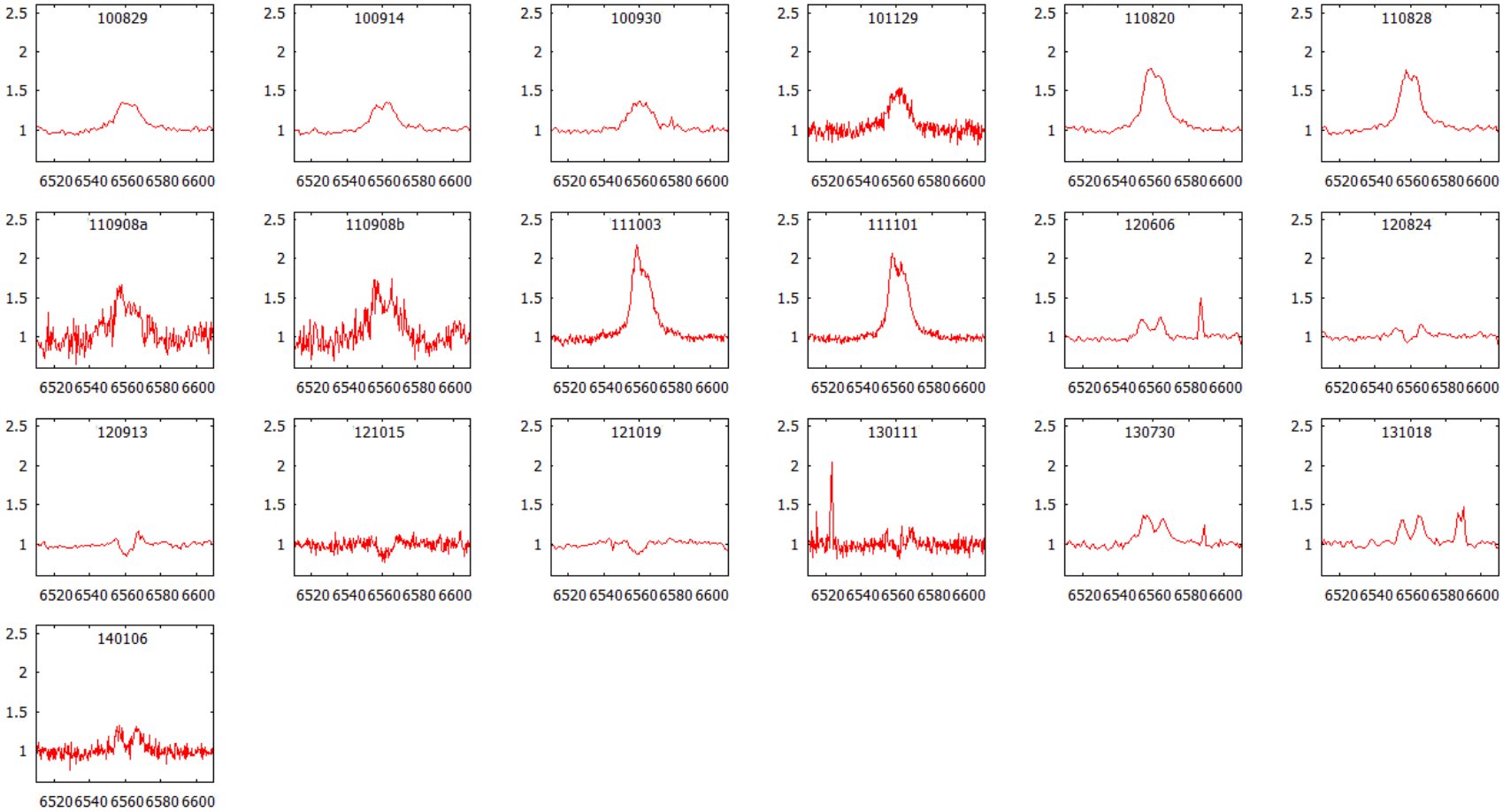
100829
100914
100930
101129
110820
110828
110908a
110908b
111003
111101
120606
120824
120913
121015
121019
130111
130730
131018
140106
2.5
2
1.5
1
6520 6540 6560 6580 6600

IGR J01363+6610

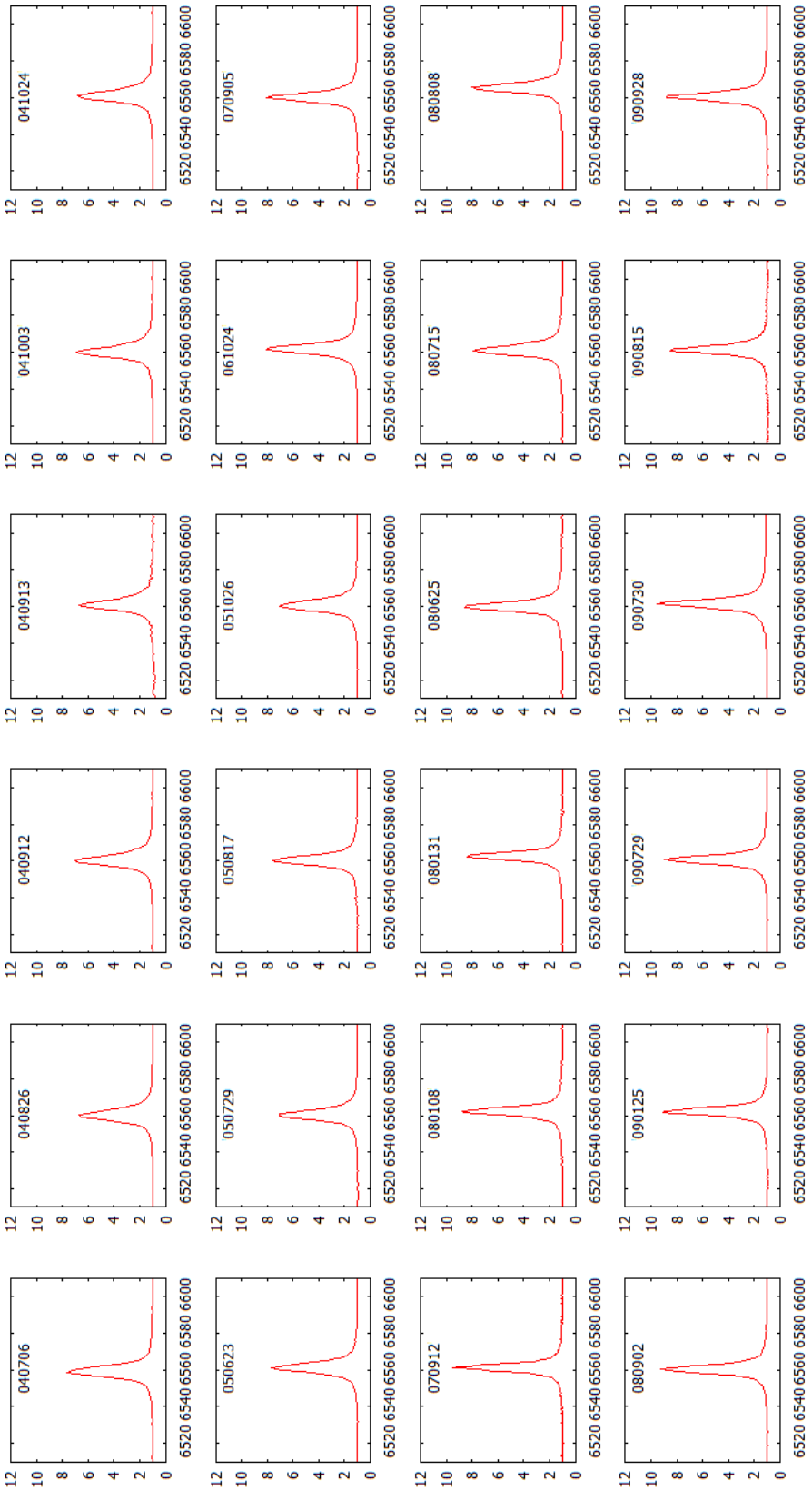

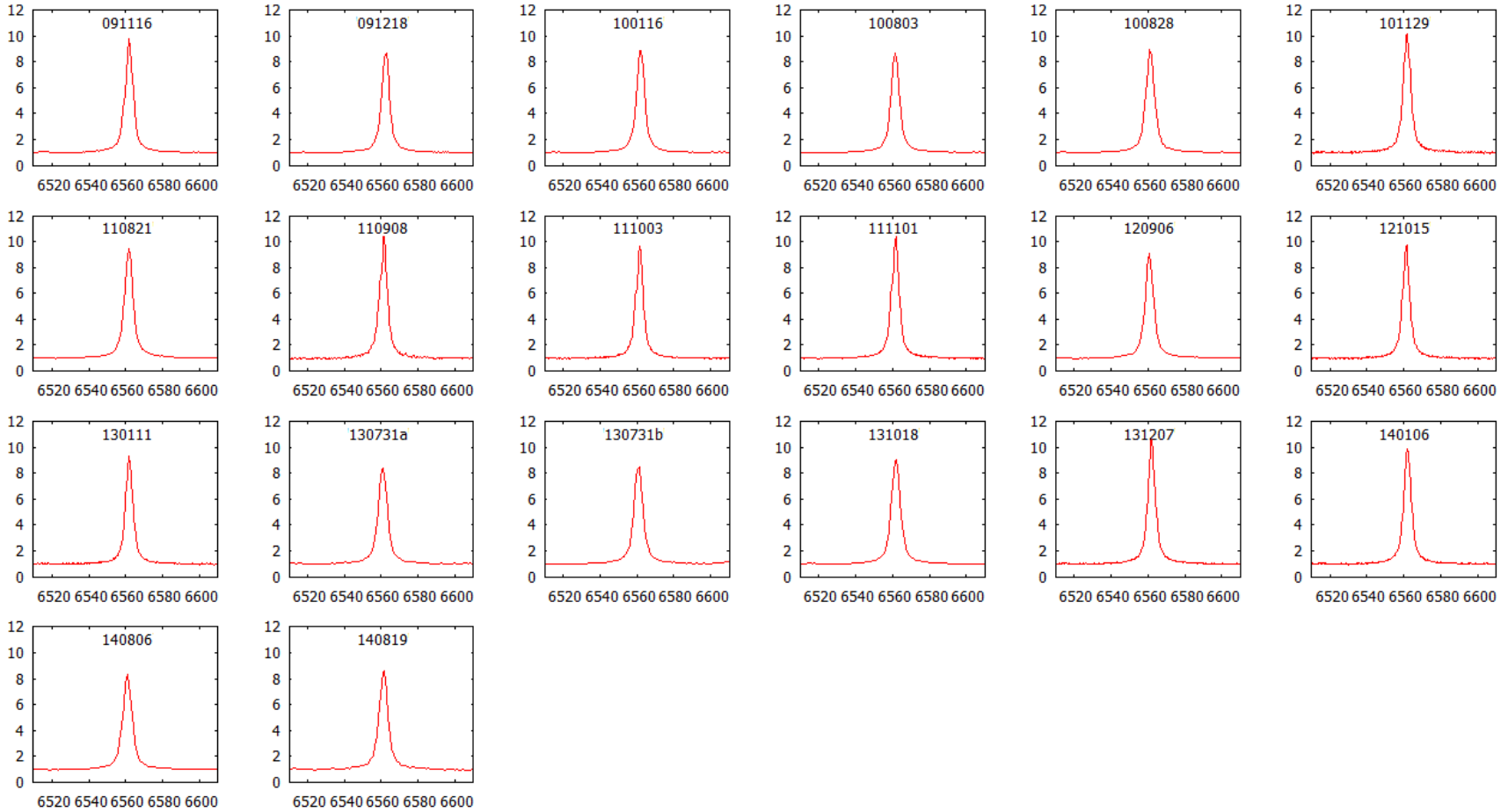
091116
091218
100116
100803
100828
101129
110821
110908
111003
111101
120906
121015
130111
130731a
130731b
131018
131207
140106
140806
140819
0 2 4 6 8 10 12
6520 6540 6560 6580 6600

RX J0146.9+6121

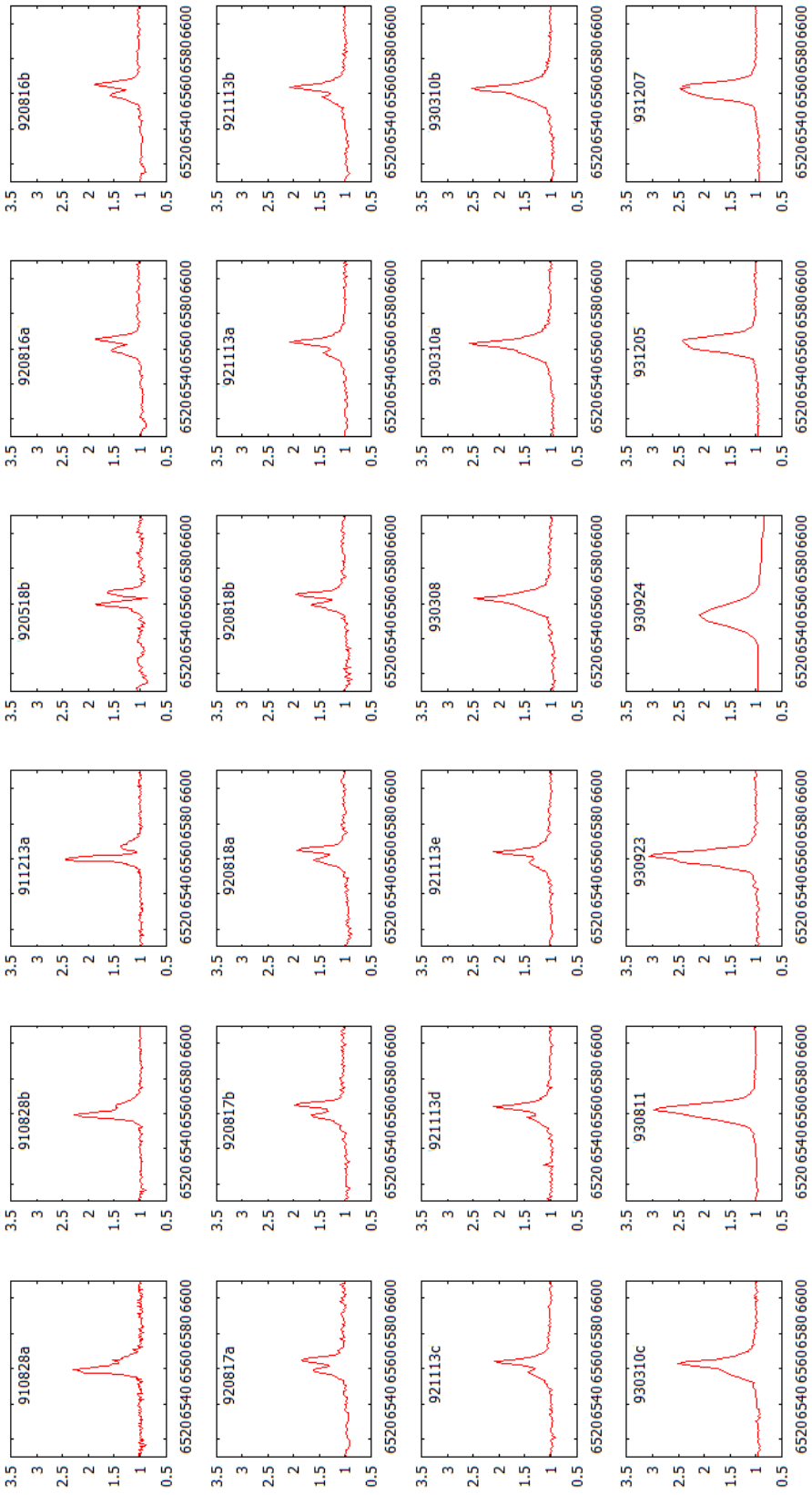

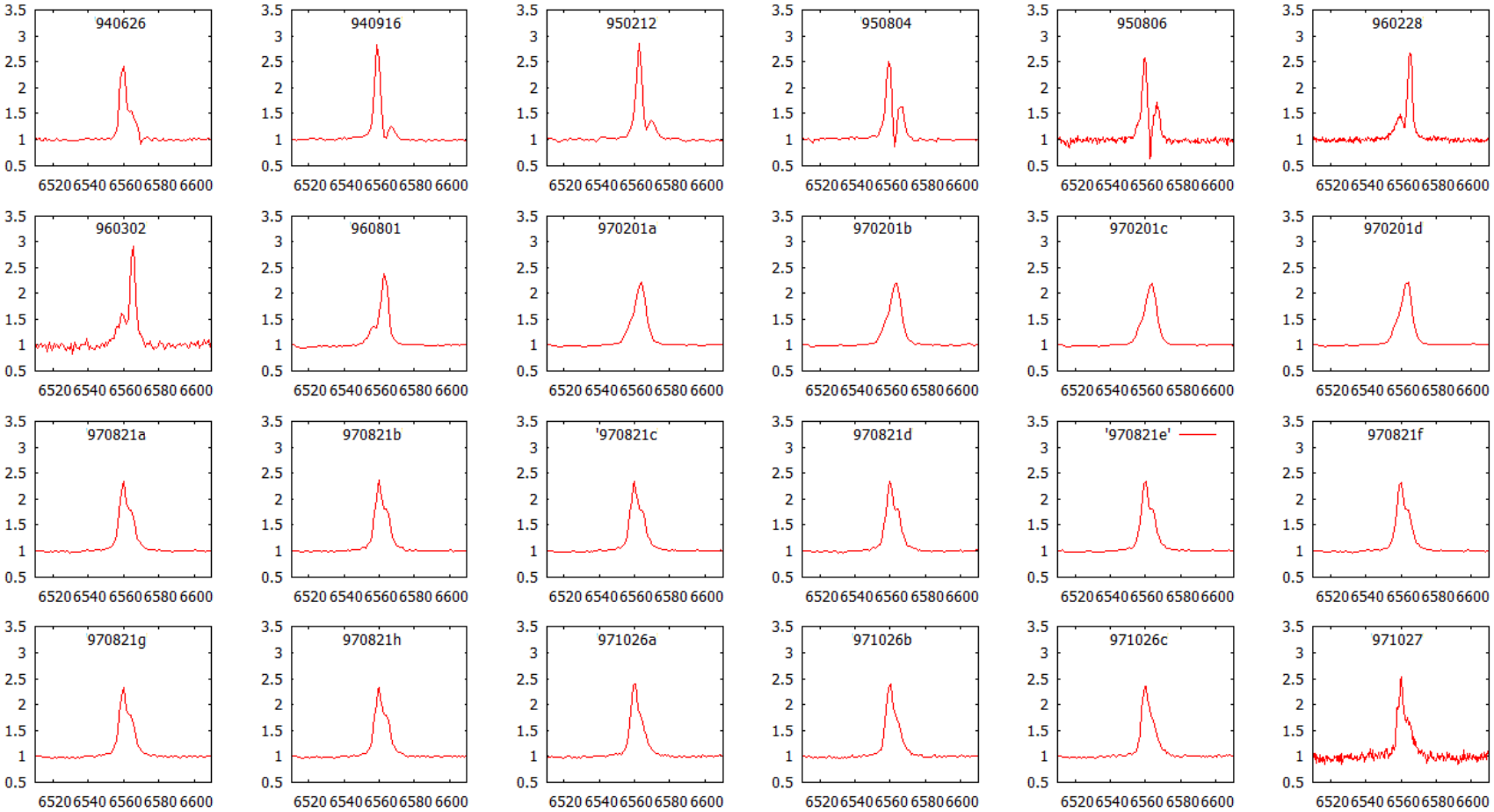
940626
940916
950212
950804
950806
960228
960302
960801
970201a
970201b
970201c
970201d
970821a
970821b
'970821c
970821d
'970821e'
970821f
970821g
970821h
971026a
971026b
971026c
971027
3.5
3
2.5
2
1.5
1
0.5
6520 6540 6560 6580 6600

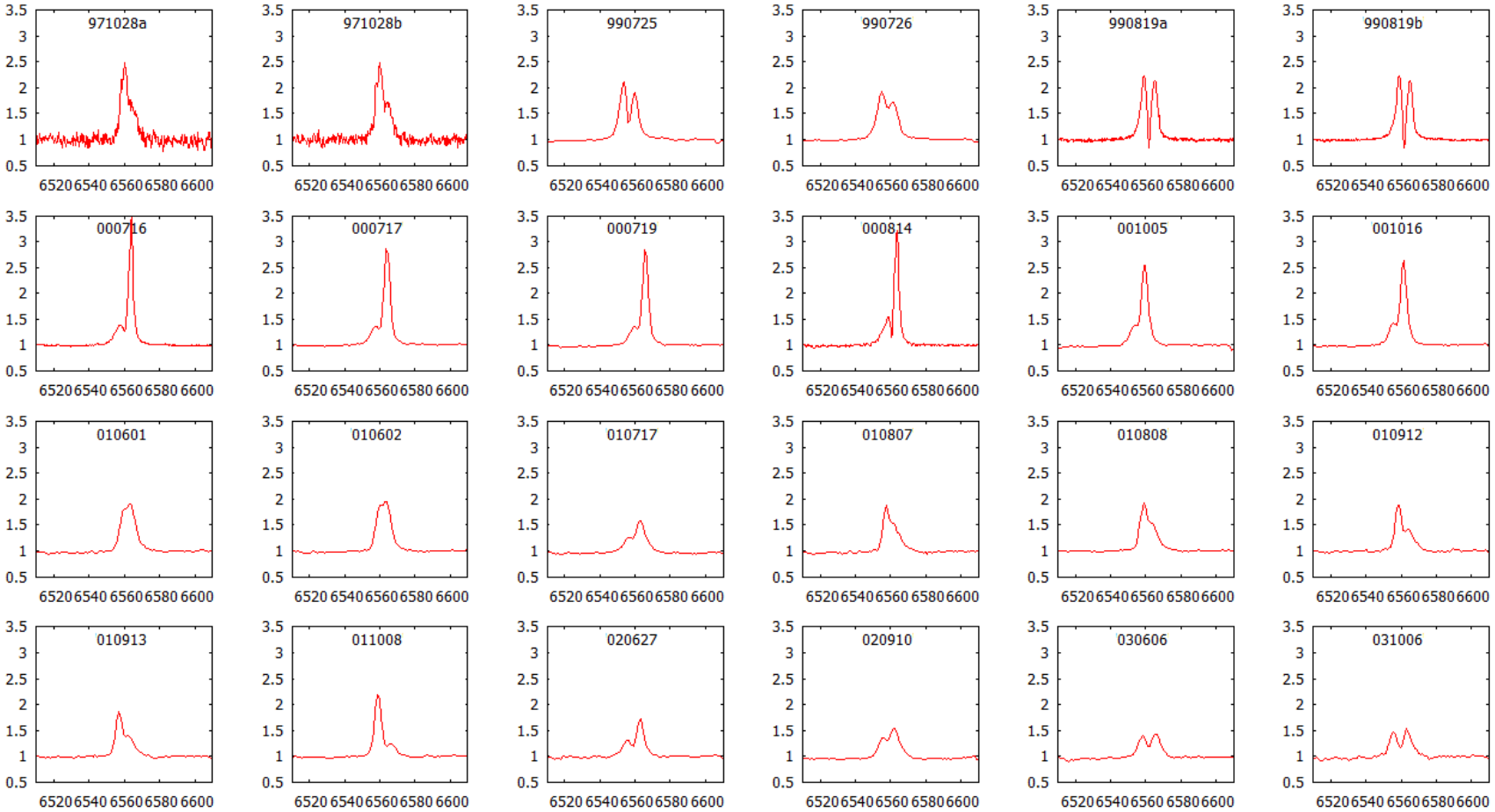
971028a
971028b
990725
990726
990819a
990819b
000716
000717
000719
000814
001005
001016
010601
010602
010717
010807
010808
010912
010913
011008
020627
020910
030606
031006
3.5
3
2.5
2
1.5
1
0.5
6520 6540 6560 6580 6600

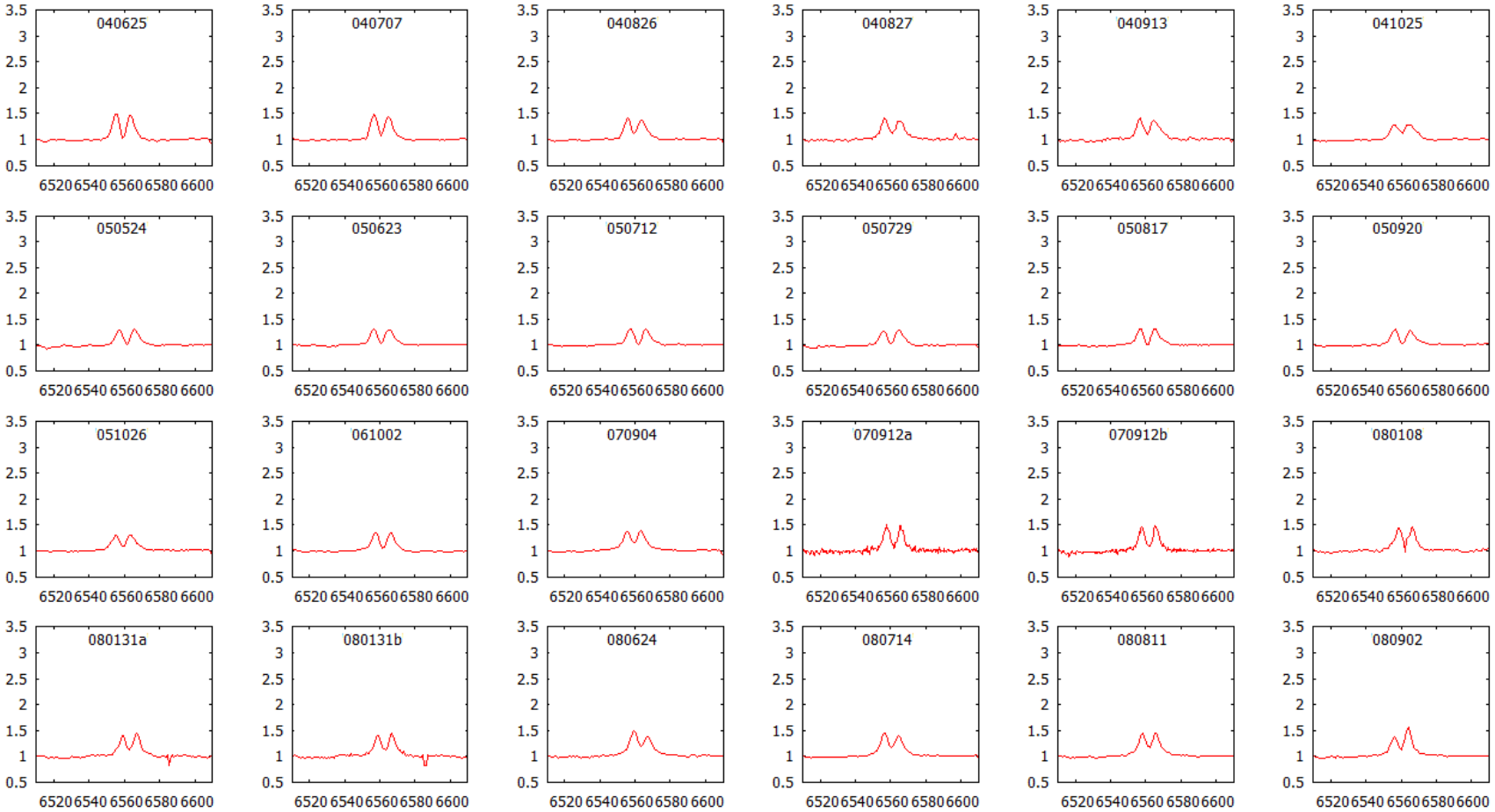
040625
040707
040826
040827
040913
041025
050524
050623
050712
050729
050817
050920
051026
061002
070904
070912a
070912b
080108
080131a
080131b
080624
080714
080811
080902
3.5
3
2.5
2
1.5
1
0.5
6520 6540 6560 6580 6600

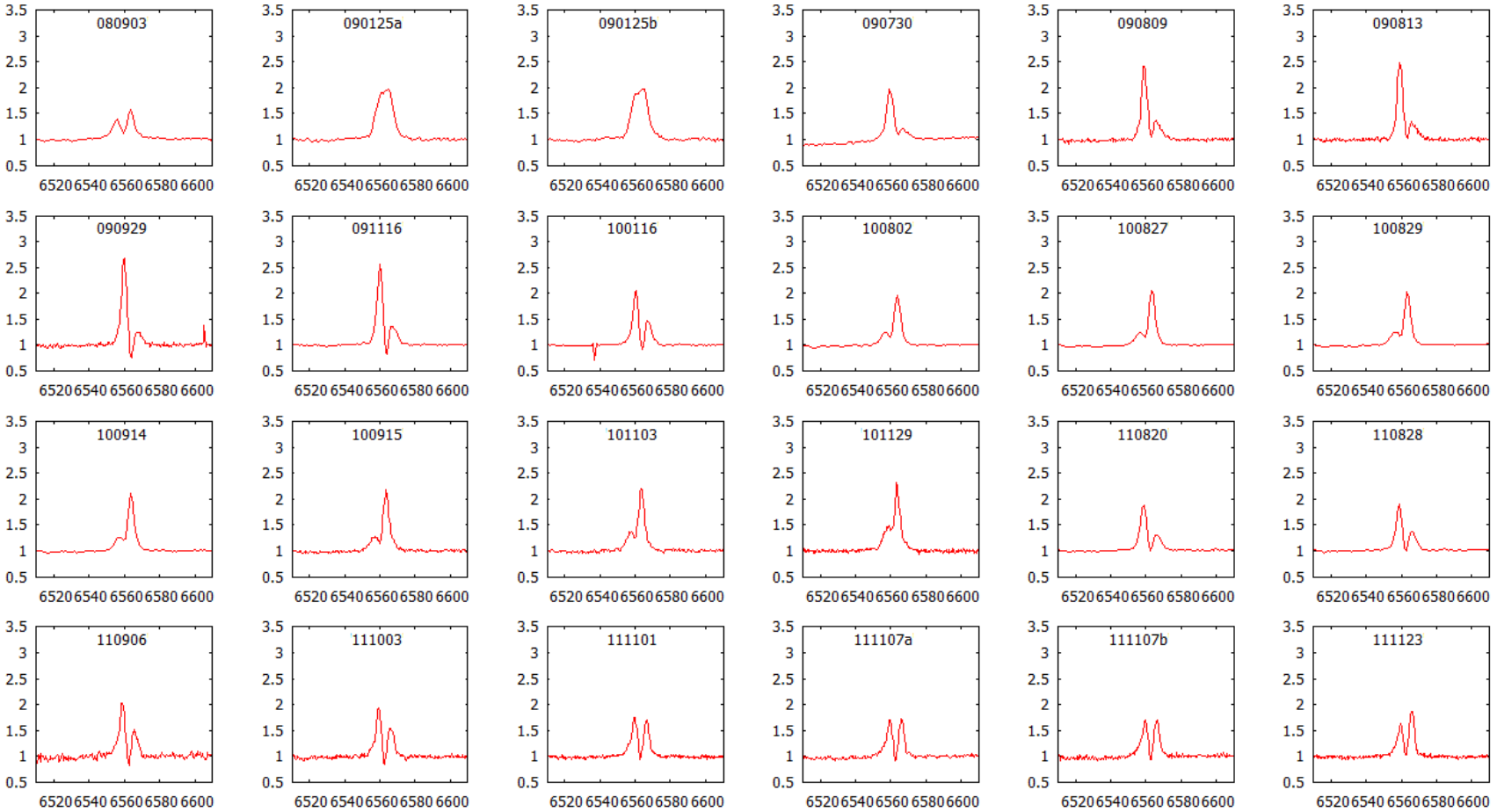
080903
090125a
090125b
090730
090809
090813
090929
091116
100116
100802
100827
100829
100914
100915
101103
101129
110820
110828
110906
111003
111101
111107a
111107b
111123
3.5
3
2.5
2
1.5
1
0.5
6520 6540 6560 6580 6600

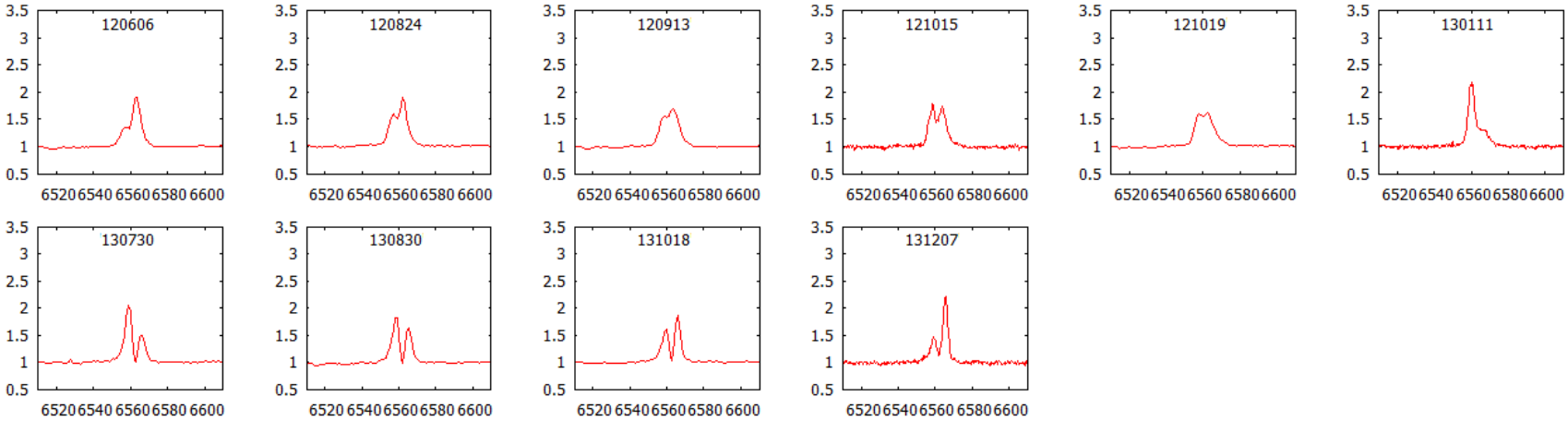
120606
120824
120913
121015
121019
130111
130730
130830
131018
131207
3.5
3
2.5
2
1.5
1
0.5
6520 6540 6560 6580 6600

IGR J01583+6713

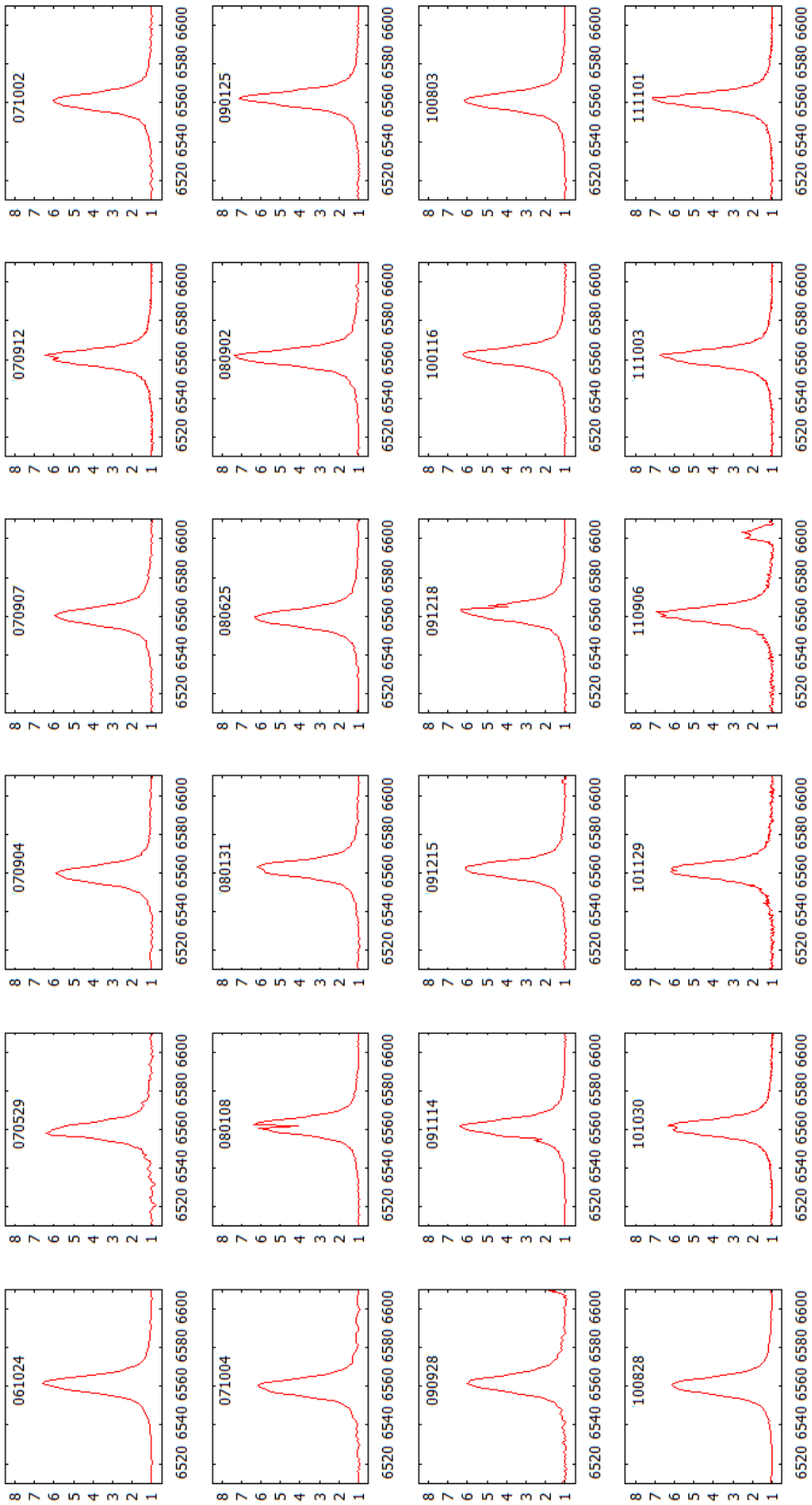

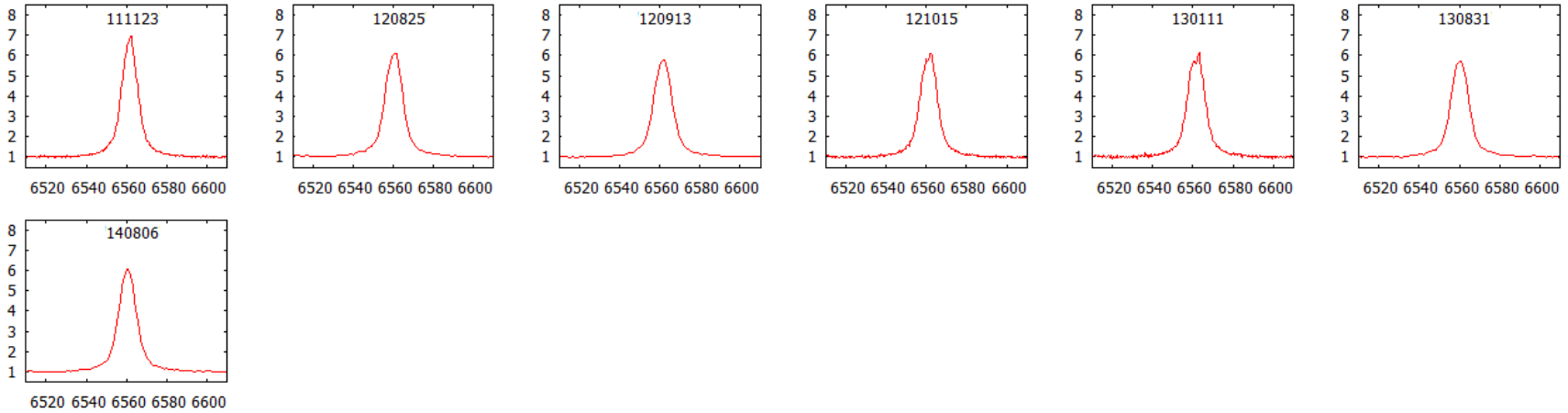
111123
120825
120913
121015
130111
130831
140806
8
7
6
5
4
3
2
1
6520 6540 6560 6580 6600

V 0332+53

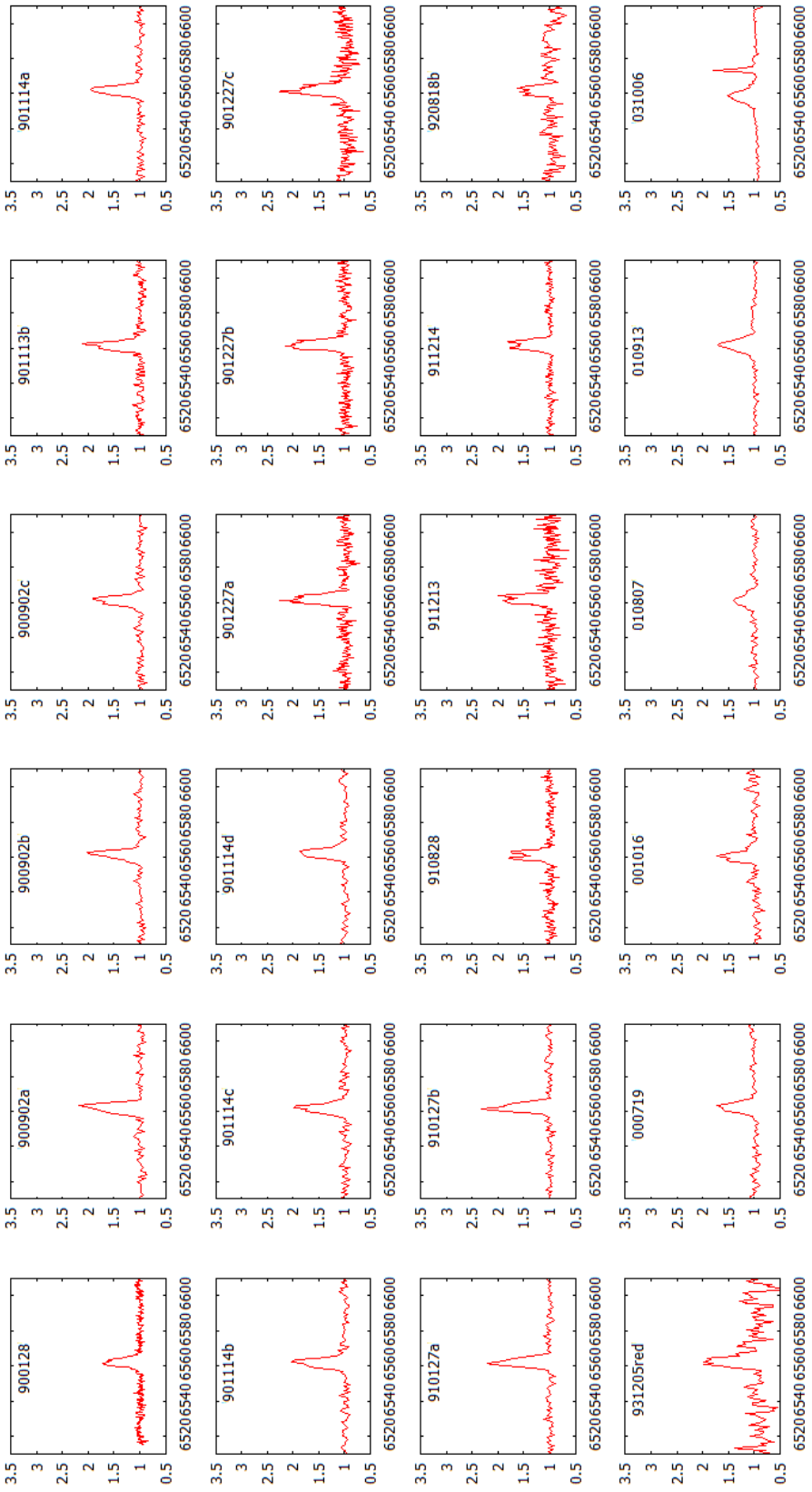
900128
900902a
900902b
900902c
901113b
901114a
901114b
901114c
901114d
901227a
901227b
901227c
910127a
910127b
910828
911213
911214
920818b
931205red
000719
001016
010807
010913
031006
3.5
3
2.5
2
1.5
1
0.5
6520 6540 6560 6580 6600

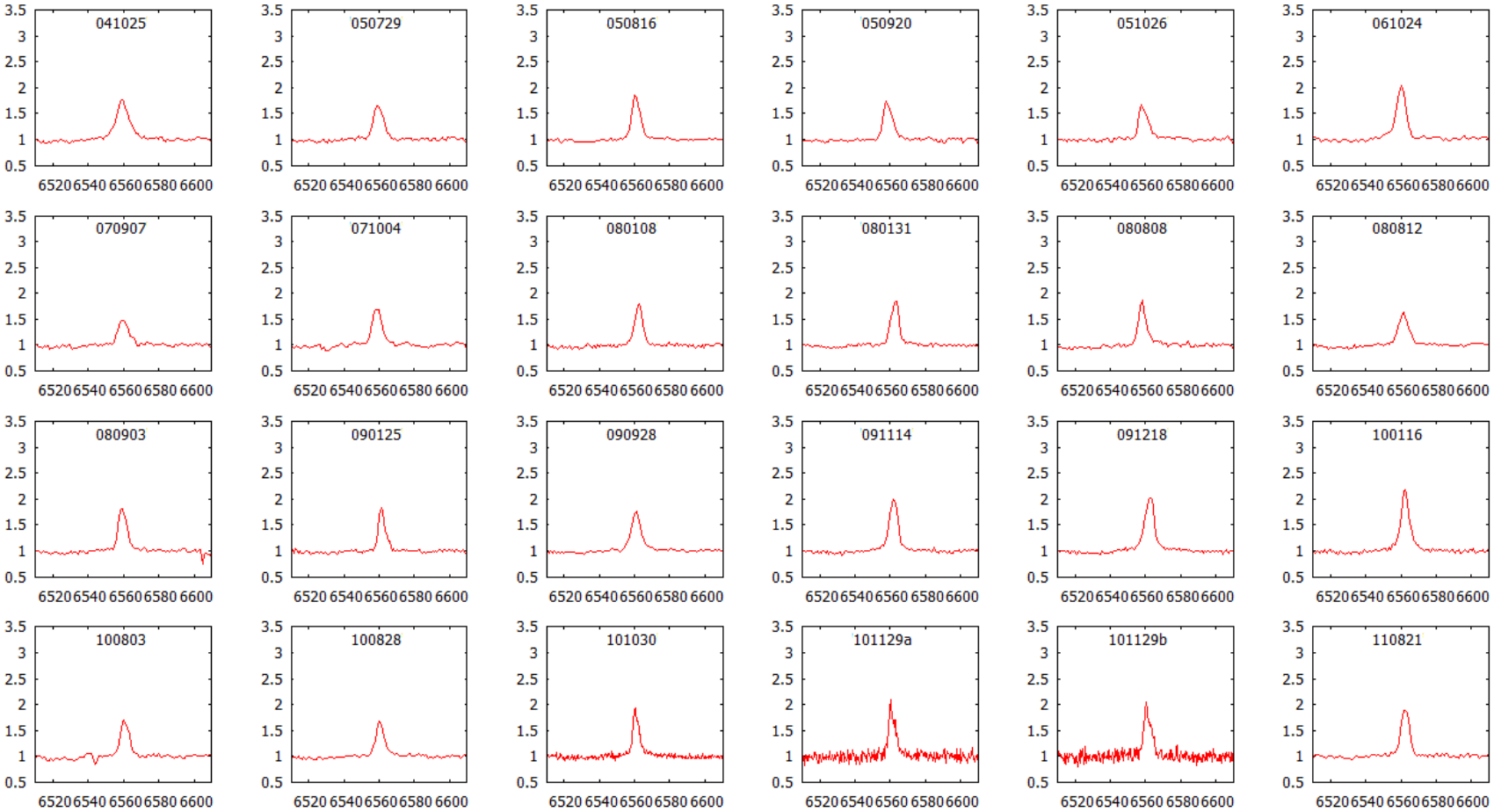
041025
050729
050816
050920
051026
061024
070907
071004
080108
080131
080808
080812
080903
090125
090928
091114
091218
100116
100803
100828
101030
101129a
101129b
110821
3.5
3
2.5
2
1.5
1
0.5
6520 6540 6560 6580 6600

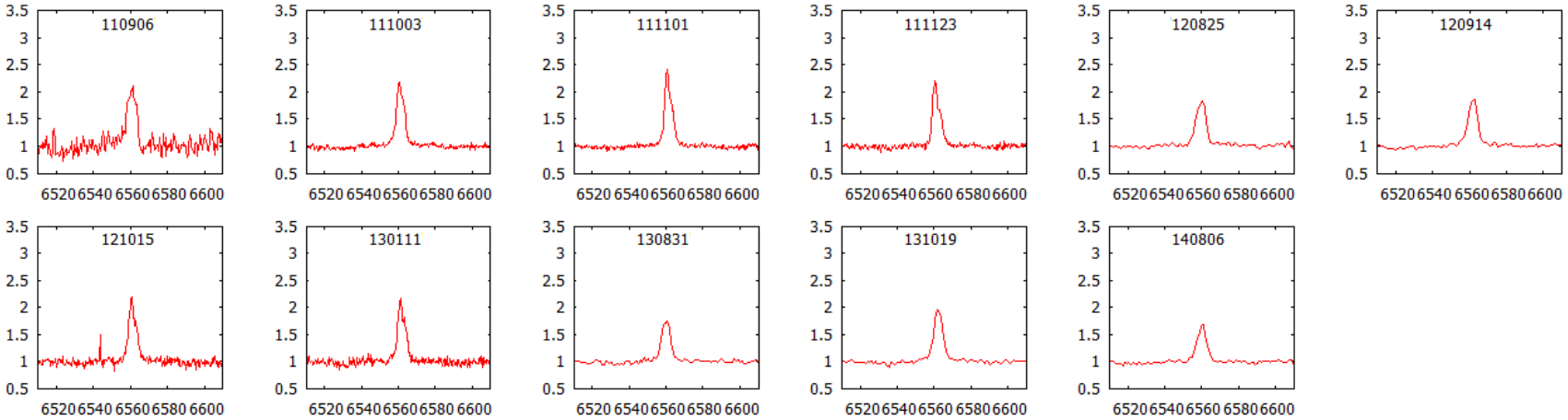
110906
111003
111101
111123
120825
120914
121015
130111
130831
131019
140806
3.5
3
2.5
2
1.5
1
0.5
6520 6540 6560 6580 6600

RX J0440.9+4431

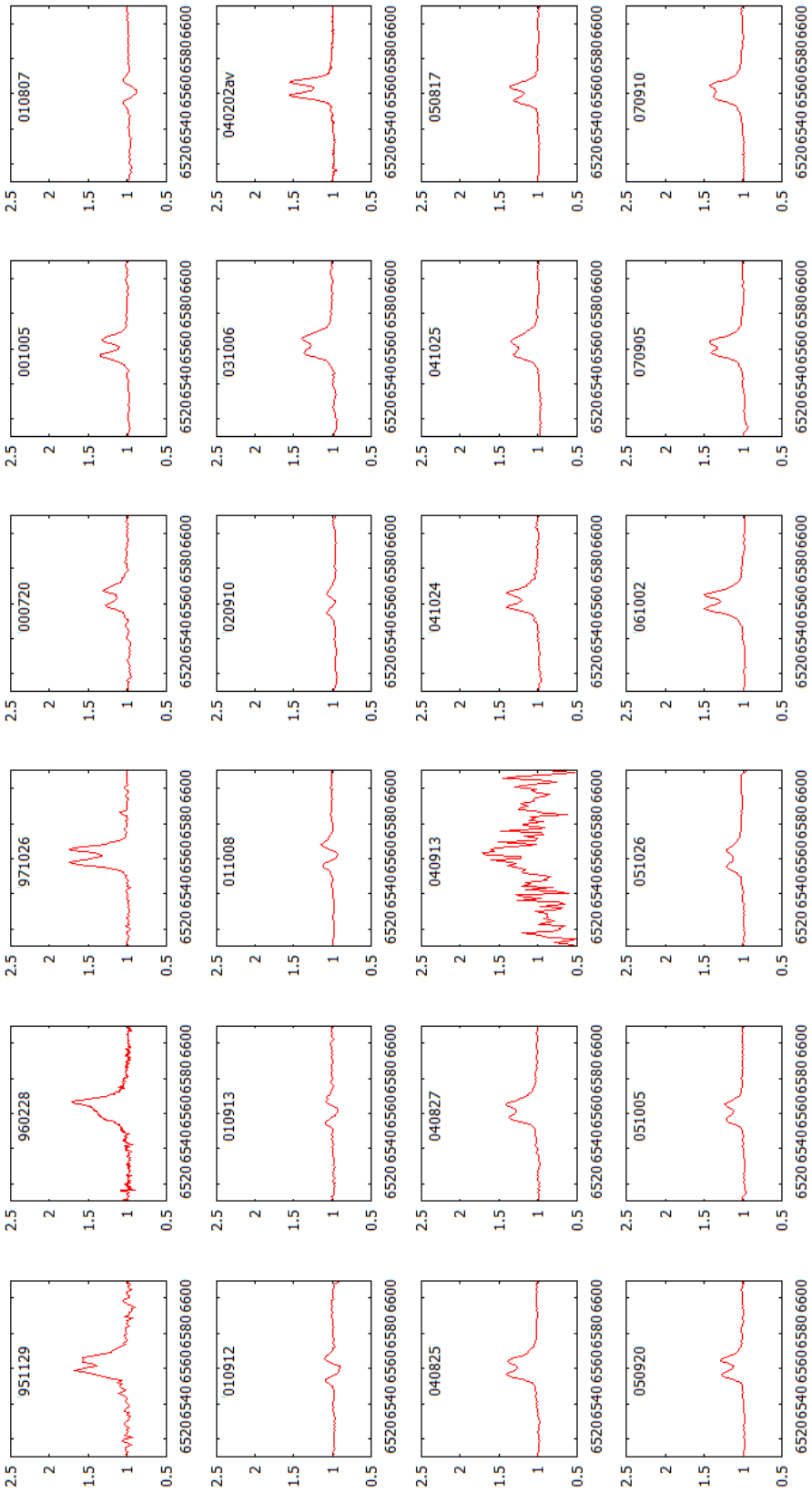

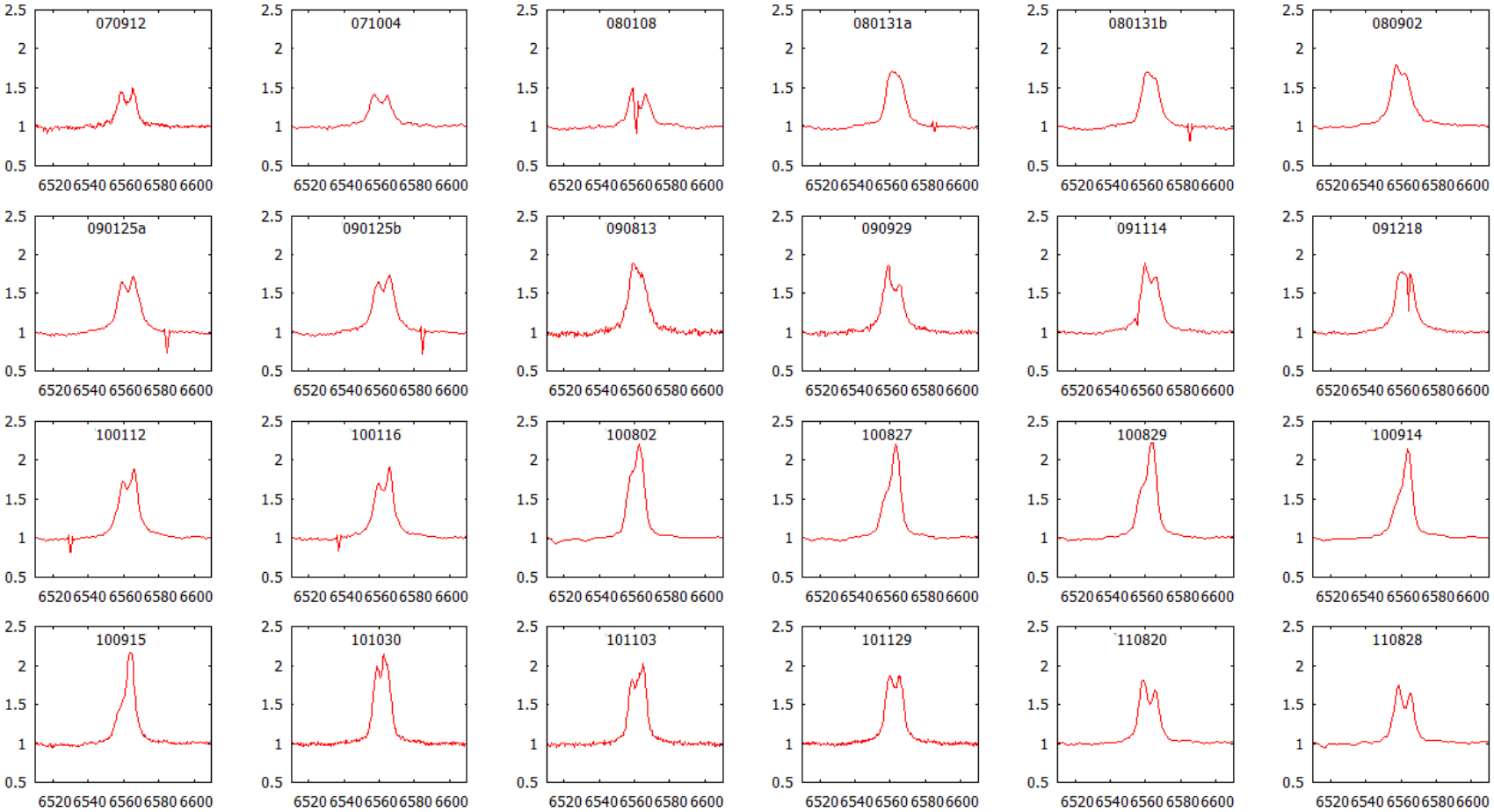
070912
071004
080108
080131a
080131b
080902
090125a
090125b
090813
090929
091114
091218
100112
100116
100802
100827
100829
100914
100915
101030
101103
101129
110820
110828
2.5
2
1.5
1
0.5
6520 6540 6560 6580 6600

111003
111101
111107av
111123
120825
120906
120914
121015
130111
130830
131018
131207
2.5
2
1.5
1
0.5
6520 6540 6560 6580 6600

1A 0535+262

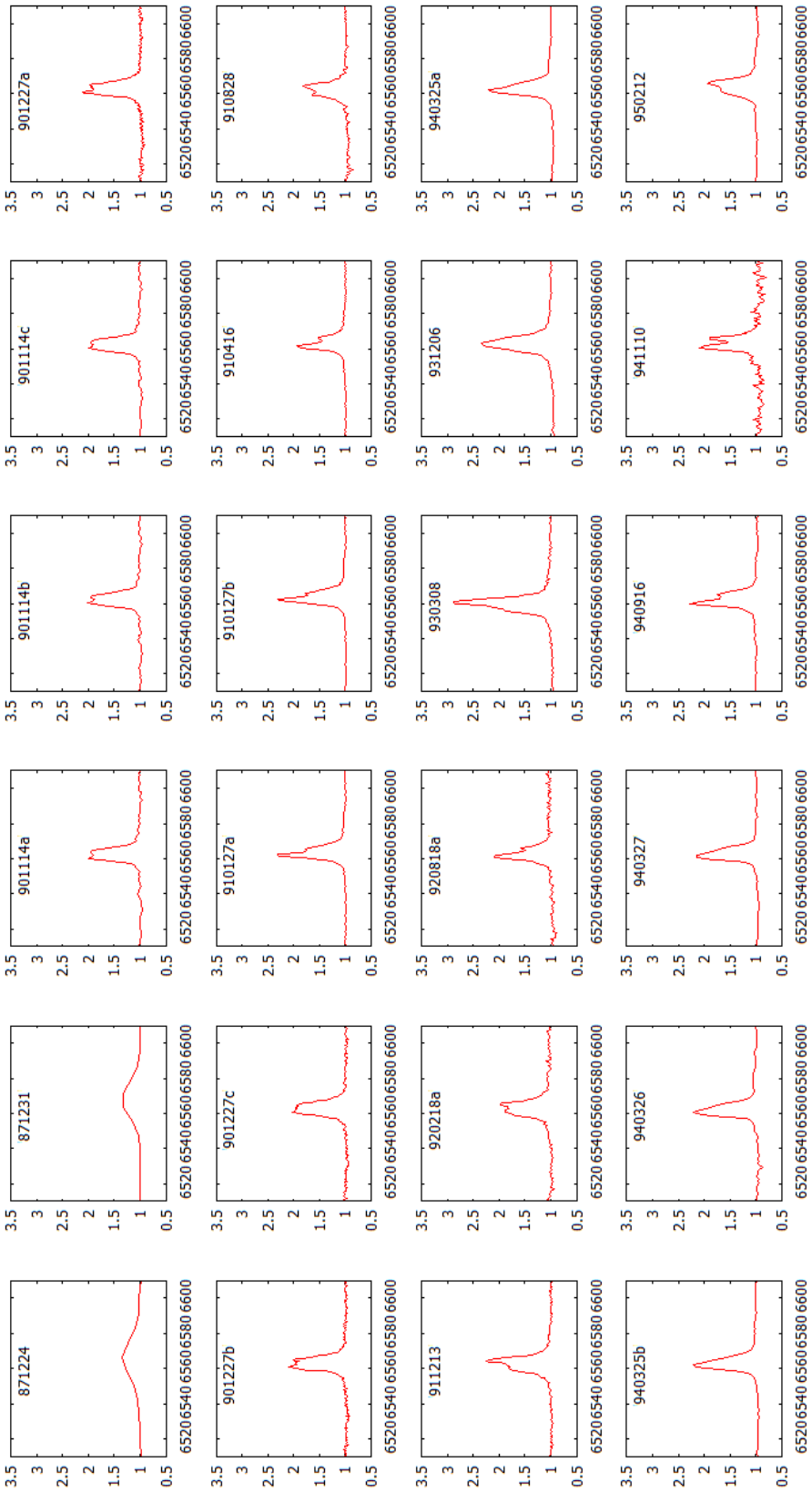
871224
871231
901114a
901114b
901114c
901227a
901227b
901227c
910127a
910127b
910416
910828
911213
920218a
920818a
930308
931206
940325a
940325b
940326
940327
940916
941110
950212

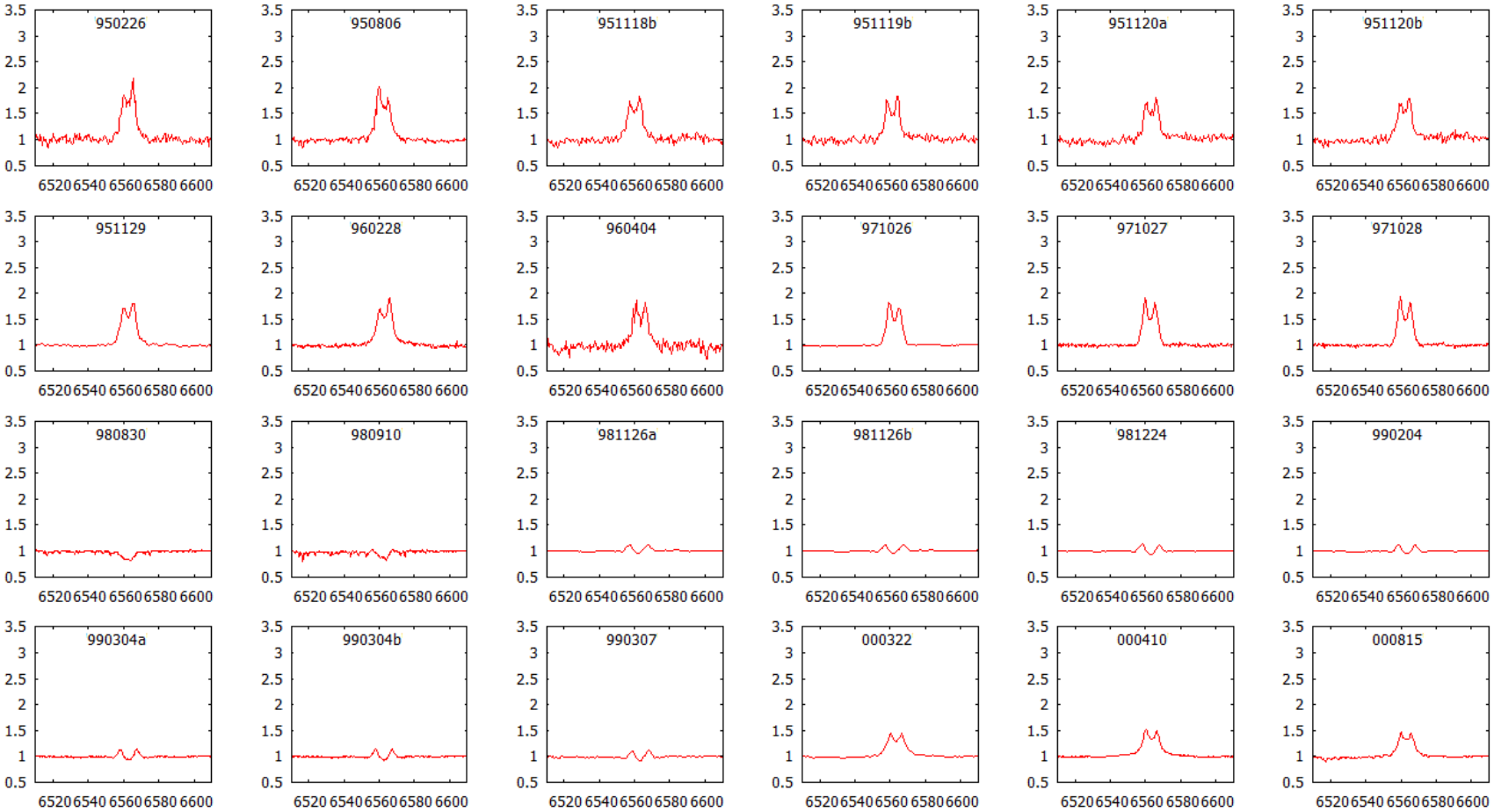
950226
950806
951118b
951119b
951120a
951120b
951129
960228
960404
971026
971027
971028
980830
980910
981126a
981126b
981224
990204
990304a
990304b
990307
000322
000410
000815
3.5
3
2.5
2
1.5
1
0.5
6520 6540 6560 6580 6600

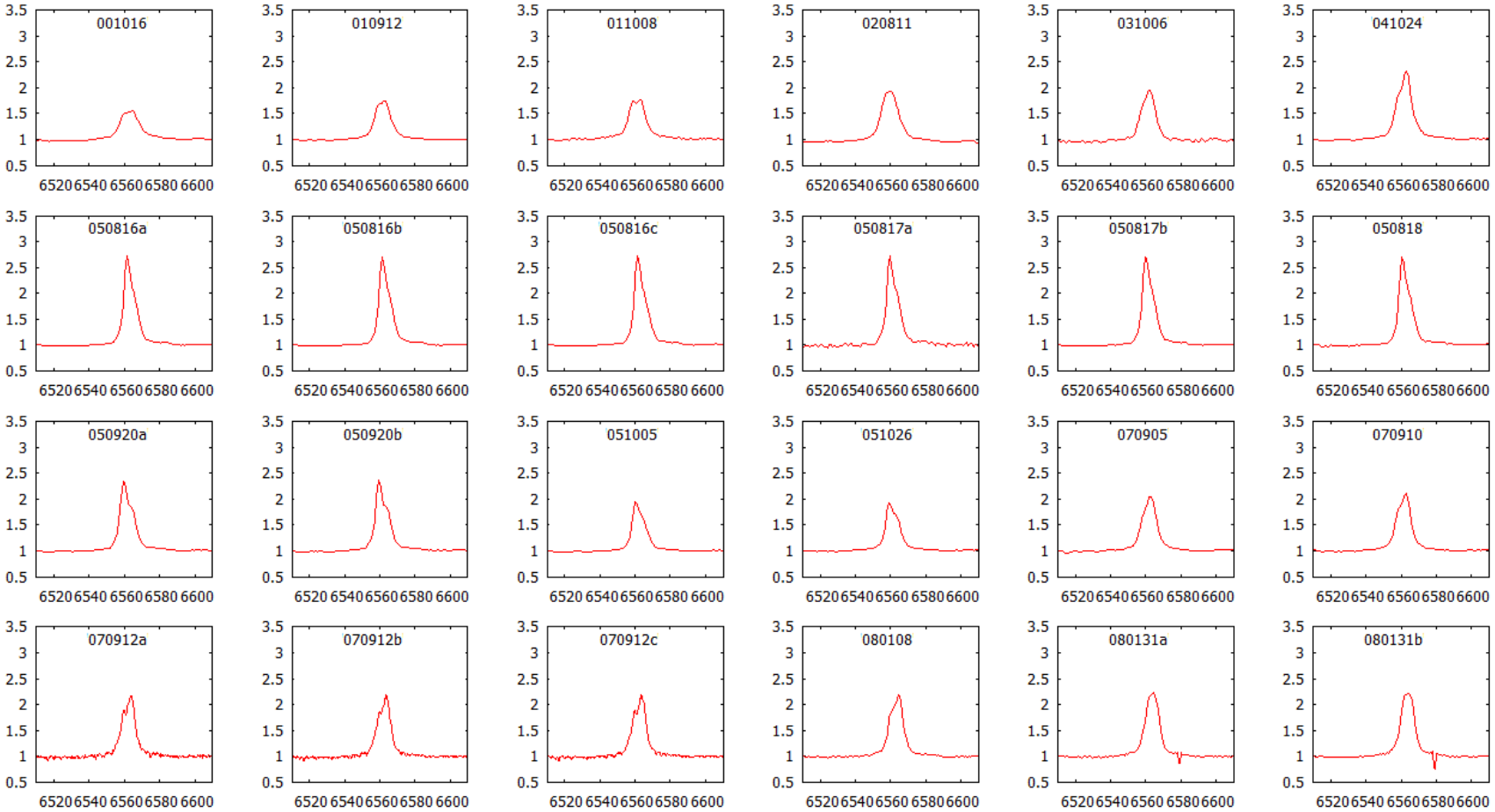
001016
010912
011008
020811
031006
041024
050816a
050816b
050816c
050817a
050817b
050818
050920a
050920b
051005
051026
070905
070910
070912a
070912b
070912c
080108
080131a
080131b
3.5
3
2.5
2
1.5
1
0.5
6520 6540 6560 6580 6600

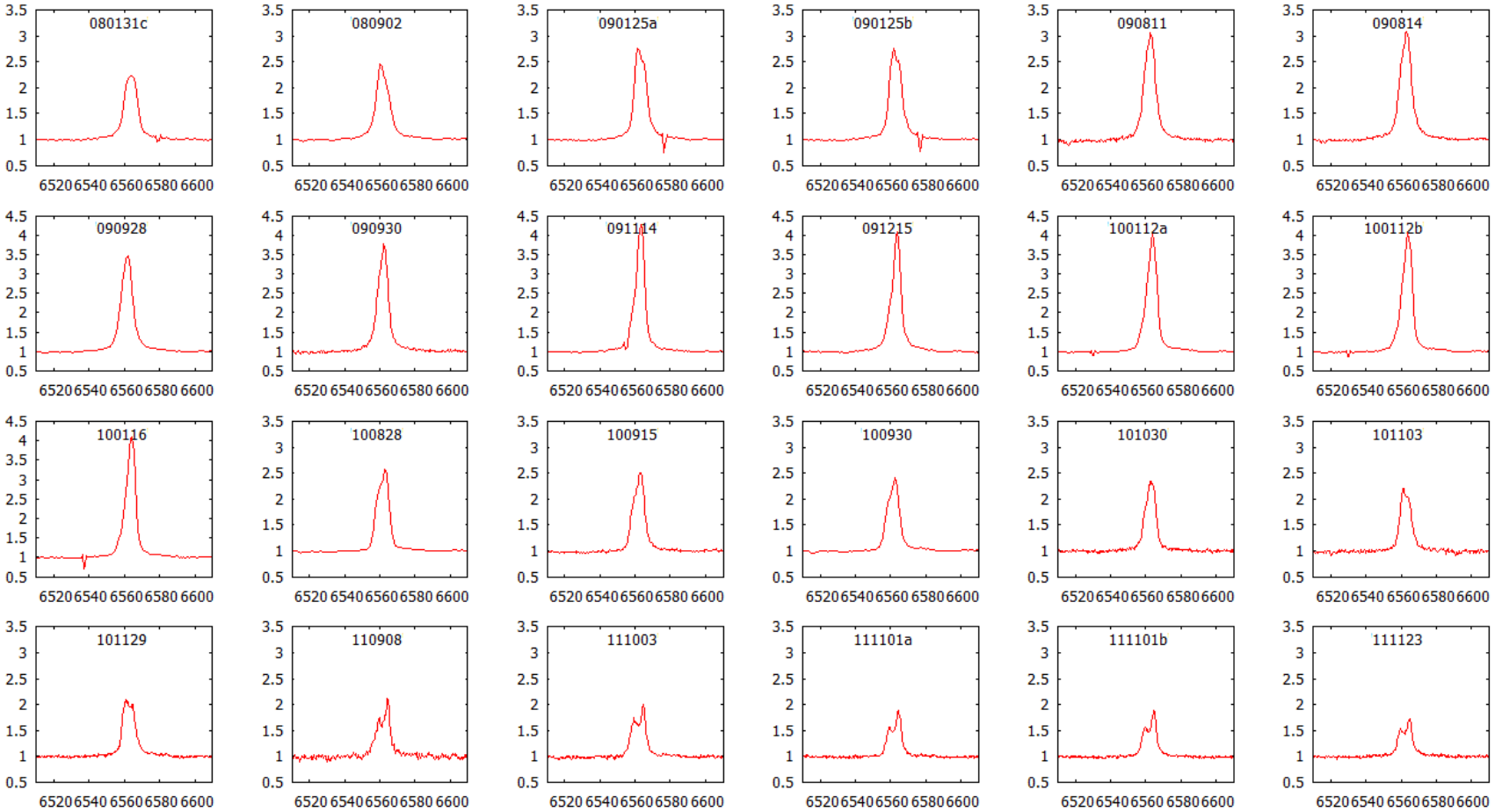
080131c
080902
090125a
090125b
090811
090814
090928
090930
091114
091215
100112a
100112b
100116
100828
100915
100930
101030
101103
101129
110908
111003
111101a
111101b
111123

120824
120913
121015
130111
3.5
3
2.5
2
1.5
1
0.5
6520 6540 6560 6580 6600

IGR J06074+2205

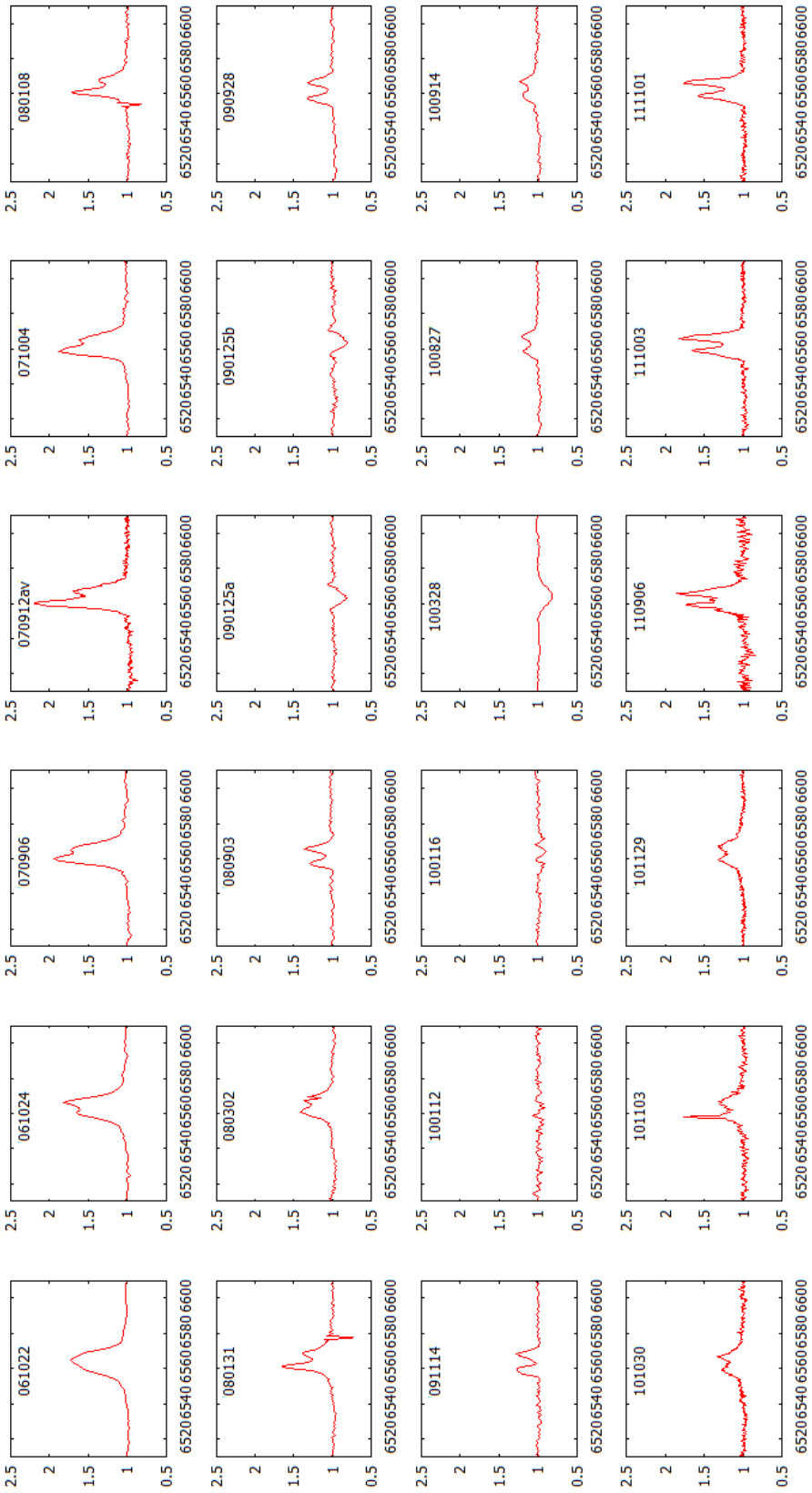

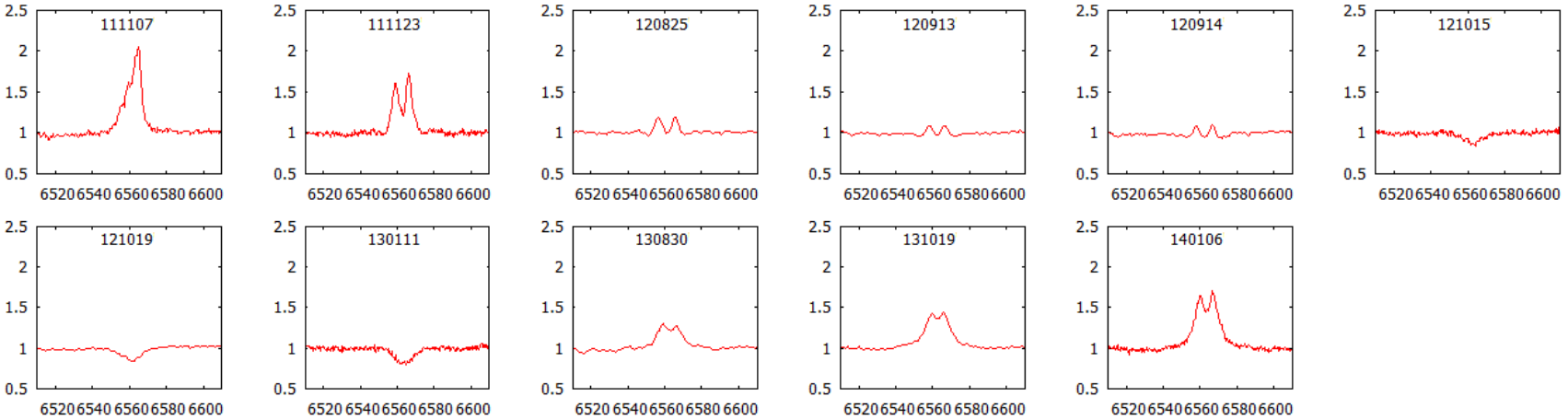
111107
111123
120825
120913
120914
121015
121019
130111
130830
131019
140106
2.5
2
1.5
1
0.5
6520 6540 6560 6580 6600

XTE J1946+274

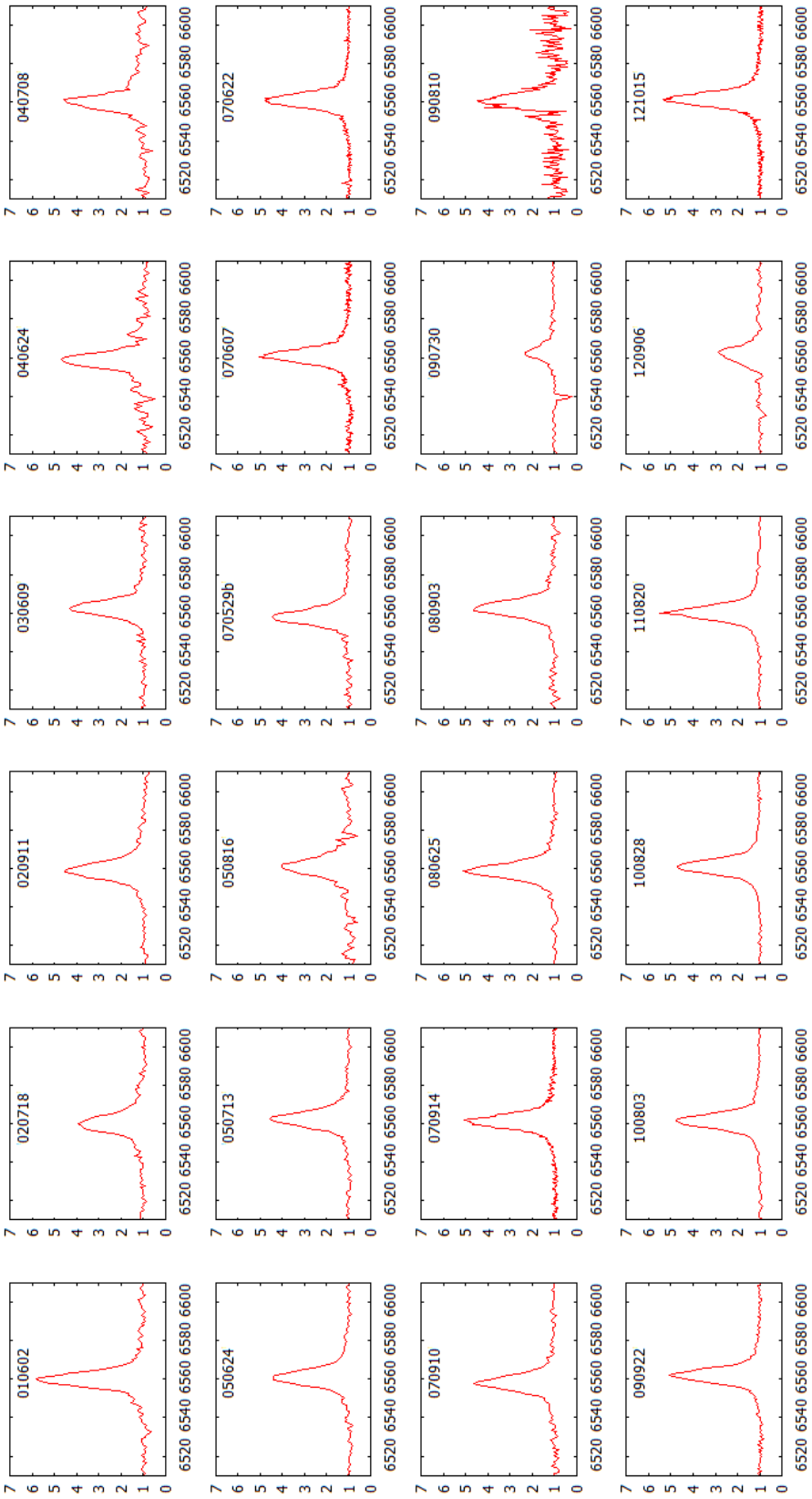

130731
140805
7
6
5
4
3
2
1
0
6520 6540 6560 6580 6600

KS 1947+300

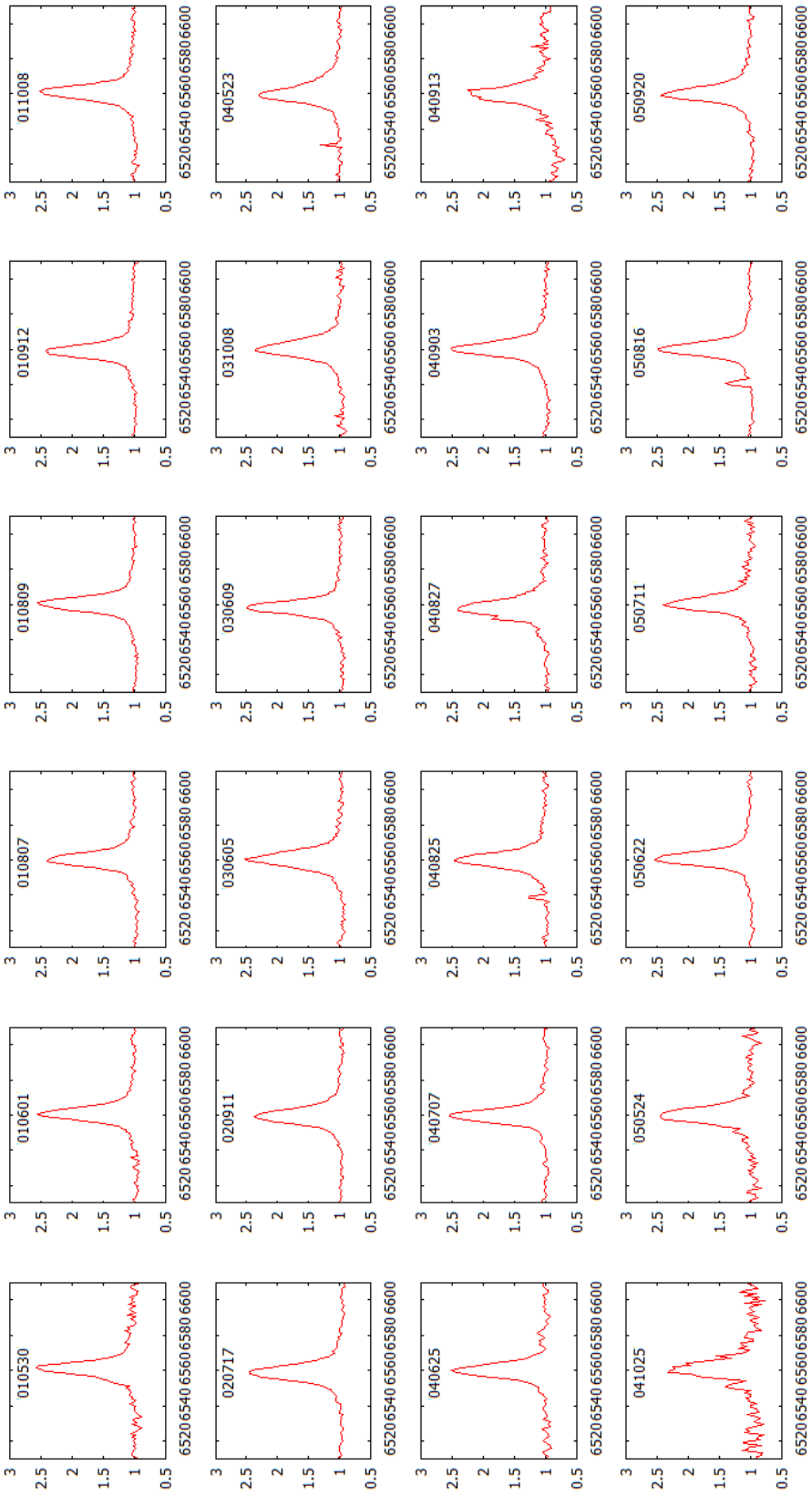
010530
010601
010807
010809
010912
011008
020717
020911
030605
030609
031008
040523
040625
040707
040825
040827
040903
040913
041025
050524
050622
050711
050816
050920

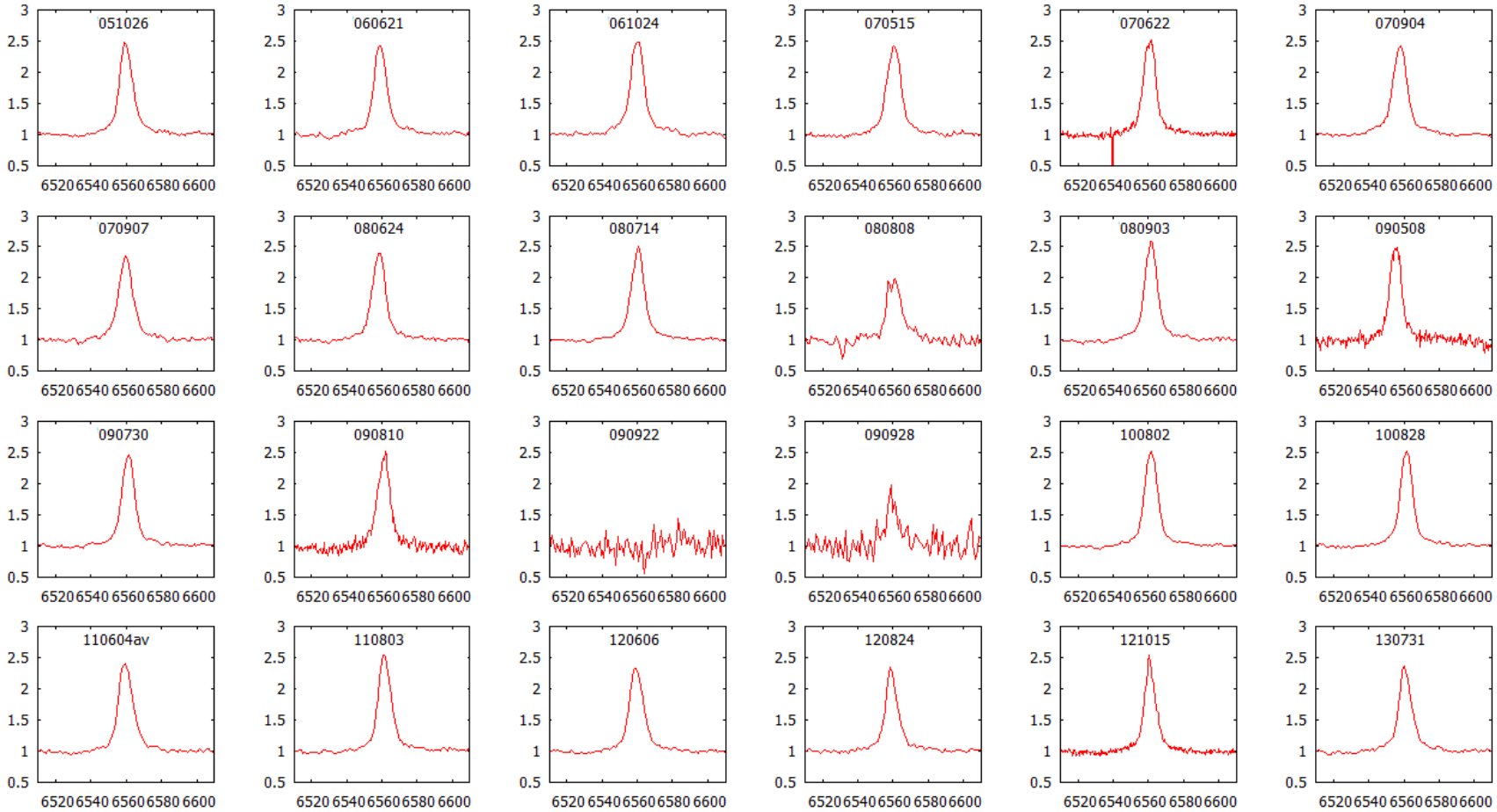
051026
060621
061024
070515
070622
070904
070907
080624
080714
080808
080903
090508
090730
090810
090922
090928
100802
100828
110604av
110803
120606
120824
121015
130731
3
2.5
2
1.5
1
0.5
6520 6540 6560 6580 6600

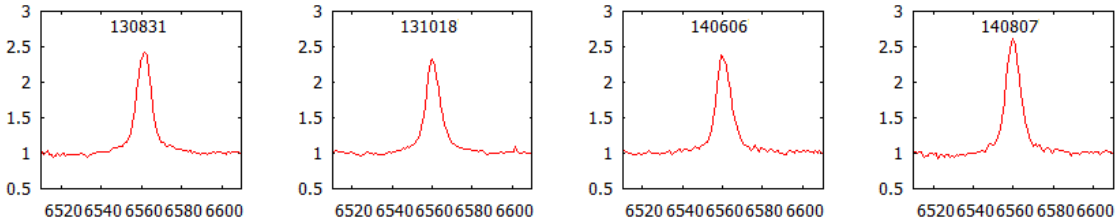
130831
131018
140606
140807
3
2.5
2
1.5
1
0.5
6520 6540 6560 6580 6600

GRO J2058+42

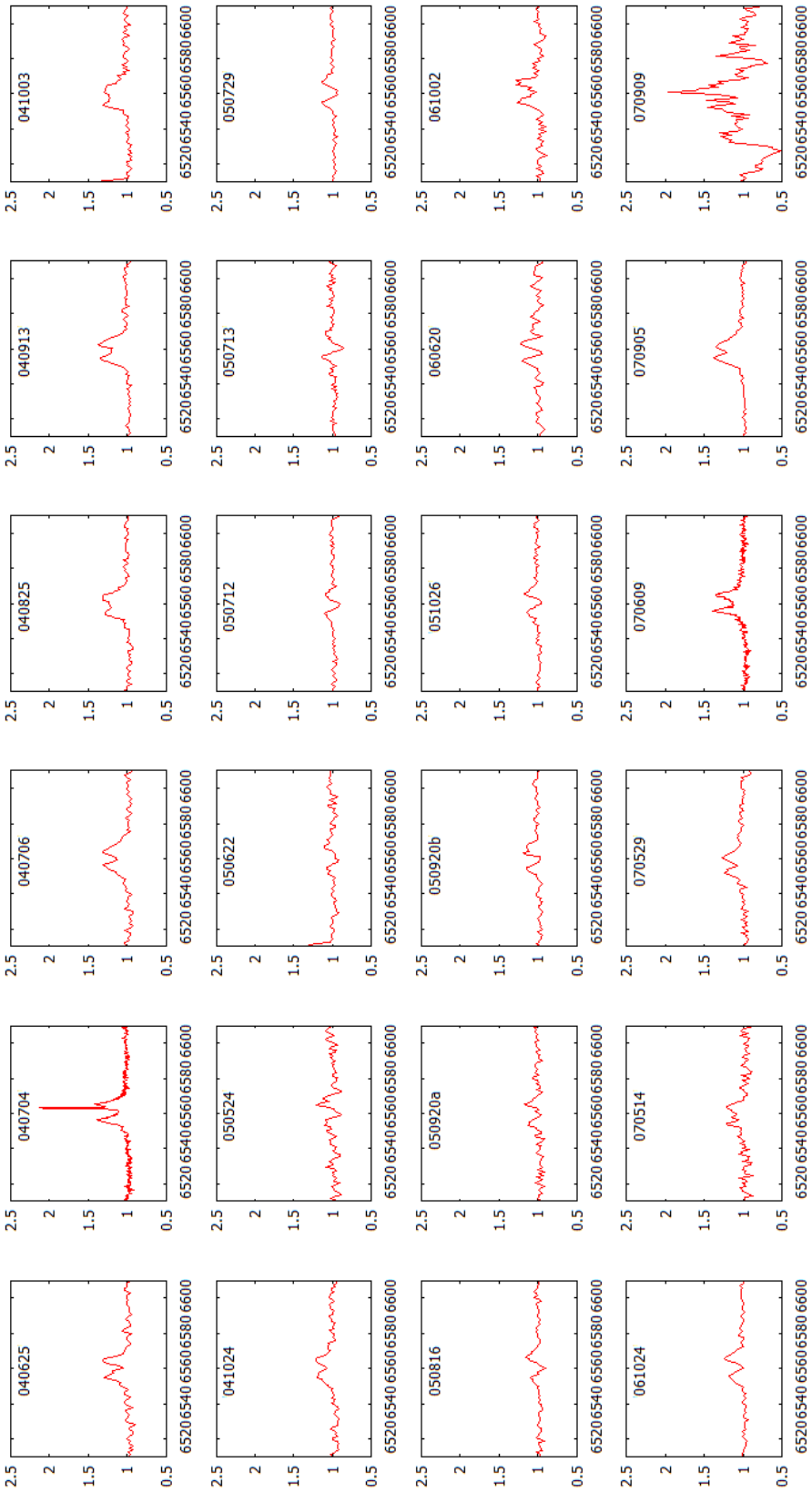
040625
040704
040706
040825
040913
041003
041024
050524
050622
050712
050713
050729
050816
050920a
050920b
051026
060620
061002
061024
070514
070529
070609
070905
070909
2.5
2
1.5
1
0.5
6520 6540 6560 6580 6600

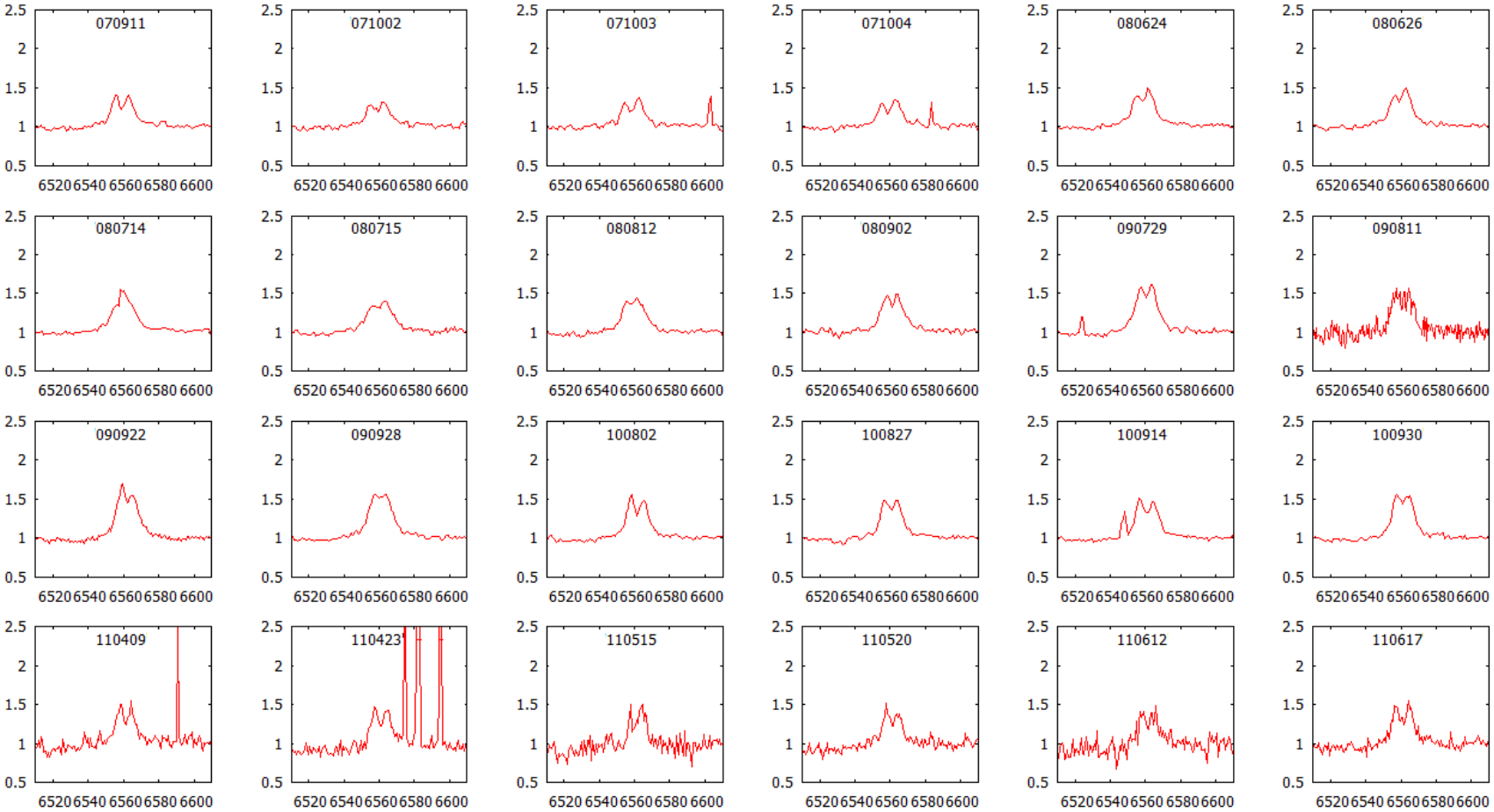
070911
071002
071003
071004
080624
080626
080714
080715
080812
080902
090729
090811
090922
090928
100802
100827
100914
100930
110409
110423
110515
110520
110612
110617
2.5
2
1.5
1
0.5
6520 6540 6560 6580 6600

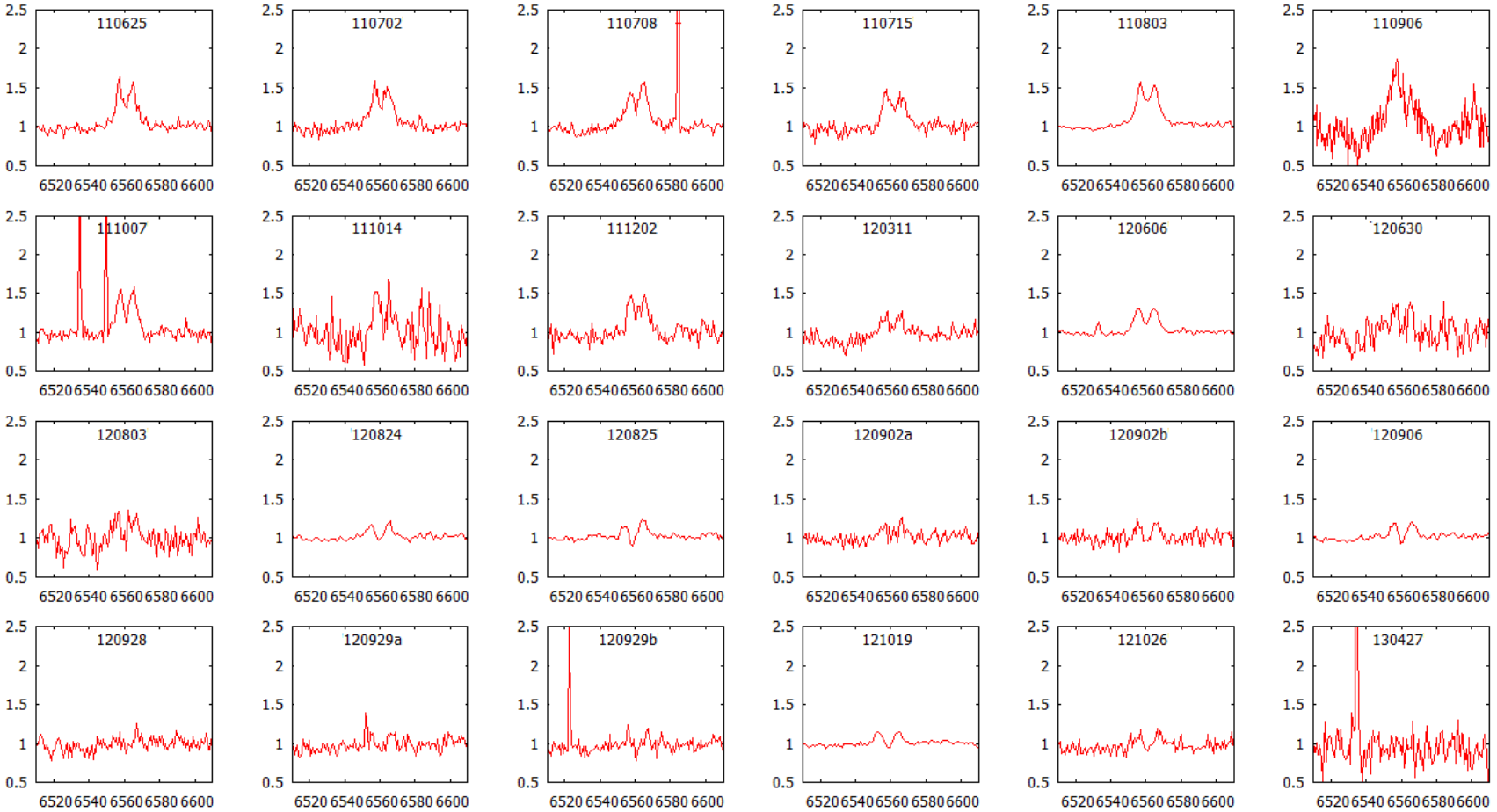
110625
110702
110708
110715
110803
110906
111007
111014
111202
120311
120606
120630
120803
120824
120825
120902a
120902b
120906
120928
120929a
120929b
121019
121026
130427
2.5
2
1.5
1
0.5
6520 6540 6560 6580 6600

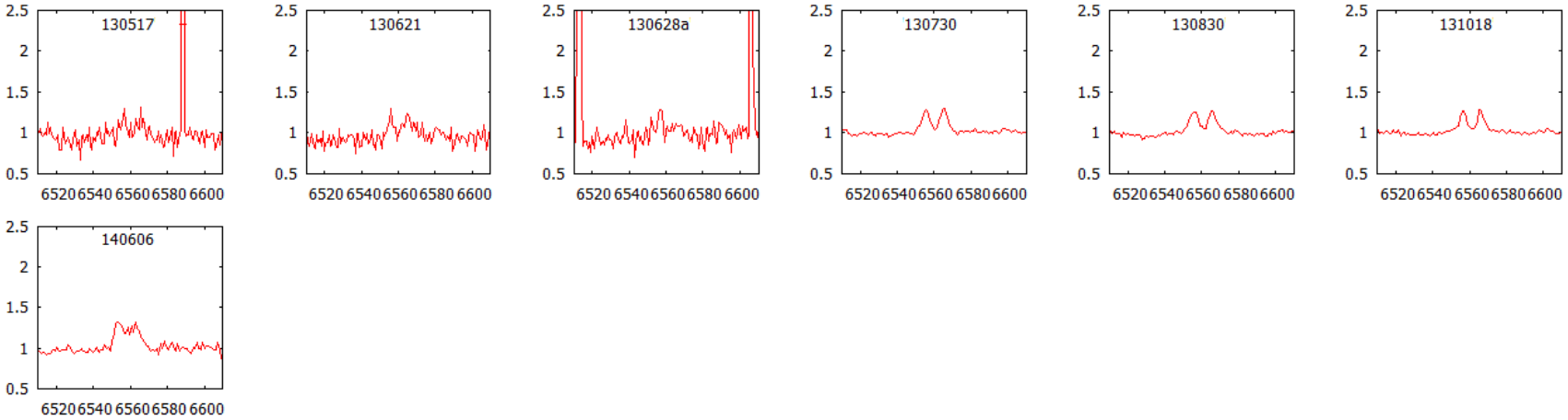
130517
130621
130628a
130730
130830
131018
140606
2.5
2
1.5
1
0.5
6520 6540 6560 6580 6600

SAX 2103.5+4545

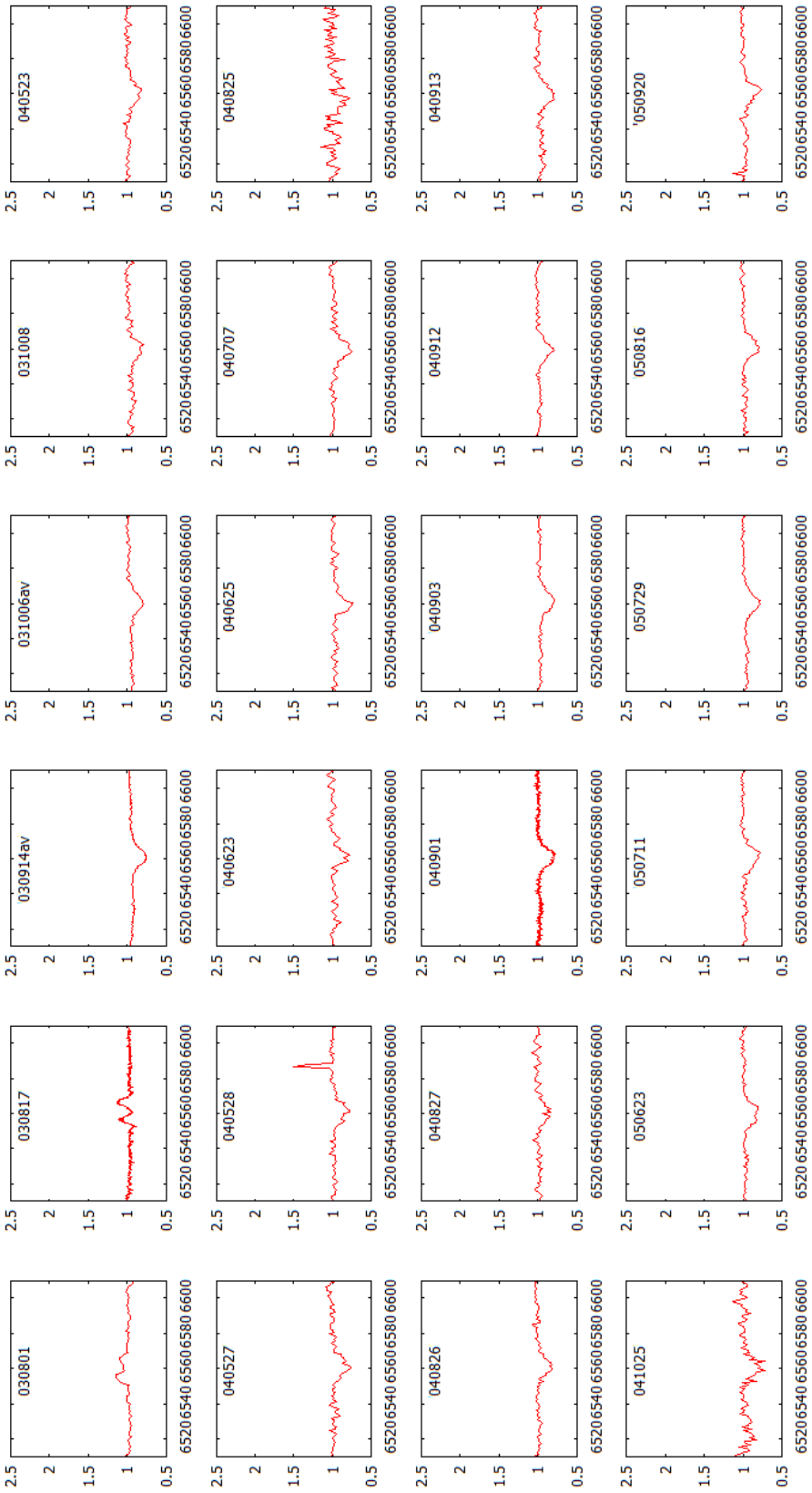

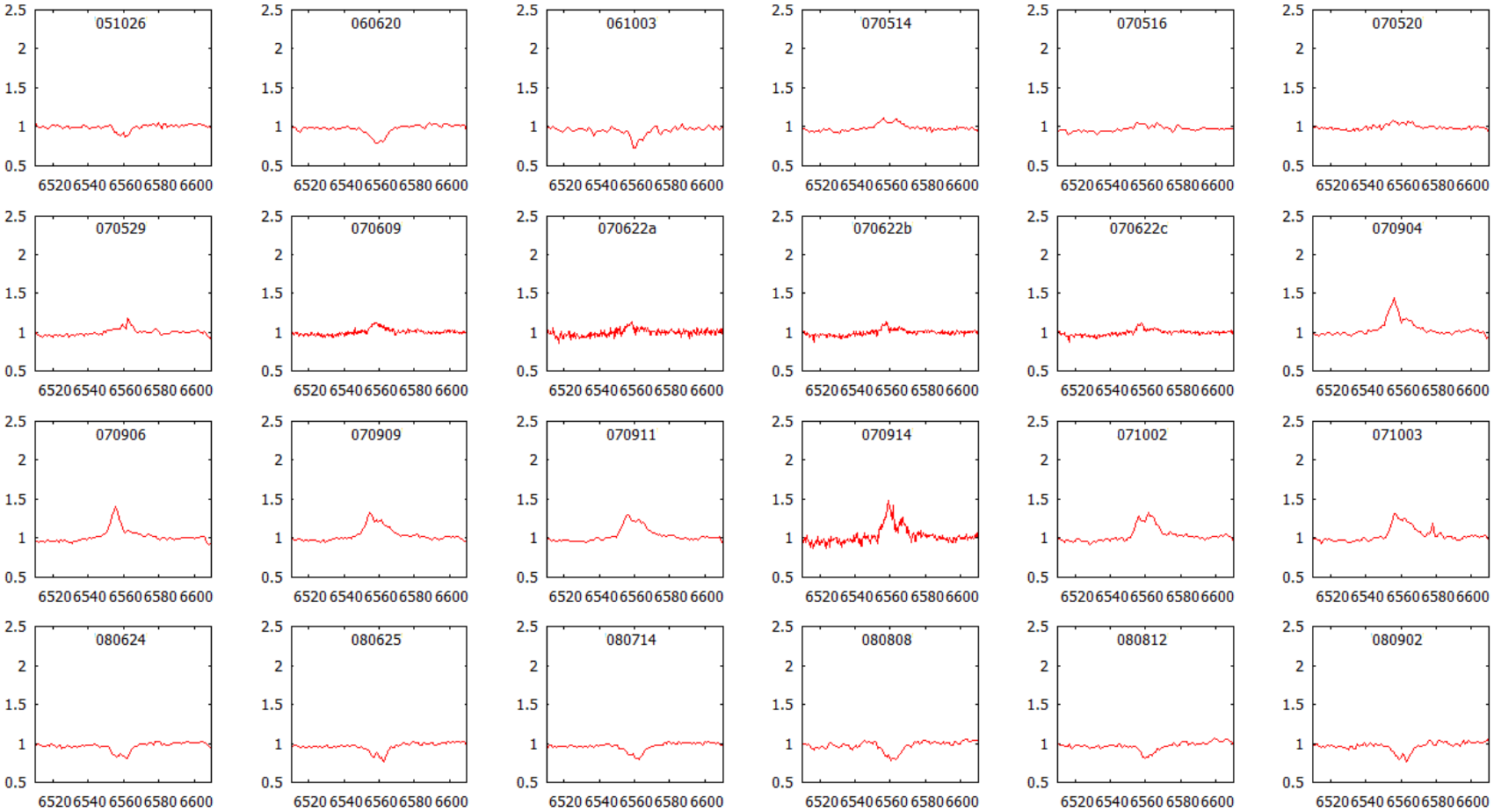
051026
060620
061003
070514
070516
070520
070529
070609
070622a
070622b
070622c
070904
070906
070909
070911
070914
071002
071003
080624
080625
080714
080808
080812
080902
2.5
2
1.5
1
0.5
6520 6540 6560 6580 6600

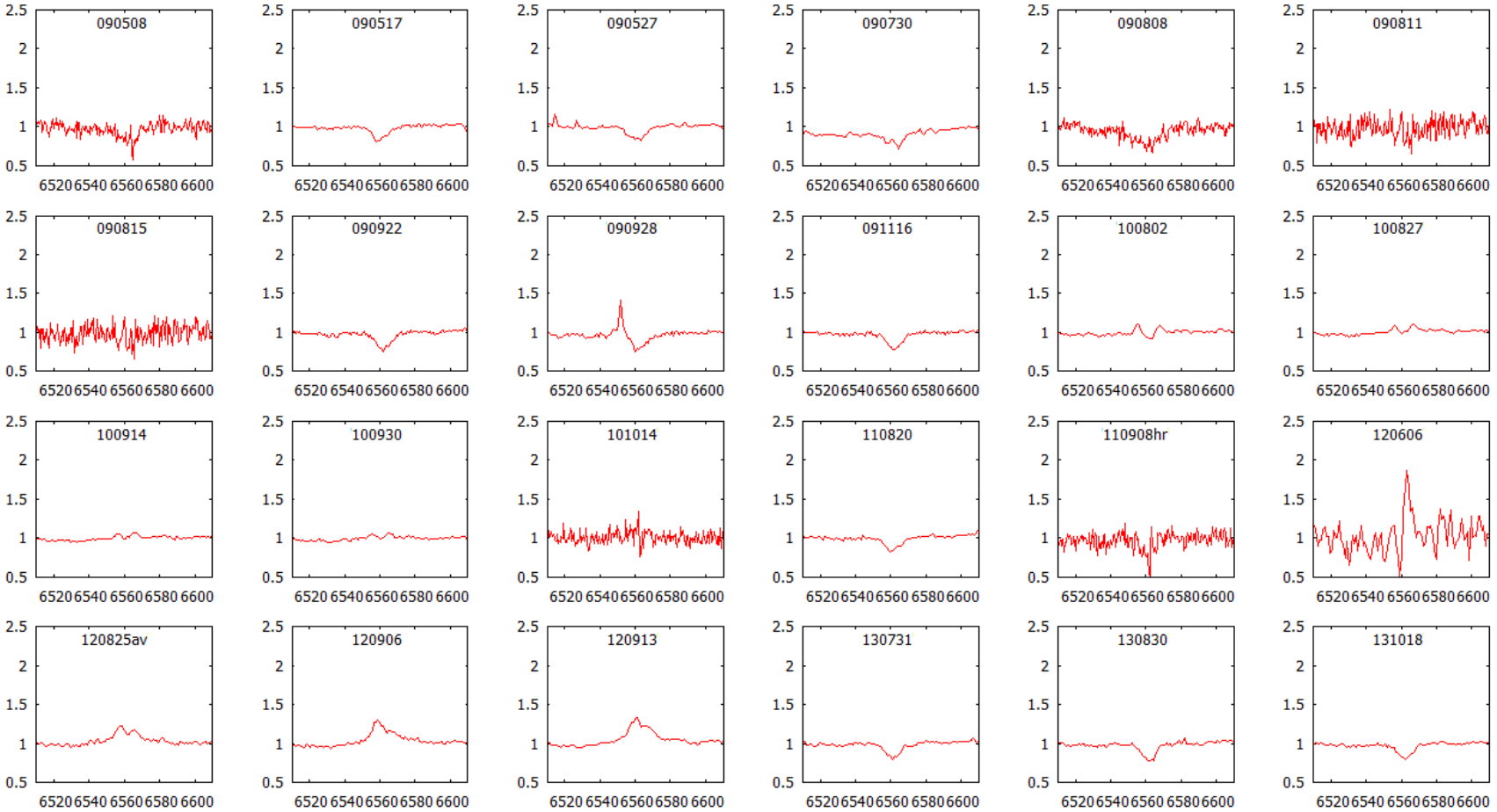
090508
090517
090527
090730
090808
090811
090815
090922
090928
091116
100802
100827
100914
100930
101014
110820
110908hr
120606
120825av
120906
120913
130731
130830
131018
2.5
2
1.5
1
0.5
6520 6540 6560 6580 6600

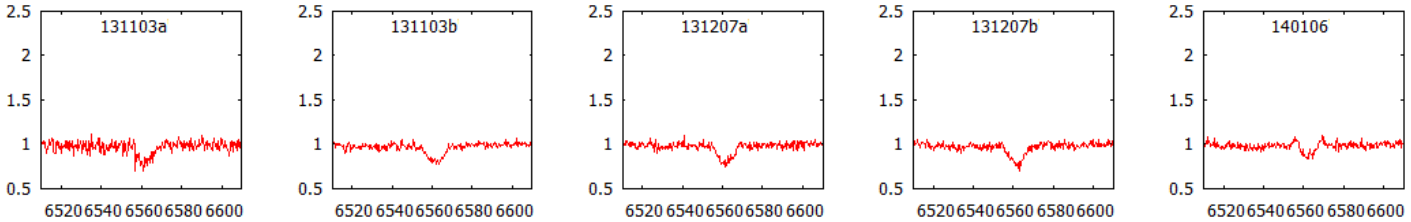
131103a
131103b
131207a
131207b
140106
2.5
2
1.5
1
0.5
6520 6540 6560 6580 6600

4U 2206+54

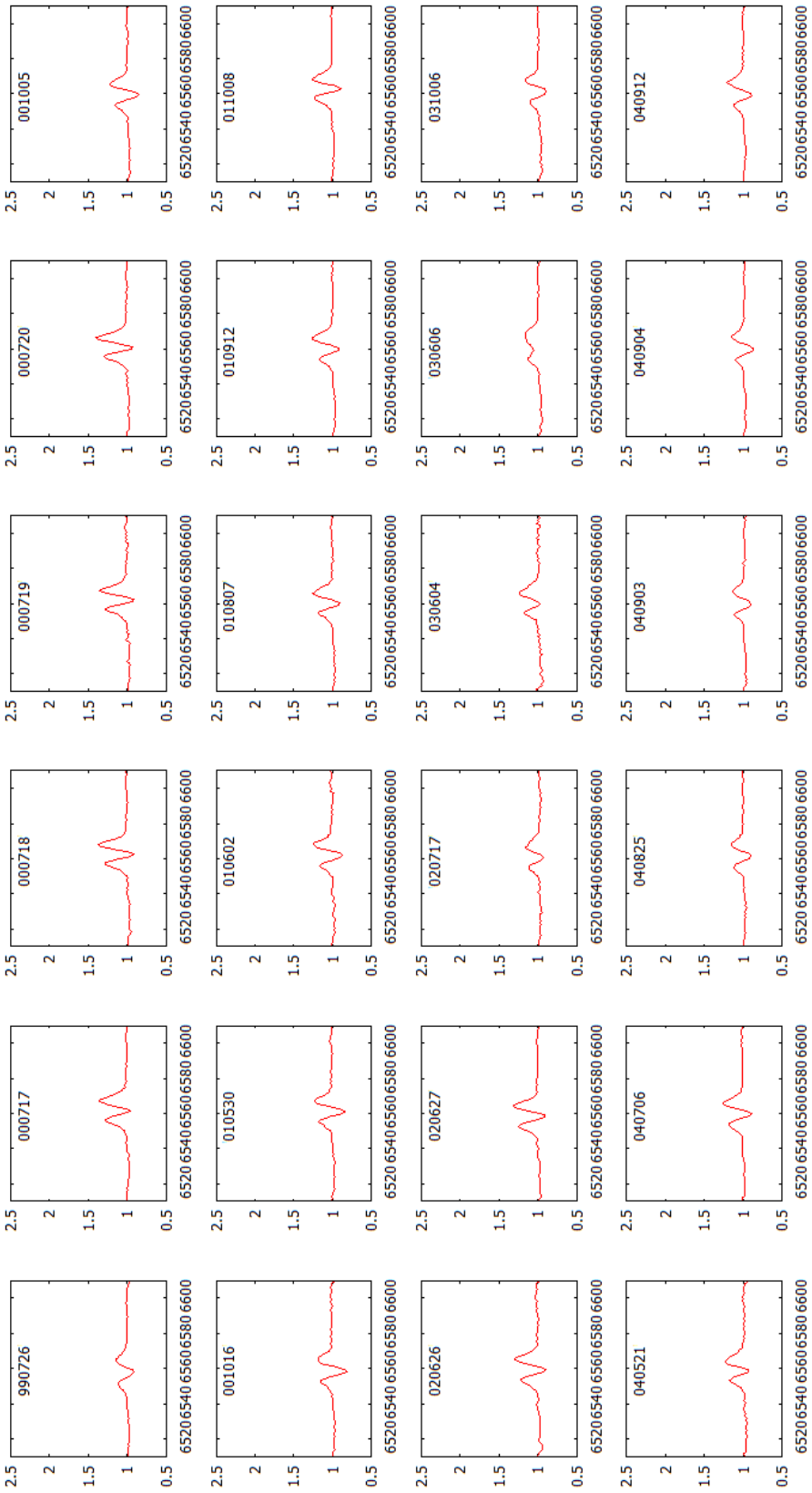
990726
000717
000718
000719
000720
001005
001016
010530
010602
010807
010912
011008
020626
020627
020717
030604
030606
031006
040521
040706
040825
040903
040904
040912
2.5
2
1.5
1
0.5
6520 6540 6560 6580 6600
6520 6540 6560 6580 6600

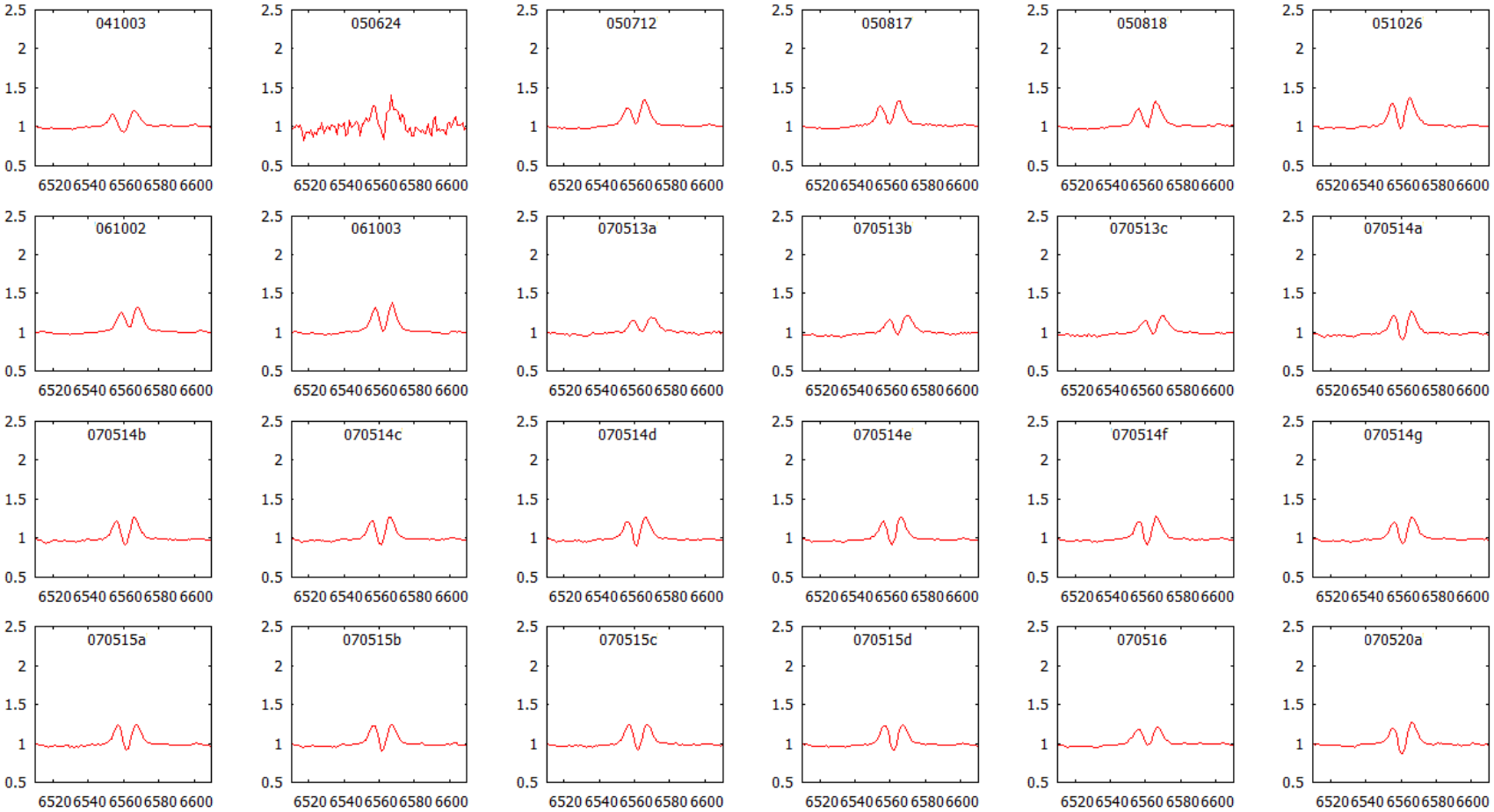
041003
050624
050712
050817
050818
051026
061002
061003
070513a
070513b
070513c
070514a
070514b
070514c
070514d
070514e
070514f
070514g
070515a
070515b
070515c
070515d
070516
070520a
2.5
2
1.5
1
0.5
6520 6540 6560 6580 6600

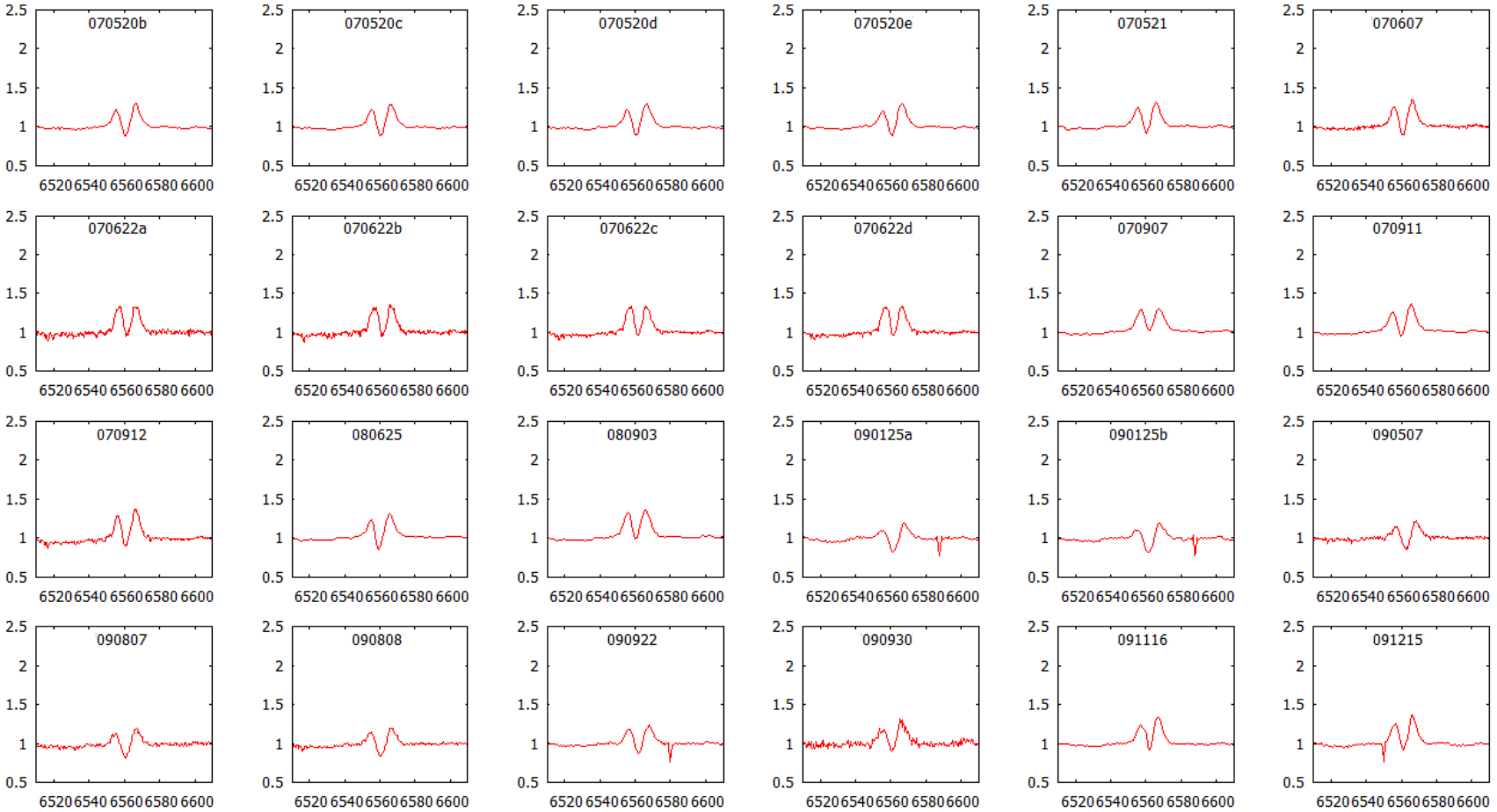
070520b
070520c
070520d
070520e
070521
070607
070622a
070622b
070622c
070622d
070907
070911
070912
080625
080903
090125a
090125b
090507
090807
090808
090922
090930
091116
091215
2.5
2
1.5
1
0.5
6520 6540 6560 6580 6600

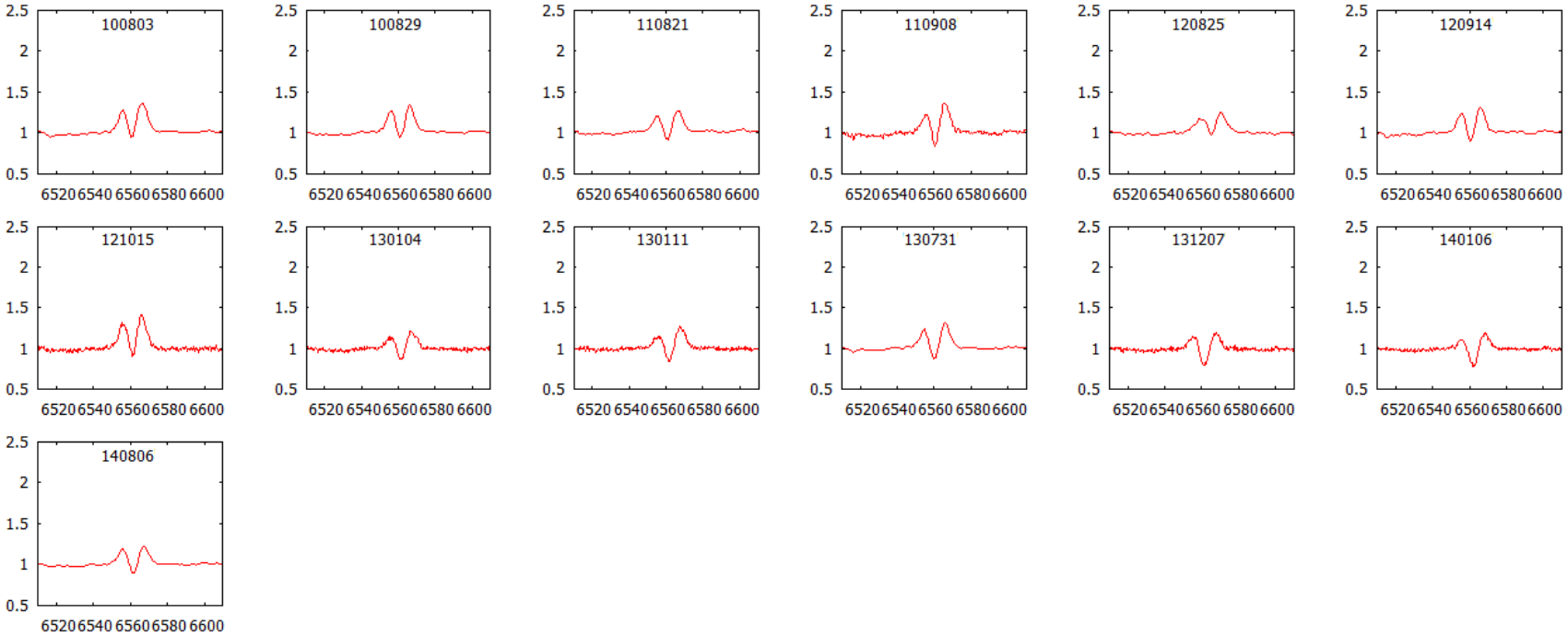
100803
100829
110821
110908
120825
120914
121015
130104
130111
130731
131207
140106
140806
2.5
2
1.5
1
0.5
6520 6540 6560 6580 6600

SAX J2239.3+6116

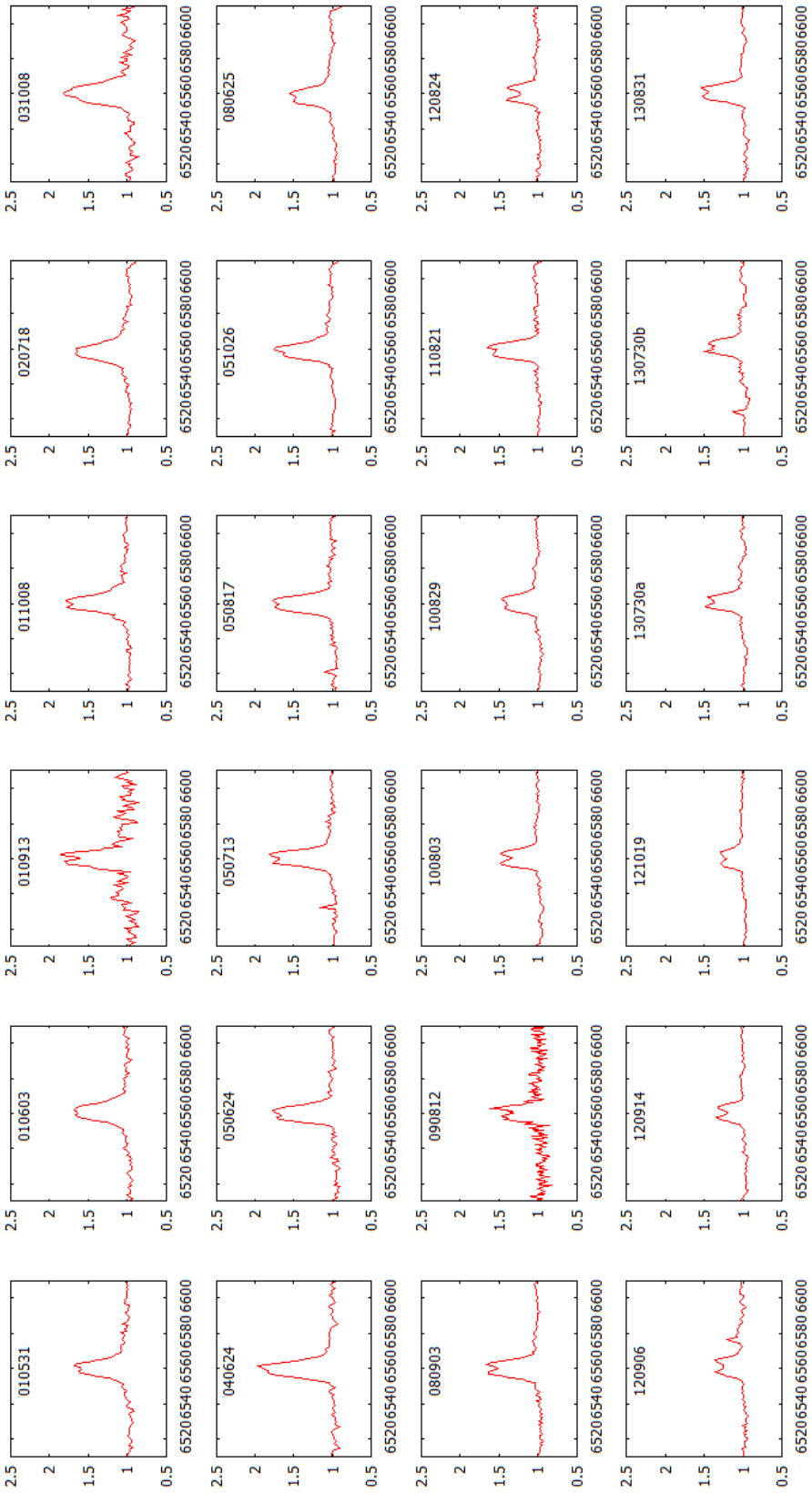

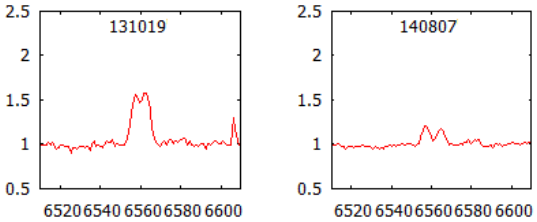
131019
2.5
2
1.5
1
0.5
6520 6540 6560 6580 6600

140807
2.5
2
1.5
1
0.5
6520 6540 6560 6580 6600

Appendix B

The Lomb-Scargle Algorithm

To find the quasi-periods in the V/R cycles we used NASA's periodogram service, and specifically the Lomb-Scargle (LS) algorithm. LS is a variation of the Discrete Fourier Transform (DFT), in which a time series is decomposed into a linear combination of sinusoidal functions. The basis of sinusoidal functions transforms the data from the time domain to the frequency domain.

The periodogram power is normalized by the inverse of the variance of the original signal data values. Horne and Baliunas (Horne 1986) showed that this scaled power has an exponential distribution for Gaussian noise data values and a large number of observations N_obs. The probability, p, of observing a power less than or equal to P_0 in one sample when the time series is a noise signal is then given by:

$$p = Pr\{P <= P_0\} = 1 - e^{-P_0} \tag{B.1}$$

The probability of seeing at least one sample exceeding this value is then given by :

$$p\nu = 1 - p^M \tag{B.2}$$

where M is the number of periods sampled.

The above expression is invalid in the limit of a small number of observations, N_obs. When N_obs is less than 50, the following formula is applied as in Zechmeister and Kurster (2009):

$$p = Pr\{P <= P_0\} = \left(1 - \frac{2P}{N-1}\right)^{\frac{N-3}{2}} \tag{B.3}$$

and, again

$$p\nu = 1 - p^M \tag{B.4}$$

where M is now the number of independent frequencies. The theoretical number of independent frequencies for a given data set lies between N and $N * (N-1)/2$ (or N choose 2). The effective number of independent frequencies is approximately equal to

$$M = \frac{maxf - minf}{df} \tag{B.5}$$

where df is the width (in frequency) of a peak (Zechmeister and Kurster 2009) that is defined as the width of the top peak in the periodogram. The beginning and ending points of a peak are defined as the frequencies at which the power is half of the peak's maximum.

Bibliography

[1] Giacconi, R., Murray, S., Gursky, H., Kellogg, E., Schreier, E., Tananbaum, H., The Uhuru Catalog of X-ray Sources, ApJ 178, 281 (1972)

[2] Huang, S.S., Profiles of Emission Lines in Be Stars, ApJ 171, 549 (1972)

[3] Scargle, J.D., Studies in Astronomical Time Series Analysis II: Statistical Aspects of Spectral Analysis of Unevenly Spaced Data, ApJ 263, 835 (1982)

[4] Bernacca, P.L., Iijima, T., Stagni, R., Identification of the Optical Counterpart of the X-ray Source V0332 + 53, A&A 132, L8 (1984)

[5] Moon, T.T., Dworetsky, M.M., Grids for the Determination of Effective Temperature and Surface Gravity of B, A and F Stars Using uvby-beta Photometry, MNRAS 217, 305 (1985)

[6] Stella, L., White, N.E., Davelaar, J., Parmar, A.N., Blissett, R.J., van der Klis, M., The Discovery of 4.4 Second X-ray Pulsations From the Rapidly Variable X-ray Transient V0332 + 53, ApJ 288, L45 (1985)

[7] Dachs, J., Hanuschik, R., Kaiser, D., Rohe, D., Geometry of Rotating Envelopes Around Be Stars Derived from Comparative Analysis of H-alpha Emission Line Profiles, A&A 159, 276 (1986)

[8] Horne, J.H., Baliunas, S.L., A Prescription for Period Analysis of Unevenly Sampled Time Series, ApJ 302, 757 (1986)

[9] Hanuschik, R.W., High-resolution Emission-line Spectroscopy of Be stars. I - Evidence for a Two-component Structure of the H-alpha Emitting Envelope, A&A 166, 185 (1986)

[10] Hanuschik, R.W., Kozok, J.R., Kaiser, D., High Resolution Emission Line Spectroscopy of Be Stars. III - Balmer Line Profiles, A&A 189, 147 (1988)

[11] Hanuschik, R.W., Stellar V sin i and Optical Emission Line Widths in Be Stars, Astrophysics and Space Science 161, 61 (1989)

[12] Okazaki, A.T., Long-term V/R Variations of Be Stars Due to Global One-armed Oscillations of Equatorial Disks, Publ. Astron. Soc. Jpn. 43, 75 (1991)

[13] Telting, J.H., Heemskerk, M.H., Henrichs, H.F., Savonije, G.J., Observational Evidence for a Prograde One-Armed Density Structure in the Equatorial Disc of a Be Star, A&A 288, 558 (1994)

[14] Hanuschik, R.W., Shell Lines in Disks Around Be Stars. 1: Simple Approximations for Keplerian Disks, A&A 295, 423 (1995)

[15] Hanuschik, R.W., Hummel, W., Dietle, O., Sutorius, E., V/R Variability and Global Oscillations in the Be Star Disks, A&A 300, 163 (1995)

[16] Finger, M.H., Wilson, R.B., Harmon, B.A., Quasi-periodic Oscillations During a Giant Outburst of A0535+262, ApJ 459, 288 (1996)

[17] Hanuschik, R.W., On the Structure of Be Star Discs, A&A 308, 170 (1996)

[18] Hanuschik, R.W., W. Hummel, E. Satorius, O. Dietle, G. Thimm, Atlas of High-Resolution Emission and Shell Lines in Be Stars. Line Profiles and Short-Term Variability, A&AS, 116, 309 (1996)

[19] Vacca, W.D., Garmany, D.C., Shull, J.M., The Lyman-Continuum Fluxes and Stellar Parameters of O and Early B-Type Stars, ApJ 460, 914 (1996)

[20] Okazaki, A.T., On the Confinement of One-armed Oscillations in Discs of Be Stars, A&A 318, 548 (1997)

[21] Reig P., Coe, M.J., Stevens, J.B., Negueruela, I., Clark, J.S., Buckley, D.A.H., Fabregat, J., Roche, P., Hard X-Ray and Ground-Based Observations of High-Mass X-Ray Binaries, ESASP 382, 175 (1997)

[22] Quirrenbach, A., Bjorkman, K.S., Bjorkman, J.E., Hummel, C.A., Buscher, D.F., Armstrong, J.T., Mozurkewich, D., Elias II, N.M., Babler, B.L., Constraints on the Geometry of Circumstellar Envelopes: Optical Interferometric and Spectropolarimetric Observations of Seven Be Stars, ApJ 479, 477 (1997)

[23] Negueruela, I., On the Nature of Be/Xray Binaries, A&A 338, 505 (1998)

[24] Negueruela, I., Reig, P., Coe, M.J., Fabregat, J., Large-scale Perturbations in the Circumstellar Envelopes of Be/X-ray Binaries, A&A 336, 251 (1998)

[25] Steele, I.A., Negueruela, I., Coe, M.J., Roche, P., The Distances to the X-ray Binaries LSI +61 deg 303 and A0535+262, MNRAS 297, L5 (1998)

[26] Wilson, A.C., Finger, H.M., Harmon, A.B., Chakrabarty, D., Strohmayer, T., Discovery of the 198 Second X-Ray Pulsar GRO J2058+42, ApJ 499, 820 (1998)

[27] Negueruela, I., Roche, P., Fabregat, J., Coe, M.J., The Be/X-ray Transient V0332+53: Evidence for a Tilt Between the Orbit and the Equatorial Plane?, MNRAS 307, 695 (1999)

[28] Steele, I.A., Negueruela, I., Clark, J.S., A Representative Sample of Be Stars. I. Sample Selection, Spectral Classification and Rotational Velocities A&AS 137, 147 (1999)

[29] Reig, P., Roche, P., Discovery of Two New Persistent Be/X-ray Pulsar Systems, MNRAS 306, 100 (1999)

[30] In't Zand, J.J.M., Halpern, J., Eracleous, M., McCollough, M., Augusteijn, T., Remillard, R.A., Heise, J., The Transient X-ray Source SAX J2239.3+6116 and Its Optical Counterpart, A&A, arXiv:astro-ph/0006335 (2000)

[31] Negueruela, I., Reig, P., On the Nature of the Hard X-ray Source 4U2206+54, A&A 371, 1056 (2001)

[32] Negueruela, I., Okazaki, A.T., The Be/X-ray transient 4U 0115+63/V635 Cassiopeiae. I. A consistent model, A&A 369, 108 (2001)

[33] Okazaki, A.T., Negueruela, I., A Natural Explanation for Periodic X-ray Outbursts in Be/X-ray Binaries, A&A 377, 161 (2001)

[34] Zamanov, R.K., Reig, P., Marti, J., Coe, M.J., Fabregat, J., Tomov, N.A., Valchev, T., Comparison of the H_α Circumstellar Disks in Be/X-ray Binaries and Be Stars, A&A 367, 884 (2001)

[35] Verrechia, F., Israel, G.L., Negueruela, I., Covino, S., Polcaro, V.F., Clark, J.S., Steele, I.A., Gualandi, R., Speziali, R., Stella, L., The Identification of the Optical/IR Counterpart of the 15.8-s Transient X-ray Pulsar XTE J1946+274, A&A 393, 983(2002)

[36] Porter, J.M., Rivinius, T., Classical Be Stars, Publ. Astron. Soc. Pac. 115, 1153 (2003)

[37] Torrejon, J.M., Kreykenbohm, I., Orr, A., Titarchuk, L., Negueruela, I., Evidence for a Neutron Star in the Non-Pulsating Massive X-ray Binary 4U2206+54, A&A 423, 301 (2004)

[38] Reig, P., Negueruela, I., Fabregat, J., Chato, R., Coe, M.J., Long-term Optical/IR Variability of the Be/X-ray Binary LS V +44 17/RX J0440.9+4431, A&A 440, 1079 (2005)

[39] Reig, P., Negueruela, I., Papamastorakis, G., Manousakis, A., Kougentakis, T., Identification of the Optical Counterparts of High-Mass X-ray Binaries Through Optical Photometry and Spectroscopy, A&A 440, 637 (2005)

[40] Tycner, C., Lester, J.B., Hajian, A.R., Armstrong, J.T., Benson, J.A., Gilbreath, G.C., Hutter, D.J., Pauls, T.A., White, N. M., Properties of the Halpha-emitting Circumstellar Regions of Be Stars, ApJ 624, 359 (2005)

[41] Blay, P., Negueruela, I., Reig, P., Coe, M.J., Corbet, R.H.D., Fabregat, J., Tarasov, A.E., Multiwavelength Monitoring of BD +53 2790, the Optical Counterpart to 4U 2206+54, A&A 446, 1095 (2006)

[42] Grundstrom, E.D., Gies, D.R., Estimating Be Star Disk Radii Using H-alpha Emission Equivalent Widths, ApJ 651, L53 (2006)

[43] Nakajima, M., Mihara, T., Makishima, K., Niko, H., A Further Study of the Luminosity-dependent Cyclotron Resonance Energies of the Binary X-Ray Pulsar 4U 0115+63 with the Rossi X-Ray Timing Explorer, Advances in Space Research 38, 2756 (2006)

[44] Negueruela, I., Smith, D.M., Reig, P., Chaty, S., Torrejon, J.M., Superginat Fast X-ray Transients: A New Class of High Mass X-ray Binaries Unveiled by Integral, ESA Spec. Publ. 604, 165 (2006)

[45] Ribo, M., Negueruela, I., Blay, P., Torrejon, J.M., Reig, P., Wind Accretion in the Massive X-ray Binary 4U 2206+54: Abnormally Slow Wind and a Moderately Eccentric Orbit, A&A 449, 687 (2006)

[46] Baykal, A., Inam, S.C., Stark, M.J., Heffner, C.M., Erkoca, A.E., Swank, J.H., Timing Studies on RXTE Observations of SAX J2103.5+4545, MNRAS 374, 1108 (2007)

[47] Reig, P., Larionov, V., Negueruela, I., Arkharov, A.A., Kudryavtseva, N.A., The Be/X-ray Transient 4U0115+63/V635 Cassiopeiae, A&A 462, 1081 (2007)

[48] Stefl, S., Okazaki, A.T., Rivinus, T., Baade, D., V/R Variations of Binary Be Stars, Publ. Astron. Soc. Pac. 361, 274 (2007)

[49] Walter, R., Zurita Heras, J., Probing Clumpy Stellar Winds With a Neutron Star, A&A 476, 335 (2007)

[50] Negueruela, I., Smith, D.M., Reig, P., Torrejon, J.M., Ribo, M., Superginat Fast X-ray Transients and Other Wind Accretors, AIP Conf. Proc. 1010, 252 (2008)

[51] Reig, P., Rapid Spectral and Timing Variability of Be/X-ray Binaries During Type II Outbursts, A&A 489, 725 (2008)

[52] Cranmer, S.R., A Pulsational Mechanism for Producing Keplerian Disks Around Be Stars, ApJ 701, 396 (2009)

[53] Sarty, G.E., Kiss, L.L., Huziak, R., Catalan, L.J.J., Luciuk, D., Crawford, T.R., Lane, D.J., Puckard, R.D., Grzybowski, T.A., Closas, P., Johnston, H., Balam, D., Wu, K., Periodicities in the High-Mass X-ray Binary System RX J0146.9+6121/LS I+61.235, MNRAS 392, 1242 (2009)

[54] Zechmeister, M., Kurster, M., The Generalised Lomb-Scargle Periodogram. A New Formalism for the Floating-mean and Keplerian Periodograms, A&A 496, 577 (2009)

[55] Finger, M.H., Ikhsanov, N.R., Wilson-Hodge, C.A., Pate, S.K., Spin-Down of the Long-Period Accreting Pulsar 4U 2206+54, ApJ 709, 1249 (2010)

[56] Reig, P., Slowikowska, A., Zezas, A., Blay, P., Correlated Optical/X-ray Variability in the High-Mass X-ray Binary SAX J2103.5+4545, MNRAS 401, 55 (2010)

[57] Reig, P., Zezas, A., Gkouvelis, L., The optical Counterpart to IGR J06074+2205: A Be/X-ray Binary Showing Disc Loss and V/R Variability, A&A 522, 107 (2010)

[58] Wang, W., Discovery of a Magnetic Neutron Star in X-ray Transient IGR J01583+6713, A&A 516, A15 (2010)

[59] Tomsick, J.A., Heinke, C., Halpern, J., Kaaret, P., Chaty, S., Rodriguez, J., Bodaghee, A., Confirmation of IGR J01363+6610 as a Be X-ray Binary With Very Low Quiescent X-ray Luminosity, ApJ 728, 86 (2011)

[60] Reig, P., Be/X-ray Binaries, Astrophysics and Space Science 332, 1 (2011)

[61] Townsend, L.J., Coe, M.J., Corbet, R.H.D., Hill, A.B., On the Orbital Parameters of Be/X-ray Binaries in the Small Magellanic Cloud, MNRAS 416, 1556 (2011)

[62] Ferrigno, C., Farinelli, R., Bozzo, E., Pottschmidt, K., Klochkov, D., Kretschmar, P., RX J0440.9+4431: A Persistent Be/X-ray Binary In Outburst, A&A 553, A103 (2013)

[63] Monageng, I.M., How Circumstellar Discs Affect Mass Accretion in Be X-ray Binaries, (2013)

[64] Arabaci, M.O., Arranz, A.C., Zurita, C., Soto, J.G., Nespoli, E., Suso, J., Kiaeerad, F., Rojas, J.G., Kiziloglu, U., Detection of a Large Be Circumstellar Disk During X-ray Quiescence of XTE J1946+274, A&A, arXiv:1412.2770 (2014)

[65] Martin, R.G., Nixon, C., Armitage, P.J., Lubow, S.H., Price, D.J., Giant Outbursts in Be/X-ray Binaries, ApJ 790, L34 (2014)

[66] Psaradaki, I., Spectroscopic Study of the Be Optical Counterpart to the High-Mass X-ray Binary Source IGR J21343+4738, (2014)

[67] Reig, P., Doroshenko, V., Zezas, A., The Quiescent State of the Accreting X-ray Pulsar SAX J2103.5+4545, MNRAS 445, 1314 (2014)

[68] Stoyanov, K.A., Zamanov, R.K., Latev, G.Y., Abedin, A.Y., Tomov N.A., Orbital Parameters of the High-Mass X-ray Binary 4U 2206+54, Astronomische Nachrichten, arXiv:1411.7561 (2014)

[69] Reig, P., Fabregat, J., Long-term Variability of High-mass X-ray Binaries. I. Photometry, A&A 574, 14 (2015)

[70] http://exoplanetarchive.ipac.caltech.edu/applications/Periodogram/docs/Algorithms.html

[71] http://www.sao.arizona.edu/help/FLWO/60/60.html

[72] http://www.astrosurf.com/buil/us/spe2/hresol7.htm

[73] http://www.stsci.edu/institute/software hardware/pyraf/

[74] http://iraf.noao.edu